# EXTREME VALUE ANALYSIS OF PEAK WIND PRESSURES ON BUILDINGS

by

J. J. Lou* and J. A. Peterka**

Fluid Mechanics and Wind Engineering Program
Fluid Dynamics and Diffusion Laboratory
Department of Civil Engineering
Colorado State University
Fort Collins, Colorado 80523

December 1981

* Graduate Research Assistant
** Associate Professor

CER81-82JJL-JAP32

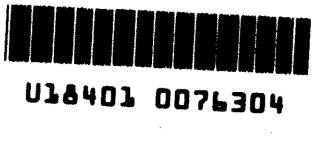

TA7
.C6
CER81-82/32
copy 2

ABSTRACT

EXTREME VALUE ANALYSIS OF PEAK WIND PRESSURES ON BUILDINGS

Extreme value statistics of pressure fluctuations on buildings in regions of impinging, separated flows and vortex formation was determined both theoretically and experimentally. Fluctuating pressure data were obtained on a scale model of an actual structure placed in a wind tunnel which simulated the characteristics of the atmospheric wind. The data were analyzed to yield probability density functions of pressure fluctuations, which are non-Gaussian for negative and for strong positive mean values of pressure coefficients. It was confirmed that the distribution of all the pressure peaks in sequence, called "continuous peaks" in this study, is of extreme value type I. Autocorrelation functions of peak sequences provided at estimate of the average effective fluctuation rate. With this value available, the probability distribution of the largest (or maximum negative) peak in a given time period was obtained, resulting in the ability to predict peak pressures on a statistical basis. Examination of some implications of the findings reveals the possibility of recovering the extreme value distributions from typical wind-tunnel pressure study data (for example, 16-second record at 250 samples per second). Applications of extreme value results also include prediction technique for peak pressures.

TABLE OF CONTENTS

TABLE OF CONTENTS (CONTINUED)

LIST OF TABLES

LIST OF FIGURES

LIST OF FIGURES (CONTINUED)

LIST OF FIGURES (CONTINUED)

## LIST OF SYMBOLS

| Symbol | Definition |
|---|---|
| $a(x)$ | Increasing function of x, Eq. (3.7) |
| CDF, $F(x)$ | Cumulative distribution function of x |
| $Cp$ | Pressure coefficient |
| $C_{\hat{p}}$ | Extreme pressure coefficient |
| $Cp_{max}$ | Peak maximum pressure coefficient |
| $Cp_{mean}$ | Mean pressure coefficient |
| $Cp_{min}$ | Peak minimum pressure coefficient |
| $Cp_{rms}$ | Root-mean-square pressure coefficient |
| $C_x(t, t+\tau)$ | Autocovariance function of random process {X(t)} at arbitrary fixed values of t and $t+\tau$, Eq. (6.8) |
| $D$ | Characteristic length of building |
| $e$ | Voltage |
| $F_{I,max}(x;\xi,\theta)$ | Type I asymptote CDF of maxima, Eq. (3.12) |
| $f_{I,max}(x;\xi,\theta)$ | Type I asymptote PDF of maxima, Eq. (3.13) |
| $F_{I,min}(x;\xi,\theta)$ | Type I asymptote CDF of minima, Eq. (3.14) |
| $f_{I,min}(x;\xi,\theta)$ | Type I asymptote PDF of minima, Eq. (3.15) |
| $g$ | Pressure spike value |
| $\hat{g}$ | Extreme pressure spike value |
| $g_d$ | Pressure gust factor, Eq. (6.11) |
| $h$ | Time interval between samples |
| $m$ | Maximum lag number |
| $m_r$ | Rth moment of power spectral density |
| $N$ | Number of independent peaks in a period of time T |
| $N$ | Sample size |
| $n$ | Exponent of mean velocity profile, Eq. (4.6) |
| $n$ | Frequency Hz |

LIST OF SYMBOLS (CONTINUED)

| Symbol | Definition |
|---|---|
| n | Sample size |
| PDF, f(x) | Probability density function of x |
| P(x), P(η) | PDF of the largest/smallest peak in time T (Extreme value PDF) |
| p(x), p(η) | PDF of continuous peaks |
| Q(x), Q(η) | CDF of the largest/smallest peak in time T (Extreme value CDF) |
| $Q_r(x)$ | CDF of the largest/smallest peak in time T |
| q(x), q(η) | CDF of continuous peaks |
| r | Lag number |
| r | Ratio of two time periods (= $T_r/T$) |
| $R^2$ | Multiple correlation coefficient |
| $\hat{R}_r$ | Autocorrelation coefficient estimate at lag number r |
| S(n) | Power spectral density function |
| S{P} | Coefficient of skewness of pressure fluctuations |
| T | Time period |
| t | Time |
| $T_r$ | Time period |
| $T_u$ | Turbulence intensity |
| U | Longitudinal velocity |
| $u_n$ | Characteristic value of $X_{(n)}$, Eq. (3.8) |
| $U_{rms}$ | Root-mean-square velocity |
| $U(\delta)$, $U_\infty$ | Free stream velocity |
| U(Z) | Velocity at height Z |
| V | Wind velocity |
| WD | Wind direction |
| X | Wind load, Eq. (6.12) |

LIST OF SYMBOLS (CONTINUED)

| Symbol | Definition |
|---|---|
| $X$ | Random variable |
| $X_i$ | Sample values of random variable X |
| $X_{(i)}$ | Sample values in ordered set, Eq. (3.1) |
| $\{X(t)\}$ | Random process |
| $Z$ | Height |
| $\Phi_{(1)}(x;n)$ | Exact CDF of $X_{(1)}$, Eq. (3.4) |
| $\phi_{(1)}(x;n)$ | Exact PDF of $X_{(1)}$, Eq. (3.5) |
| $\Phi_{(n)}(x;n)$ | Exact CDF of $X_{(n)}$, Eq. (3.2) |
| $\phi_{(n)}(x;n)$ | Exact PDF of $X_{(n)}$, Eq. (3.3) |
| $\theta$ $(= 1/\alpha_n)$ | Location factor of extreme value distribution |
| $\xi(= - u_n)$ | Scaling factor of extreme value distribution |
| $\nu$ | Average effective fluctuation rate |
| $\rho$ | Density of air |
| $\mu$ | Absolute viscosity of air |
| $\delta$ | Boundary layer thickness |
| $\sigma_p^2$ | Variance of pressure fluctuations |
| $\eta$, x | Standardized variate |
| $\hat{\chi}^2$ | Chi-square statistic |
| $\tau$ | Time lag |

Subscripts

| | |
|---|---|
| p | Prototype full scale |
| M | Model |

Superscript

| | |
|---|---|
| - | Time average |

# Chapter 1

## INTRODUCTION

Instantaneous local wind pressures on building surfaces result in large forces which have caused a substantial number of glass breakage and cladding failures or dislodgment in recent years. Rational design of glass and cladding which must withstand the effects of rare events such as peak wind pressures requires consideration of the risks involved for any particular choice of design capacity. Given a design, the engineer often wants to estimate the maximum pressure or suction which the design can withstand and seek an estimate of the probability that in a given time period this peak value will be exceeded. Cermak (1975), in "Application of Fluid Mechanics to Wind Engineering--A Freeman Scholar Lecture," has written an extensive review of wind engineering including wind loading of structures. He pointed out that research on the determination of extreme value statistics for pressure fluctuations in regions of separated flow, reattachment and vortex formation is urgently needed. The present work addresses this goal.

Fluctuations in pressure are caused by turbulence in the flow approaching the structure and by flow disturbances generated by the structure itself. The mean wind profile, mean wind speed, turbulence scales and intensities, direction of the approach flow, and the geometry and roughness of the building have significant influence. Because of the random nature of wind direction and amplitude, records of pressure measured on a building surface also indicate a continual random variation. The primary sources of information on wind effects on buildings have been measurements on small-scale models and on actual structures. Quantities of interest are often the mean, the root-mean-square pressure coefficients and the range of the data. The

probabilistic description of pressure fluctuations is achieved through the use of the probability density function (PDF). However, in the study of wind loads, much of the concern is for the extreme loads as indicated before. Since the extremes are rare events, many more data are required to define the main body of the PDFs of the extremes than to define the main body of the PDFs of the parent pressure fluctuations.

In this study, more than 5 million fluctuating pressure data points were obtained from a scale model in a boundary-layer wind tunnel. Local pressure measurements were made at points in regions of impinging, separated flows and vortex formation. The present work provides a theory which attempts to embrace the distinctive features of previous findings on peak wind pressures on buildings. The distribution of all the peaks in sequence is verified to be of extreme value type 1. The effective fluctuation rate $\nu$ is provided by examining the autocorrelation coefficients between peaks at various lag times. This parameter is used with theory to obtain the distribution of the largest peak in a given time period T (at a particular tap), allowing the peak at any desired probability level to be predicted. One important application of the present work is the possibility of recovering the extreme value distribution from typical wind-tunnel pressure study data (e.g. 16 sec. record at 250 Hz). The new theory is also compared with Davenport's (1964) peak value theory and Dalglish's (1979) "spike" theory.

# Chapter 2

## BACKGROUND

Advances in structural materials and architectural concepts have promoted the design and construction of building with increasing slenderness and decreasing structural damping. The use of lighter cladding and more extensive glass areas has also increased in recent years. All of these features produce vulnerability of structure to damage by wind loading. Many failures of various exterior building elements indicate the need of an improved evaluation of local wind loading.

Fluctuating pressures on bluff obstacles in turbulent flows are caused directly by upstream turbulence and the unsteady velocity field produced by the obstacles themselves. Vickery (1966) pointed out that "in both smooth and turbulent flow the fluctuating pressures are sufficiently large to warrent attention in regard to both the dynamic response of a structure and the magnitude of instantaneous local pressures on a face." The local pressure fluctuations, when combined with pressure due to the mean wind, thus produce high instantaneous loading on the surfaces of an obstacle (such as a high-rise building). In wind engineering applications, one is often concerned with the largest value. For cladding design, the mean pressure loading is not adequate. Instead, the gust effects must be taken into account, which means knowledge of peak pressures (maximum pressure or suction) expected to act on the structure during its projected lifetime is essential for rational design of glass and cladding.

Conversion from mean wind speed to mean pressure can easily be achieved through mean pressure coefficients obtained from model tests

in a wind tunnel and/or from full-scale measurements. Determination of wind turbulence effects remains difficult since the local pressure fluctuates in a random manner. Davenport (1961, 1964), in his papers on the buffeting of structures by gusty wind, suggested expressions for estimating the largest instantaneous values occuring during samples of some specific duration of a stationary random function. His analysis was intended to apply to all aspects of a structure subjected to gust loading. This means the stationary random function here could be the turbulent velocity fluctuation, the fluctuating aerodynamic force induced on the structure thereby, or the structure's response in terms of deflection, stress, bending moment, etc. A probability distribution for the maximum peak value expected during a given time period, T, has been obtained by Davenport assuming a stationary Gaussian process. This prediction technique requires the value of the average effective fluctuation rate $\nu$ in peaks per second. The physical interpretation of $\nu$, according to Davenport, is the frequency at which most of the energy in the spectrum is concentrated. He provided an estimate of $\nu$ based on the earlier statistical work of Rice (1944, 1945) using the appropriate moments of the power spectrum of the random process. A so-called "gust factor" was proposed to relate the peak loads to the mean. His definition of a gust factor was the number of rms values by which the peak response exceeds the mean in some specified recurrence period. This gust factor is dependent on the statistical characteristics of wind turbulence, the mean wind speed profile, and the size and dynamic properties of the structure. Vellozzi and Cohen (1968) introduced the gust response factor which is a measure of the effective dynamic load produced by gust, and is intended to translate the dynamic response

phenomena produced by gust loading into simpler static design criteria. The gust loading factor approach is undoubtedly a notable advance in obtaining design pressures in practice. This technique is, in fact, the basis of the wind loading provisions of the American National Standard Building Code ANSI A58.1-1972 (1972). Vickery (1970) determined that "The gust factor relates only to the overall loads in the direction of mean wind. Lateral loads or local pressures are not predictable by the gust factor." It is apparent that the simplified gust factor approach cannot be considered entirely adequate.

Dalgliesh (1971) presented a summary of statistical information derived from actual pressure measurements on a tall building. The maximum peaks observed from all the records were plotted as probability distribution and compared with the theoretical distribution defined by Davenport (1964) for a stationary, Gaussian process. The observed distributions are in good agreement with Davenport's theory for cladding positions on the positive-pressure upwind side of the building. Only one distribution for a negative pressure on the leeward side of the building was reported, and discrepancies occur as the distribution tends to be more widely scattered and centered at higher peak value than the theoretical curve. A rather extensive discussion on the crucial quantity $\nu$ (effective fluctuation rate) was given since it provides useful information for the checking and improvement of theoretical methods for predicting peak pressures. Dalgliesh found that $\nu$ tends to increase with decreasing lengths of record and the actual number of peaks per second is an upper bound for the effective fluctuation rate. Again, he used the gust factor approach: the number of standard deviations from the mean at which the peak pressures fall.

Peterka and Cermak (1975) performed the first systematic and extensive model tests on local pressure fluctuations in a wind tunnel. They suggested that the probability densities of pressure fluctuations fall into two basic classes - one for $Cp_{mean}$ (mean pressure coefficient) > - 0.1 and another for $Cp_{mean}$ < -0.25. Probability densities in the class for $Cp_{mean}$ > -0.1 are nearly Gaussian while those in the class for $Cp_{mean}$ < -0.25 (flow speration regions) are very skew and far from Gaussian. This innovative grouping of the distributions of the fluctuating pressures conveniently summarizes some distinguishing features of the aerodynamic process. An extreme value analysis of peak pressures was also performed. It was found that probability densities for the maximum positive peak pressure in time T for $Cp_{mean}$ > -0.1 agree well with the theoretical prediction by Davenport based on a Guassian pressure fluctuation distribution. However, in regions of high negative pressure ($Cp_{mean}$ < -0.25), probability densities for the maximum negative peak pressure in time T do not agree well with Davenport's theory based on a Gaussian pressure fluctuation distribution. Their results indicate that the statistics of laboratory and field pressure distributions behave in a similar manner. Information about how the parent distribution affects its extreme value distribution was implied by Peterka and Cermak, where concern was centered on the validity of the Gaussian assumption of parent pressure fluctuations. In fact, the approach taken previously to the prediction of largest value distribution can be extended to parent distributions other than Gaussian. Davenport (1976) pointed out that the tails of the distribution of the strong negative pressures are roughly exponential in form. The largest value distribution is then of extreme value

type I. Details concerning type I model of peak pressure distributions will be discussed thoroughly in this thesis.

The probability density functions of the peak pressures in time T obtained by Akins and Cermak (1976) are very similar to those found by Peterka and Cermak (1975). Akins and Cermak reported that, for the pressure fluctuations studied in both stagnation and separated regions, the effective fluctuation rate $\nu$ was approximately 20. A design technique was also suggested by them. They argued that a technique which utilizes the mean and rms pressure coefficient would be more accurate than a procedure which merely recorded the maximum or minimum pressure observed at a particular location. Templin and Cermak (1976) examined the effect of mullions on the local pressure fluctuations on building while Zambrano and Peterka (1978) studied wind loading interaction on an adjacent building. Both groups employed the technique by Peterka and Cermak (1975) to analyze local peak pressures.

Dalgliesh et al. (1979) proposed a method of treating peak pressures based on the fit of an exponential distribution to a population of "significant independent events," called pressure spikes. They resolved the difficulty of applying a Gaussian distribution to the points making up certain time records of fluctuating pressures by arguing that sudden spikes of turbulence are superimposed on a record that is otherwise Gaussian in nature. They aimed at these spikes rather than the entire population of points in the time record. Two rules were provided to determine these spike values which form a new parent population of a negative exponential distribution. The extreme value distribution of peaks, where each peak in the distribution is the maximum spike value from a sampling interval, is then related to the

above negative exponential distribution by one parameter n, the average number of spikes per interval. This distribution was found to provide a good fit to both full-scale and wind tunnel results. A discussion of time scaling was also presented which enables comparison of model and full-scale measurements.

Sockel (1979) fitted pressure fluctuation data with a Kth order Weibull distribution which implies its extreme value distribution is of type I. This is actually in line with Mayne and Cook's (1979) opinion: "... whichever distribution is a correct description of the parent distribution, the extreme value distribution will be type I." Mayne and Cook (1979) also proposed a fully probabilistic design procedure; the design load is formed by the combination of the extreme hourly-mean wind speed with the extreme loading coefficient in that hour of wind.

The present work provides a theory and new data which attempts to embrace the distinctive features of previous findings on peak wind pressures. In the future, progress in the understanding of the phenomena related to peak pressures will depend heavily on experimental investigations. And these experimental investigations should serve as inputs to the modification of existing theoretical results.

# Chapter 3

# THEORETICAL CONSIDERATIONS

## 3.1 General Remarks

The statistical theory of extreme values has, in recent years, been very useful in connection with a variety of applied problems. The largest or smallest order statistics of a sample is often the relevant inference function in engineering applications in statistics. For example, in building aerodynamics, rational design of glass and cladding on structures requires a knowledge of peak pressures expected to act on the structure during its lifetime. The present work attempts to confirm that the cumulative distribution of peak pressures is of type I extreme value distribution. With the knowledge of probability density of largest (or smallest) peaks in a period together with the information regarding distribution of extreme winds, a probabilistic approach can be embodied in the design procedures for wind loading.

## 3.2 Order Statistics

Since we are interested in the minimum and maximum pressures, the need to consider order statistics arises (see Bury, 1975).

If we have $n$ sample values $X_i$, we can rearrange this given set of measurements into an ordered set

$$X_{(1)} \leq X_{(2)} \leq \cdots \leq X_{(r)} \leq \cdots \leq X_{(n)} \tag{3.1}$$

Thus the given observations are relabeled by a subscript in parentheses to indicate their order in magnitude, i.e. $X_{(1)}$ being the smallest measurement and $X_{(n)}$ the largest. The order statistics $X_{(r)}$ are random variables associated with a statistical model (probability density function PDF, $f(x)$ and cumulative distribution function CDF,

$F(x)$, where $F(x) = \int_{-\infty}^{x} f(x)dx$). The order statistics $X_{(1)}$ and $X_{(n)}$ often provide more important information than the mean $\bar{X}$ or some other property of the underlying model $F(x)$. These two order statistics are called the "extreme values" of a set of $n$ measurements.

### 3.3 Exact Models of Order Statistics

Consider the largest sample value $X_{(n)}$ among $n$ independent sample values $X_i$ with model $F(x)$. The distribution of $X_{(n)}$ is obtained as follows (Epstein, 1960):

$$\begin{aligned}\Phi_{(n)}(x;n) &= \text{Prob}\{X_{(n)} \leq x\} \\ &= \text{Prob}\{\text{all } X_i \leq x\} \\ &= \text{Prob}\{X_1 \leq x,\ x_2 \leq x,\ \ldots\ X_n \leq x\} \\ &= [F(x)]^n \end{aligned} \tag{3.2}$$

The PDF of the nth order statistic $X_{(n)}$ is obtained as

$$\phi_{(n)}(x;n) = \frac{d\Phi_{(n)}}{dx} = n[F(x)]^{n-1} f(x) \tag{3.3}$$

Similarly, if the smallest sample value $X_{(1)}$ is larger than a given value $x$, it follows that all sample values $X_i$ must be larger than $x$.

$$\begin{aligned}[1 - \Phi_{(1)}(x;n)] &= \text{Prob}\{X_{(1)} > x\} \\ &= \text{Prob}\{\text{all } x_i > x\} \\ &= \text{Prob}\{X_1 > x,\ X_2 > x,\ \ldots\ X_n > x\} \\ &= [1 - F(x)]^n \\ \therefore\ \Phi_{(1)}(x;n) &= 1 - [1 - F(x)]^n \end{aligned} \tag{3.4}$$

The equivalent PDF of $X_{(1)}$ is

$$\phi_{(1)}(x;n) = n[1 - F(x)]^{n-1} f(x) \tag{3.5}$$

## 3.4 The Type I Extreme Value Model

The sampling model of interst is the distribution of an extreme value in a sample from an underlying, "parent" distribution. When the parent distribution $F(x)$ is known, the exact extreme value models are provided by Eq. (3.2), (3.3) or (3.4), (3.5). When $F(x)$ cannot be specified, asymptotic distributions can be used to model the extreme value of interest. Note that these distribution are valid only for large sample size $n$ of the underlying variable $X$.

Since an extreme value is a rare event, it occurs less frequently than other values of the underlying variable $X$. This large value usually ends up in the tail of $f(x)$. In other words, the nature of the corresponding tail of the parent distribution will affect the distribution of the extreme value more strongly than the bulk of $f(x)$. The type I extreme value model arises from parent distributions that are unlimited in the direction of the extreme value, provided the relevant tail of the parent PDF $f(x)$ falls off in an exponential manner, i.e. $f(x)$ is of exponential type (Gumbel, 1958).

Since for any sample of size $n$ it is true that

$$\min_i \{X_i\} = - \max_i \{-X_i\} \tag{3.6}$$

We shall now focus on the derivation of the asymptotic extreme-value distribution of largest value only. Our interest is in underlying distribution $F(x)$ having an upper tail of the exponential type

$$F(x) = 1 - \exp\{-a(x)\} \tag{3.7}$$

with $a(x)$ an increasing function of $x$. It follows, from this condition, that the normal, log-normal, gamma, and Weibull distributions are of this general type. Only a simplified argument is presented here. The reader is referred to Gumbel (1958) for details. We introduce what is known as the characteristic value $u_n$ of $X_{(n)}$. It is defined to equal that value of $x$ for which

$$F(x) = 1 - \frac{1}{n} \tag{3.8}$$

For the exponential-type case under consideration here, we can write

$$F(u_n) = 1 - \frac{1}{n} = 1 - \exp\{-a(u_n)\}$$

Thus

$$e^{-a(u_n)} = \frac{1}{n}$$

and

$$\frac{1}{n} e^{a(u_n)} = 1 \tag{3.9}$$

Consider now the distribution of $X_{(n)}$, Eq. (3.2):

$$\Phi_{(n)}(x;n) = [F(x)]^n$$

If $n$ is large, $X_{(n)}$ will almost certainly take on values only in the upper tail of the distribution of $X$. Thus in the region of interest

$$\Phi_{(n)}(x;n) = [1 - e^{-a(x)}]^n$$

Using the factor equal to unity [Eq. (3.9)],

$$\Phi_{(n)}(x;n) = [1 - \frac{1}{n} e^{a(u_n)} e^{-a(x)}]^n$$

$$= \{1 - \frac{1}{n} e^{-[a(x) - a(u_n)]}\}^n \tag{3.10}$$

If $x$ is "not far" from $u_n$, then we can replace $a(x)$ by a linear approximation. The Taylor expansion of $a(x)$ about $x = u_n$ gives:

$$a(x) \simeq a(u_n) + \left[\frac{da(x)}{dx}\Big|_{u_n}\right] (x - u_n)$$

$$= a(u_n) + \alpha_n(x - u_n)$$

in which $\alpha_n$ depends only on $n$ and not on $x$. Therefore,

$$a(x) - a(u_n) \simeq \alpha_n (x - u_n)$$

Substituting into Eq. (3.10)

$$\Phi_{(n)}(x;n) \simeq [1 - \frac{1}{n} e^{-\alpha_n(x - u_n)}]^n = (1 - \frac{\beta}{n})^n$$

where $\beta = e^{-\alpha_n(x - u_n)}$. As the size $n$ of the initial sample increases, the nth-order statistic $X_{(n)}$ increases and so does the characteristic value $u_n$. It can therefore be expected that the term $\{a(u_n) - a(x)\}$ (and hence $\beta$) tends to a constant as $n$ grows. Therefore the type I asymptote is written

$$F_{I,max}(x) = \lim_{n\to\infty} \Phi_{(n)}(x;n)$$

$$= \lim_{n\to\infty} (1 - \frac{\beta}{n})^n$$

$$= \lim_{n\to\infty} [1 - \frac{n}{n}\beta + \frac{n(n-1)}{2!n^2}\beta^2 - \ldots]$$

$$= 1 - \beta + \frac{1}{2!}\beta^2 - \frac{1}{3!}\beta^3 \ldots$$

$$= e^{-\beta}$$

Substituting for $\beta$

$$F_{I,max}(x) = \exp\{-\exp[-\alpha_n(x - u_n)]\} \tag{3.11}$$

The quantity $\alpha_n$ is recognized as a scale factor and $u_n$ is a location factor. Expressing these quantities in the notation of this thesis,

$$\alpha_n = \frac{1}{\theta}$$

$$u_n = - \xi$$

The type I asymptotic Eq. (3.11) is then written

$$F_{I,max}(x;\xi,\theta) = \exp[-\exp(\frac{x + \xi}{\theta})] \tag{3.12}$$

The extreme value PDF is obtained by differentiating Eq. (3.12):

$$f_{I,max}(x;\xi,\theta) = - \frac{1}{\theta} \exp[\frac{x + \xi}{\theta} - \exp(\frac{x + \xi}{\theta})] \tag{3.13}$$

The type I asymptote for largest extremes is related to the type I asymptote for smallest extremes as follows:

From Eq. (3.6), we know that

$$\min_i\{X_i\} = - \max_i\{-X_i\} \tag{3.6}$$

Hence the type I asymptote of minimum values is obtained from (3.12) as

$$F_{I,min}(x;\xi,\theta) = 1 - \exp[-\exp(\frac{x + \xi}{\theta})] \tag{3.14}$$

with PDF

$$f_{I,min}(x;\xi,\theta) = \frac{1}{\theta} \exp[\frac{x + \xi}{\theta} - \exp(\frac{x + \xi}{\theta})] \tag{3.15}$$

It is seen that $f_{I,min}(Z_e)$ is the image of $f_{I,max}(Z_e)$ about $Z_e = 0$, where $Z_e = \frac{x + \xi}{\theta}$.

## 3.5 Peak Pressures on Buildings

It has been shown in Sec. 3.4 that the statistics of the parent population points are related to those of extremes. To predict peak wind loading on a structure, Davenport (1964) has provided a peak value theory for wind loads based on the assumption of a Gaussian pressure distribution. If the parent population is Gaussian, a type I double exponential distribution has been shown to apply to peak pressures on windward faces of a building (Peterka and Cermak, 1975; and Dalgliesh, 1971). Extensive model studies in wind tunnels by Peterka and Cermak have shown that the forms of the PDFs fall into two basic classes, one for direct "impinging" and the other for "separated" flows. The densities in the former class are nearly Gaussian (but not necessarily, see Chapter 6), yet the densities for the latter class are highly skewed. This thus explained why predictions based on the Gaussian assumption for separated regions fall far short of observations.

Nevertheless, it is reasonable to believe that both classes meet the necessary requirements for the distributions of the positive-going and the negative-going extremes to be of the type I form (Peterka, personal communication, 1979). The cumulative density function of peaks in sequence (see Chapter 5 for details), q(x), has the form (Peterka, personal communication, 1979)

$$q(x) = \int_{-\infty}^{x} p(x)\,dx = \begin{cases} \exp[-\exp(\frac{x+\xi}{\theta})] & \text{for positive peaks} \quad (3.16) \\ 1 - \exp[-\exp(\frac{x+\xi}{\theta})] & \text{for negative peaks} \quad (3.17) \end{cases}$$

where

$p(x)$ = probability density function of peaks

$\xi, \theta$ = empirical location and scaling factors;

$\xi,\theta$ can be selected by "least-squares" fit of experimental data.

Then

$$p(x) = \frac{dq(x)}{dx} = \begin{cases} -\frac{1}{\theta}\exp[\frac{x+\xi}{\theta} - \exp(\frac{x+\xi}{\theta})] & \text{for positive peaks} \quad (3.18) \\ \frac{1}{\theta}\exp[\frac{x+\xi}{\theta} - \exp(\frac{x+\xi}{\theta})] & \text{for negative peaks} \quad (3.19) \end{cases}$$

But in the peak loading problem, we are not primarily concerned with the distribution of all the peaks, but only with the largest (or smallest) of these in a period of time T.

If the peaks are independent, then the probability density function of largest peak in time T, P(x), is given by

$$P(x) = \frac{dQ(x)}{dx} = \frac{d[q(x)]^N}{dx} = N[q(x)]^{N-1}\, p(x) \qquad (3.20)$$

where

Q(x) = cumulative distribution of largest peak in time T

N = number of independent peaks in time T

= $\nu$T

And $\nu$ is the effective fluctuation rate, number of independent peaks per unit time.

$$\begin{aligned} Q(x) &= [q(x)]^N \\ &= \exp[-N\exp(\frac{x+\xi}{\theta})] \\ &= \exp\{-\exp[\frac{x+(\xi+\theta\,\ell n\,N)}{\theta}]\} \end{aligned} \qquad (3.21)$$

The largest observation Q(x) has also a type I model, with location shifted by the factor $\theta\ \ell n\ N$, the scale parameter $\theta$ being unchanged.

The model Eq. (3.17) also features a reproductive property. That is, the smallest extreme value from the model Eq. (3.17) has the exact

distribution with Eq. (3.17) being shifted to the left by amount $\theta \ell n N$.

Note the expressions (3.20) and (3.21) are valid for all $N$ not for large $N$ only. A problem arises as to how to determine $N$, and thus $\nu$ in a given time $T$. The effective fluctuation rate, $\nu$, varies with frequency response of the measurement system and is not an easily measured quantity. A new mechanism was proposed to find $\nu$ in this thesis. It was achieved by examining the autocorrelation coefficients between peaks for various lag times (Peterka, 1979). Details concerning the new method will be discussed in Section 3, Chapter 6.

# Chapter 4

# EXPERIMENTAL APPARATUS AND PROCEDURES

## 4.1 General

The intention of this study was to determine extreme value statistics for surface pressure fluctuations on structures. During the past decade, wind tunnels capable of modeling the wind forces on structures have been developed (Cermak, 1958) and there is a growing confidence that careful simulation of the flow field and the near-by structures will produce pressure fluctuations that accurately model the full-scale situation (Dalgliesh, 1975). With the versatility of modern high speed digital computers, large amounts of data at various locations on a model (structure) subjected to many wind directions can be obtained to facilitate an extensive analysis of peak wind pressures on buildings. The data analyzed in this thesis originated from a wind engineering study (Peterka and Cermak, 1979) of a preliminary design of the Mountain Bell Utah State Headquarters Building, Salt Lake City, Utah (Fig. 4.2). The wind-tunnel test was performed in the Meteorological Wind Tunnel in the Fluid Dynamics and Diffusion Laboratory at Colorado State University, Fort Collins, Colorado. Measurements of a different test building were made in the Industrial Aerodynamics Wind Tunnel in order to check the consistency of the data obtained.

## 4.2 Scaling Requirements

### Physical Modeling

Modeling the aerodynamic loading on a structure requires special consideration of flow conditions in order to produce similitude between model and prototype. Cermak (1975) detailed the similarity requirements and their wind tunnel implementation. In summary the requirements may be stated as follows:

(1) Undistorted scaling of boundary geometry (geometric similarity).

(2) Kinametric similarity of approach flow (distributions of mean velocity and turbulence characteristics).

(3) Reynolds number equality.

These criteria are satisfied by constructing a scale model of the structure and its surroundings and performing the model studies in wind tunnels specially designed to model the important characteristics of atmospheric boundary layer flows. Reynolds number constancy requires that the quantity $\frac{UD\rho}{\mu}$ be similar for model and prototype. If the same fluid is used (the kinematic viscosity, $\frac{\mu}{\rho}$ , is identical for both), Reynolds number can not be made precisely equal with reasonable wind velocities. Wind velocity in the wind tunnel would have to be the model scale factor times the prototype wind. Such a value is well above the velocity of sound in air and can result in appreciable effects of compressibility. To compensate for this apparent dilemma is the circumstance that duplication of prototype Reynolds number for sharp-edged bluff bodies is not directly necessary. In fact, for sufficiently high Reynolds number ($> 2 \times 10^4$) a pressure coefficient at any location on the building will essentially be constant with Reynolds number if the model is characterized by sharp corners. Typical values encountered are $10^7$ to $10^8$ for the full-scale and $10^5$ to $10^6$ for the wind tunnel model. Thus acceptable flow similarity is achieved without precise Reynolds number equality.

Time Scaling

Time scaling is essential to relate peak pressures on the model to those in full-scale situation. The concept of the reduced velocity is

frequently applied to time scaling (Akins, 1976). This dimensionless parameter is, in fact, the reciprocal of the Strouhal number. The equality required in the model and prototype is given by:

$$\left(\frac{\bar{U}}{n_o D}\right)_M = \left(\frac{\bar{U}}{n_o D}\right)_p \tag{4.1}$$

where $\bar{U}$ is the mean velocity of wind, $n_o$ is a characteristic frequency, and $D$ is an appropriate dimension of the building under consideration. Equation (4.1) can be rearranged to

$$T_M = \left(\frac{\bar{U}_p}{\bar{U}_M}\right)\left(\frac{D_M}{D_p}\right) T_p \tag{4.2}$$

since $n_o = \frac{1}{T}$. For a fixed geometric scale and velocity ratio, Eq. (4.2) can be used to obtain a time scaling.

As shown in Chapter 3, theoretical analysis of extreme value statistics requires a knowledge of the number of independent peaks in time $T$, $\nu T$, where $\nu$ is the effective fluctuation rate. The use of a nondimensional wavenumber leads to a scaling for $\nu$

$$\left(\frac{\nu D}{\bar{U}}\right)_M = \left(\frac{\nu D}{\bar{U}}\right)_p \tag{4.3}$$

or

$$\nu_M = \left(\frac{\bar{U}_M}{\bar{U}_p}\right)\left(\frac{D_p}{D_M}\right) \nu_p \ . \tag{4.4}$$

This scaling together with Eq. (4.2) gives the relationship

$$(\nu T)_M = (\nu T)_p \ . \tag{4.5}$$

With a time scaling factor established, the wind-tunnel measurements of pressure fluctuation rates can be compared with available full-scale measurements.

## 4.3 Wind Tunnels

Measurements of the Utah Mountain Bell Building were made in the Meteorological Wind Tunnel located in the Fluid Dynamics and Diffusion Laboratory of Colorado State University, Fort Collins, Colorado. A schematic of the tunnel is shown in Fig. 4.1. This is a closed-circuit type wind tunnel with a 9 to 1 contraction ratio driven by a 250 hp variable-pitch, variable-speed propeller. The available velocity in the test section ranges from 0.3 to 37 mps (1 to 120 fps). All of the data reported in this thesis were taken at a free stream velocity of 16 mps (50 fps) measured at the top of the boundary-layer. This velocity is well above that required to ensure Reynolds number similarity between the model and prototype as discussed in Sec. 4.2. The ceiling of the wind tunnel is adjustable to maintain a zero pressure gradient in the vicinity of the model.

The long test section in conjunction with spires, barriers and roughness elements were used to develop the proper approach mean velocity and turbulence characteristics. Descriptions of this type of approach to obtain thick boundary layers have been provided by Cermak (1976). The velocity profile developed had a mean profile following a power-law of the form

$$\frac{\bar{U}(Z)}{\bar{U}(\delta)} = \left(\frac{Z}{\delta}\right)^{n} \tag{4.6}$$

where $\bar{U}(Z)$ and $\bar{U}(\delta)$ are the mean velocities at an arbitrary height, $Z$, and at the top of the boundary layer, $\delta$ respectively. The exponent $n$ is an indication of terrian roughness upstream of the modeled area. For this study $n$ had a value of 0.24--which would be classified as suburban or type B exposure as designated by the ANSI Standard (1972).

Mean velocity and turbulence intensity profiles were measured upstream of the model and are shown in Fig. 4.3. The turbulence intensity is defined as the root-mean-square (about the mean) of the longitudinal velocity fluctuations divided by the local mean velocity $\bar{U}(Z)$,

$$T_u = \frac{U_{rms}(Z)}{\bar{U}(Z)} \tag{4.7}$$

Properties of the wind tunnel boundary layer, such as velocity spectra, autocorrelation function and coherence function are reported by Akins and Cermak (1976). The reader is referred to this report for a more complete discussion of simulation of boundary layers.

## 4.4 The Model

The Mountain Bell Building was modeled along with a region of the city with 300 m (985 ft) radius centered at Mountain Bell Building. The model was constructed to the scale of 1:200 to give the largest possible size that did not produce significant blockage in the wind tunnel test section. The model was built of 0.013 m (1/2 in.) thick Lucite plastic and fastened together by metal screws. The surrounding buildings were built of styrofoam. The completed model is shown in Fig. 4.2.

To measure pressures, holes were drilled in the model 0.0016 m (1/16 in.) in diameter normal to the plastic surface. A brass tube with inside diameter of 0.0016 m was connected to each pressure tap with the tube extending into the interior of building. Flexible "Tygon" tubing (0.0016 m ID, 0.003 m OD) was used to connect each tap directly to a pressure transducer. The tube length is 0.013 m. The dimensions and the locations of the taps on the building are shown in Fig. 4.4.

The model was mounted on a turntable at the downstream end of the test section. The turntable was supported by a large inertial mass to

isolate the model from any vibrations in the wind tunnel. The wind directions were measured clockwise from true north. The reference for the azimuth was set using an optical alignment technique. Other building orientations could be set using a graduated scale located on the base of the turntable. The scale is readable to within 0.25 degree.

Details concerning the experimental configuration of this study can be found in the "Wind-Tunnel Study of Mountain Bell Utah State Headquarters Building, Salt Lake City" by Peterka and Cermak (1979).

## 4.5 Pressure Measurements

Fluctuating pressure data used for study in this thesis were obtained from selected pressure taps on the model building. The instantaneous pressure was transmitted through a very short tube length (0.013 m) to the positive sides of one differential pressure transducer. The negative or reference side of the transducer was connected to the static side of Pitot-static tube located directly above the model at the top of the boundary layer. In this way, the transducer measured the instantaneous difference between the local pressures on the surface of the building and the static pressure in the free stream above the model. The fluctuating signal from the transducer was fed to a high-speed digital data-acquisition system. A block diagram of the system is shown in Fig. 4.5. The digital technique and data processing procedure will be discussed in more detail in Chapter 5 titled "Data Acquisition, Processing and Reduction." Note that in this study, pressure measurement was made at each tap at a time.

The pressure transducer used was a Setra Low Range Pressure Transducer (Model 237) with 0.1 psi range. It was selected because of its favorable signal-to-noise ratio and linearity in the required

working range. The transducer was calibrated to yield a calibration factor which converted the voltage signal into physical units (psi). The calibration is linear and repeatable to within 0.5 percent.

# Chapter 5

# DATA ACQUISITION, PROCESSING AND REDUCTION

## 5.1 Digital Techniques

Before the continuous time series of the fluctuating voltages can be converted into a discrete digital time series, the digitizing sample rate must be considered. Sampling at points which are too close together will yield correlated and highly redundant data, and thus unnecessarily increase the time and cost of calculations. In contrast, sampling at points which are too far apart will cause higher frequency components to be "folded" at lower frequencies. (Bendat and Piersol, 1971 have a more detailed description of concepts discussed in this section). In this case, misrepresentation and improper conclusions about the original data may result. One practical method exists for handling this aliasing problem, i.e. to select the sample rate to be at least two times greater than the maximum anticipated frequency in the original data. Previous studies in pressure fluctuations on buildings indicate that most of the energy content is associated with frequencies less than 100 Hz. The data, then, were digitized at 250 samples per second so that all significant information was obtained for the probabilistic study. However, since the frequency response of the pressure measurement system in this study is sufficiently high (over 500 Hz), data were then taken at a sample rate of 1000 Hz in situations where power spectra were to be measured. Because the energy content of fluctuating pressures were much less than the frequency response of the transducer, no influence of transducer frequency response on results was expected.

A sophisticated digital-data-acquisition system at the Fluid Dynamics and Diffusion Laboratory at Colorado State University was used

for the pressure measurements. The analog-to-digital (A/D) convertor (Preston Scientific GMAD-4), Hewlett-Packard-1000 computer, disk unit, and Digi-Data digital tape drive are an integrated system. An operator can control the system through a teletype. The data-taking program sampled from the A/D on one channel and saved time series segments of length 16,384 ($2^{14}$) on the 9-track magnetic tape for transfer to the Cyber 172 for later analysis. Each segment of 16,384 data was broken into 4 tape-records of 4,096 ($2^{12}$) although the 16,384 points constitute a continuous time series. This is expecially helpful when the spectral density estimation by digital means is to be computed by the Cooley-Tunkey Fast-Fourier Transform (FFT) method (Akins and Peterka, 1975).

Seven representative pressure taps on the wind tunnel models, subjected to various wind directions, were selected. Each was sampled at 1000 Hz for 4 minutes (16 segments, each of 16,384 points) for spectral analysis; while data for probabilistic study were obtained by sampling at 250 Hz for 25 minutes (24 segments, each of 16,384 points) for each tap. The long record of pressure fluctuations provided an acceptably large sample of peaks for determination of extreme value distribution as will be discussed later.

## 5.2 Basic Data Processing and Reduction

The raw data on digital tapes obtained from the A/D converter consisted of 16-bit binary words representing the continuous pressure-transducer voltages. These 16-bit binary words (from HP-1000) were then transformed into 60-bit binary words (Cyber 172) by byte manipulation routines (CSU Computer User's Manual, 1976). Special attention must be given to the feature of representing negative numbers in the

HP-1000 16-bit binary. Those numbers which are greater than 32767 ($2^{15}$-1) are actually negative numbers and the value 65535 ($2^{16}$-1) must be subtracted from them to determine correct original values. All the digital data in this study were processed using the Cyber 172 at the Computer Center of Colorado State University.

The digital tape contained a record of a voltage signal e[t] in a discrete form, consisting of N values obtained by sampling at intervals of $\Delta t$. The total length of record in seconds, T, is then equal to $N\Delta T$. The first step in data reduction was to convert the voltage signal into physical units of pressure. The use of linear pressure transducers makes this operation a simple multiplication. The discrete form of the record in physical units was expressed as $P_i$. The sample mean value, $\bar{P}$, the variance, $\sigma_P^2$, and the coefficient of skewness, S{P}, are computed in the usual manner; thus for large sample size, N

$$\bar{P} = \frac{1}{N} \sum_{i=1}^{N} P_i$$

$$\sigma_P^2 = \frac{1}{N} \sum_{i=1}^{N} (P_i - \bar{P})^2 \qquad (5.1)$$

$$S\{P\} = \frac{1}{N} \sum_{i=1} (P_i - \bar{P})^3 / \sigma_P^3$$

Non-dimensional pressure coefficients, Cp, were obtained from the surface pressures on the models. The mean, rms, peak maximum, and peak minimum pressure coefficients are defined as follows:

$$Cp_{mean} = \frac{\overline{(P_i - P_{static})}}{\frac{1}{2}\rho\{\bar{U}(\delta)\}^2} \tag{5.2}$$

$$Cp_{rms} = \frac{\overline{\{(P_i - P_{static}) - \overline{(P_i - P_{static})}\}^2}^{1/2}}{\frac{1}{2}\rho\{\bar{U}(\delta)\}^2}$$

$$Cp_{max} = \frac{(P_i - P_{static})_{max}}{\frac{1}{2}\rho\{\bar{U}(\delta)\}^2} \quad \text{maximum in record}$$

$$Cp_{min} = \frac{(P_i - P_{static})_{min}}{\frac{1}{2}\rho\{\bar{U}(\delta)\}^2} \quad \text{minimum in record}$$

The data records used in obtaining these coefficients were taken at a sample rate of 250 Hz for a period of 16.38 sec. (Peterka and Cermak, 1979). These coefficients will descirbe the general characteristics of pressure taps chosen in this study.

The probability density function (PDF) can be defined for the midpoint of the ith bin for K bins over the data range [a,b] as

$$\hat{f}_i(\eta) = \frac{Prob[d_{i-1} < \eta \leq d_i]}{w} = \left(\frac{N_i}{N}\right)\left(\frac{K}{b-a}\right) \quad i = 1, 2, \ldots K \tag{5.3}$$

where $\eta = \dfrac{Cp - Cp_{mean}}{Cp_{rms}}$, the reduced variate

$w = (b-a)/K$, the width of each bin

$N$ = sample size

$d_i = a + iW$, and

$N_i$ = number of $\eta$ such that $d_{i-1} < \eta \leq d_i$.

The PDF for parent distributions of pressure fluctuations on the structure were calculated for each tap location using 64 bins to

subdivide the range of fluctuations. Each distribution consisted of 16,384 data samples.

The power spectral density function, which describes the frequency composition of the data in terms of the contributions of the fluctuations at a given frequency to the variance of the signal, was computed directly from the data records using Fast-Fourier Transform techniques. The programs used in the data analysis of this thesis and a detailed description of their use has been discussed by Akins and Peterka (1975).

## 5.3 Treatments of Peak Pressures

The probability density function of all peaks in sequence for each pressure tap was constructed. These peaks are actually "relative" extrema (relative maxima or minima) in the time series. Figure 5.1 shows how these peaks were selected according to the "screening" technique. The local extremum must be, at least, 2 analog-digital steps (~.0096 volt) away from its two neighboring points to avoid A/D noise. Distributions of this kind are referred to as "probability density of continuous peaks" $p(\eta)$. The cumulative probabilities of peak distributions $q(\eta)$ were also calculated. The cumulative distribution function (CDF) is the probability that the value of $\eta$ will not exceed a certain value. It is the integral of the probability density function from $-\infty$ to $\eta$. In our case,

$$q(\eta) = \int_{-\infty}^{\eta} p(\eta)\, d\eta \tag{5.4}$$

Each peak distribution consisted of 10,000 peaks selected from 24 segments, each 16,384 data points long. The task was then to fit these peak distributions $q(\eta)$ (CDF) by type I extreme value distributions,

$$q_{max}(\eta) = \exp\{-\exp(\frac{\eta + \xi}{\theta})\} \quad \text{for maximum} \tag{5.5}$$

$$q_{min}(\eta) = 1 - \exp\{-\exp(\frac{\eta + \xi}{\theta})\} \quad \text{for minimum} \tag{5.6}$$

The parameters used in the assumed theoretical distribution were determined by least-squares fit of the observed values. A multiple correlation coefficient indicates how good the fit is. While at the same time, the chi-square goodness of fit test was used to test the null hypothesis that the observed probability density function and the assumed theoretical density function are the same. The chi-square statistic for K class intervals is

$$\hat{\chi}^2 = \sum_{i=1}^{K} \frac{(f_i - F)^2}{F} = \text{sum of normalized squared deviations} \tag{5.7}$$

where $f_i$ = the observed frequency in the ith bin and F = the expected frequency of the theoretical distribution. The number of degrees of freedom of the chi-square, $\chi^2$, distribution is (K-1) minus the number of parameters of the assumed distribution.

The probability density for largest (or smallest) peak in time T was obtained for each tap location. Since the extremes are rare events, many more data are required to define the main body of the PDFs of extremes than to define the main body of the PDFs of the parent variate. The long record mentioned above (24 segments, each of 16,384 data points) provided 288 5-sec sampling intervals. Each sampling interval provides only one maximum/minimum. The extreme value distribution applies to a collection of maxima/minima derived from many such intervals. These distributions for the largest peak in time T were presented in hystograms. Note that these hystograms of extreme pressures

were developed from only one tap at a time, not from groupings of two or more taps. This will give us some understanding about extreme value distributions of pressure taps under different approach wind conditions.

A value of $\nu$, the number of independent peaks per unit time, was required to obtain the theoretical extreme value distribution. A new mechanism was proposed to form $\nu$. It was achieved by examining the autocorrelation coefficients between peaks for various lag times. Details concerning the new scheme will be discussed again in Chapter 6 when the data are examined and interpreted.

## 5.4 Accuracy and Repeatability

The overall accuracy of experimental measurements can be obtained by considering each instrument involved in the measurements. However, in wind-tunnel tests many factors in addition to the accuracy of each individual instrument are involved in the overall accuracy of the final measurement. As shown by Akins (1976), in order to include all relevant factors in an assessment of the accuracy of a measurement, the repeatability of each measurement serves as a more reliastic measure of the quality of the measurement even though this is not a measure of the absolute accuracy of each measurement.

A total of five repeatability checks were conducted for the pressure measurements. It was found that consistency exists among these measurements. No significant differences were observed.

# Chapter 6

# RESULTS AND DISCUSSION

Over five million pressure fluctuation data were recorded during the course of this thesis study. This huge amount of data could only be obtained and examined by taking advantage of the high speed and versatility of a digital computer. Much attention has been given to the statistical aspects of experimental design and data evaluation. A computer software package was developed for the acquisition and reduction of fluctuating pressures on buildings in regions of impinging, separated flows and vortex formation. The first section of this chapter presents mean, rms, maximum and minimum pressure coefficients of all pressure taps selected. Parent pressure distributions are discussed in the second section. We then transfer our attention from parent loading coefficients to their extremes. An extensive extreme value analysis of peak wind pressures on buildings is performed in the third section. The last section examines some implications of the findings relative to the wind tunnel model study and to the probabilistic approach of design pressures.

## 6.1 Pressure Coefficients

Figure 6.1 shows the mean and the rms of surface pressure fluctuations as well as the associated maximum and minimum of five pressure taps selected for the peak wind pressures study. Each pressure tap was sampled at 250 samples/second for a total of 4080 samples (16 sec. data). The maximum (or the minimum) pressure coefficient refers to the largest (or the smallest) Cp value in the 4080 data samples.

Each tap, which subjected to one specific wind direction, is in certain region of the flow around the tall building. For instance, Tap 116 is in the stagnation zone where the wind direction is zero degree relative to the true north. This is the case with wind direction normal to the upwind face. High mean pressure coefficient can be expected. We term the phenomenon "strong positive." Tap 417 lies in the impinging region with flow direction slightly oblique to the upwind face (WD = 165°). Tap 613 is very close to the corner of the building where speration occurs. This results in a stronger negative $Cp_{mean}$ value than that of Tap 419, which is downstream in the separated region. On top of the flat roof of the building lies Tap 701 where the effect of vortex formation is evident. The ambient flow direction is 30° relative to the south wall of the right angle corner. A very low (strong negative) mean pressure coefficient was found and is consistent with previous research findings (see, for example, Ostrowski et al., 1967). Illustration of typical flow pattern around a tall building in a boundary-layer flow is shown in Figure 6.2a. Figure 6.2b demonstrates the effect of vortex formation on the mean pressure distribution over a flat-roof building. Attention on the mean pressure coefficient and its possible related flow region should be emphasized.

## 6.2 Parent Distributions of Pressure Fluctuations

The most important function for the probabilistic description of a variate is the probability density function (PDF). The PDF's for parent distributions of pressure fluctuations on the structure were calculated for each tap location using 64 bins to subdivide the range of flucutation amplitudes. Each distribution consisted of 16,384 data samples at a sample rate 250 samples/second.

Test for stationarity of data must be made before one can actually perform the probabilistic analysis of fluctuating pressures. It was found in this study that the pressure flucutation process is stationary at least in the mean (first moment) and the rms (second moment). The sampling record of each pressure tap was broken up into sixteen successive short time intervals (16.4 sec at 250 s/s). The mean and rms of each interval were computed for all tap locations. The ensemble averaged properties of each tap computed over these intervals do not vary significantly from one interval to another. Typical results (obtained from Tap 116) are shown in Table 6.1. The data were then normalized in the usual way by extraction of the mean and division by the rms, ready for the probabilistic analysis.

The distributions were found to fall into two distinct categories: (1) those associated with direct wind impingement on the structure with positive mean pressure coefficients; and (2) those associated with separated and vortex formation regions with negative pressure coefficients. Figure 6.3 shows the probability density associated with the positive $Cp_{mean}$. These distributions are skewed to the right, contrary to the general belief that local pressures on the upwind face of the structure follow a Gaussian distribution. The PDF of Tap 417 is almost Gaussian, yet a close visual examination reveals the fact that its positive tail extends more than a normal distribution would predict. This phenomenon is much more pronounced for the case of Tap 116, which was termed "strong positive" in the previous section. In order to determine the extent to which the frequency of large positive values exceeds the normal distribution, probability for the positive side of the distribution was plotted on a logarithmic scale (Figure 6.4).

Deviations from the Gaussian distribution, at the tail, are evident, especially for Tap 116. The probability of a pressure at the 3.5 standard deviation level is 2 to 5 times that predicted by a normal distribution. The higher peaks of both distributions near zero were found shifted slightly to the negative side. This implies that, in the regions of the structure exposed to impinging flow, the pressure would be close to its mean value and also positive more frequently than would be predicted by a Gaussian distribution.

Two parameters prove to be helpful in understanding the nature of pressure distributions, i.e., the mean pressure coefficient ($Cp_{mean}$) and the coefficient of skewness of pressure fluctuation signals (S{P} as defined in Section 2, Chapter 5). For the strong positive case (Tap 116 with $Cp_{mean}$ = 0.442 and S{P} = 0.423), the positive tail deviates more from a normal distribution than the relatively moderate case (Tap 417 with $Cp_{mean}$ = 0.407 and S{P} = 0.285). It is, perhaps, more beneficial to focus attention on the skewness coefficient S{P} since it indicates the preferred direction of fluctuation. For a positive skewed random signal, the areas above and below the mean are equal, but the positive amplitudes are greater than the negative perturbations. With a higher S{P} value (= 0.423), the distribution of Tap 117 is more skewed to the right than the distribution of Tap 417 whose S{P} value equals 0.285. In other words, the distribution of pressure fluctuations can be thought of as nearly Gaussian as long as its corresponding $Cp_{mean}$ and S{P} values are comparatively small. For pressure fluctuation process, intermittent bursts of turbulence might explain the occurrence of strong spikes of pressure. A higher S{P} value tends to indicate more spikes will occur. These spikes, because

of their large values, end up in the tail of the probability distribution and usually this tail is the only part of the distribution which is not Gaussian. The tail of the distribution is, of course, the only part that is of interest for extreme value analysis.

The same argument applies as well to the distribution associated with negative mean pressure coefficient. On faces where the flow is completely separated (including the separated regions over building roof), the mean pressures are negative and intensive vortex motions are generated within these areas. Very strong negative spikes of pressure can be expected. It should not be surprising that the distributions of pressure fluctuations in the separated regions are highly skewed to the left as shown in Figure 6.5. Significant deviations from the Gaussian distribution are evident immediately. The most important deviation occurs on the negative tail of the curve. Large numbers of points are past 5 standard deviations from the mean indicating a much higher probability for values in this region than a normal distribution would predict. For comparison purposes, distributions are again displayed on a logarithmic scale (Figure 6.6). The severe deviation case goes to Tap 701, which is in the vortex formation region, with $Cp_{mean}$ = -0.813 and an S{P} value as low as -0.983 as compared with -0.616 for Tap 417 and -0.257 for Tap 613. Note deviation from normality is more eminent for negative $Cp_{mean}$ tail than for positive $Cp_{mean}$ tail. The probability of a negative pressure at 4 standard deviation level is 10 to 20 times the predicted value by a normal distribution. This information is particularly significant since the dominant loads on a structure's cladding or glass are usually due to the negative pressures in sensitive areas of the structure near corners and roof lines. Results

concerning distributions in the separated regions are in agreement with the findings of Peterka and Cermak (1975). The reader is referred to their report for details.

In order to check the consistency of results obtained above, an alternative building was tested in the Industrial Aerodynamics Wind Tunnel in the Fluid Dynamics and Diffusion Laboratory, Colorado State University. A schematic diagram of the tunnel is shown in Figure 6.7. Functionally speaking, this tunnel does not differ from the Meteorological Wind Tunnel, which was used for the measurements of the Mountain Bell Utah Headquarters Building. Two taps were selected: one is in the direct wind impinging region, the other separated region. The Setra Low Range Pressure Transducer was flushly mounted (without the 0.013 m short tubing). The same testing procedures were followed. Results from this alternate building show excellent consistency with those from the Mountain Bell Utah Building as can be seen from Figures 6.4 and 6.6. The alternate building was placed in an urban environment but without any tall structures immediately upstream. The mean velocity profile developed has an exponent $n = 0.4$, while the turbulence intensity at the ground level is approximately 35%.

Based on the above study, it may be concluded that the distribution of pressure fluctuations throughout the direct impinging region on the structure is skewed to the right, while the distribution of pressure fluctuations throughout the separated region on the structure is skewed to the left. The probability of large negative pressures is orders of magnitude larger than a prediction based on a normal distribution. For large positive pressures, however, the deviation from a normal distribution is less pronounced and usually can be

neglected. The assumption that pressures on windward faces of a building follow a Gaussian distribution thus seems natural and appropriate. Two parameters, namely, the mean pressure coefficent ($Cp_{mean}$) and the coefficient of skewness of pressure fluctuations (S{P}) are believed to summarily describe the nature of local pressure fluctuations at certain location of a building.

## 6.3 Extreme Value Analysis and Estimates of Average Effective Fluctuation Rates

The peak pressures were picked sequentially from the fluctuation time series at each pressure tap. These peaks in sequence, called continuous peaks, are actually relative extrema (local maxima or minima) in the time series. Figure 5.1 shows how these peaks were screened out. The eligible extremum was chosen to be 2 analog-digital steps (>0.0096 volts) away from its two neighboring points (one on the right and the other on the left). Later study showed that screening with 0.5 analog-digital steps (>0.0024 volts) yielded essentially same results. This can easily be understood by considering the quantization operation of digitizers. Since the magnitude of each data sample is expressed by some fixed number of digits, only a fixed set of levels are available for approximating the infinite number of levels in the continuous data. If the quantization is done properly (which is the case of this study), the true level is approximated by the quantizing level closest to it. Screening with 0.5 A/D steps is equivalent to screening with 1 A/D step. And if the number of levels is large enough, screening with 1 A/D step doesn't make much difference from screening with 2 A/D steps.

A long record of pressure flucutations at each tap is available for the collection of the continuous peaks. Each long record, sampled at a rate of 250 samples/second, consists of 24 segments of data. Each segment has 4 records and one record comprises 4,096 data points. The first 10,000 continuous peaks were picked up from each long record to construct CDF and PDF of fluctuating pressures for the corresponding tap. The CDF's from these experimental data are expressed in terms of dotted lines, shown in Figures 6.7a, c, e, g and i. Similarly, the PDF's are given in Figures 6.7b, d, f, h and j. The dotted lines are adopted merely as symbols to express curves, that is to say, each dot does not necessarily represent the calculated result of experimental data. One word worth mentioning here is that approximately 10 records of data provide 10,000 continuous peaks. We can say that, on the average, each record (4,096 data points) gives 1,000 continuous peaks. This is of particular interest if the distribution of these 1,000 continuous peaks does not differ significantly from that of 10,000 continuous peaks. This clue leads to the possibility of recovering the extreme value distribution from the regular wind-tunnel pressure study data. Refer to Section 6.4i for detailed discussion.

In Chapter 3, recall that the statistics of the parent population of points in the sampling intervals are related to those of the extremes (continuous peaks in this case). An expression for the distribution of continuous peaks can be derived from the parent population. If the tail of interest of the parent distribution is of exponential type, a type I double exponential distribution has been shown to apply to peaks. The CDF of peaks in sequence, $q(x)$, has the form (see Section 5, Chapter 3)

$$q(x) = \int_{-\infty}^{x} p(x)dx = \begin{cases} \exp[-\exp(\frac{x+\xi}{\theta})] & \text{for positive peaks} \quad (3.16) \\ 1 - \exp[-\exp(\frac{x+\xi}{\theta})] & \text{for negative peaks} \quad (3.17) \end{cases}$$

where $x$ = standardized variate

$p(x)$ = PDF of continuous peaks

$\xi$, $\theta$ = empirical location and scaling factors.

Values of the distribution parameters $\xi$ and $\theta$ are obtained by least-squares fit.

The least-squares fit employed in this study is simply the search for the best linear function to predict the sample data by regression method. The method consists of plotting the magnitude of the extreme against the so-called "Gumbel's reduced variate" $y$, estimated from

$$y = \ell n[-\ell n\, q(x)] = \frac{x+\xi}{\theta} \text{ (shown for positive case only)}$$

This has the effect of transforming the Type I CDF given by

$$q(x) = e^{-e^{\frac{x+\xi}{\theta}}}$$

to a straight line. Values of the distribution parameters $\xi$ and $\theta$ are then obtained by fitting a straight line through the plotted points. The fitted Type I distribution results are shown, in solid lines, in Figure 6.7 for each pressure tap selected. A multiple correlation coefficient ($R^2$) for each fit is also obtained to indicate how good the fit is. For every fit, the corresponding coefficient is well above 0.98. This means each least-squares fit is statistically significant. Visual examination of the plots in Figure 6.7 may also help judge the goodness of fit. The "best" fit observed goes to Tap

701 (in the vortex formation region of the building) with fitted and experimental results almost undistinguishable. However, result from chi-square goodness of fit test for each fit (with Tap 701 an exception) suggests the hypothesis that the observed PDF and the assumed theoretical PDF are the same be rejected. Chi-square test result for Tap 701 is shown in Table 6.2. It indicates that the model be accepted. While on the other hand, it is not even necessary to carry out the whole calculation process as what was done in Table 6.2 to show the rejection of the model for other taps. Take Tap 419 for example. Sum of normalized squared deviations of only 2 class intervals around the mode (PDF) yields very large a number already $[(1039-1175.5)^2/1175.5 + (931-1189.5)^2/1189.5 = 72]$. Possible explanation for failure to accept the model may attribute to the sample size used. It should be attended that 10,000 observations were used for each curve fitting. The $\chi^2$ test under this circumstance may be mathematically insignificant but the fit is physically meaningful.

Based on the finding in Figure 6.7, it is thus concluded that the distribution of continuous peaks of pressure fluctuations is of the Type I form. As was proved in Chapter 3, this Type I property for extremes holds no matter what type of parent distribution it might be as long as its tail of interest is of exponential type. The finding is believed to be the first successful attempt to prove the distributions of the positive-going and the negative-going pressure extremes to be of Type I form through wind-tunnel model test.

The distribution of continuous peak pressures at a point, q(x), has been obtained. However, in the gust loading problem, we are not primarily concerned with the distribution of all the maxima/minima,

only with the largest/smallest of these which occurs in a period of time T. Consider, for instance, a sample of N independent maxima in time T, the PDF P(x) that the largest of them has the value, x, is the probability that one of the maxima has this value while the rest are smaller, i.e.

$$P(x) = \frac{d\,Q(x)}{dx} = \frac{d\,q(x)^N}{dx} = N[q(x)]^{N-1}\,p(x) \tag{3.20}$$

where Q(x) = CDF of the largest peak in time T

q(x) = CDF of continuous maxima.

From Equation (3.20), note that

$$Q(x) = [q(x)]^N$$

$$= \exp[-N \exp(\frac{x + \xi}{\theta})]$$

$$= \exp\{-\exp[\frac{x + (\xi + \theta\,\ell n\,N)}{\theta}]\} \tag{3.21}$$

With q(x) available, Q(x) can be determined provided that the number of independent maxima, N, during a period, T, is known. The largest observation Q(x) has also a type I model, with location shifted by the factor $\theta\,\ell n\,N$, the scale parameter $\theta$ being unchanged as compared with q(x) -- the initial model. Similarly, the distribution of smallest peak in time T is also a product of this reproductive property -- with its initial model (distribution of continuous minima) being shifted by the amount $\theta\,\ell n\,N$ while the shape is preserved. The distribution of the largest/smallest peak in time T is often termed as "extreme value distribution" in this thesis. Experimental results of extreme value distribution of a scaled model in the wind tunnel were obtained so that a comparison is possible with the shifted distribution of continuous peaks.

In the past, a few theories have been presented to cope with the problem as how to determine the number of independent peaks in time T -- in other words, the effective fluctuation rate $\nu$. For the time being, a new technique, which employs the autocorrelation coefficients between peaks for various lag times, is proposed to find $\nu$. Comparison is then made among these different theories as opposed to the experimental extreme value distribution from wind-tunnel test.

Autocorrelation coefficients are established by direct computation of average products among the continuous peaks at various lag times. For N data values $X_n$, n = 1, 2, ..., N, from a transformed record $\{X(t)\}$ which is stationary with zero mean, the estimated autocorrelation function at the displacement rh is defined by the formula

$$\hat{R}_r = \hat{R}_x(rh) = \frac{1}{N-r} \sum_{n=1}^{N-r} X_n X_{n+r}, \quad r = 0, 1, 2, \ldots, m \qquad (6.3)$$

where r is the lag number, m is the maximum lag number, h is the time interval between samples, and $\hat{R}_r$ is the estimate of the true value $R_r$ at lag r, corresponding to the displacement rh. A normalized value for the autocorrelation function is obtained by dividing $\hat{R}_r$ by $\hat{R}_0$ where

$$\hat{R}_0 = \hat{R}_x(0) = \frac{1}{N} \sum_{n=1}^{N} (X_n)^2 = \overline{X^2}$$

Note that the quantity $\hat{R}_0$ is a sample estimate of the true mean square value in the data.

The very same 10,000 continuous peaks, which give rise to the distributions of continuous peaks (shown in Figure 6.8), were used to obtain autocorrelation coefficients according to the computation

technique described above. Take Tape 701 for example, which is located in the vortex formation region of the building. There are 24 segments of pressure fluctuation data, sampled at 250 Hz, each of size 16,384. The segment is further broken into 4 tape-records with 4,096 samples in each. Table 6.3 keeps track of how many continuous peaks were provided by each tape-record as we accumulate, through the long time series, those 10,000 continuous peaks needed for the distributions. Each tape-record takes 4096/250 = 16.38 sec. and provides, on the average, 1147 continuous peaks. So the average time interval between peaks is 16.38/1147 = .0143 sec. Note that the sampling rate is much higher than the energy frequencies of fluctuating pressures; thus, there are enough data points to ensure detection of all peaks. It should also be noted that, from Table 6.3, the number of peaks per unit time is almost independent of the sampling rate. Autocorrelation coefficients were computed at 0, 1, 2, 5, 10, and 15 lag numbers, which correspond to lag times of 0.0, 0.0143, 0.0286, 0.0715, 0.143, and 0.215 sec., respectively. Results are shown in Table 6.4. Plot of autocorrelation coefficients versus average lag times can be found in Figure 6.9. The same procedure was followed to obtain autocorrelation coefficients for pressure flucutation data sampled at 1,000 Hz. Results were compared with those of previous case (sample rate = 250 Hz). Figure 6.9 illustrates the agreement in $\hat{R}$'s at corresponding lag times between two sets of data: one sampled at 250 Hz, the other 1,000 Hz. The average fluctuation rate, $\nu$, can thus be determined from Figure 6.9. At $\hat{R} = 0.2$ level, the average time per independent peak is found to be .023 sec/indep pk. The reciprocal of this quantity gives

$$\nu = \frac{\text{no. of independent peaks}}{\text{sec.}}$$

$$= \frac{1}{.023 \text{ sec./indep pk}} \simeq 45 \text{ indep pk/sec.}$$

At $\hat{R} = 0.1$ level,

$$\nu = \frac{1}{.065 \text{ sec./indep pk}} \simeq 15 \text{ indep pk/sec.}$$

These two $\nu$'s are differed by a factor of 3. They agree reasonably well with values reported by Akins (1976) [$\nu$ approximately 20 in both separated and stagnation regions]. Zambrano (1978), in his study of wind load interaction on an adjacent building, found $\nu$ to be approximately 20 with no upstream building interference. Values of $\nu$, ranged from approximately 5 up to approximately 45, were also reported for cases with different degrees of interference by the upwind building. Peterka and Cermak (1974) reported $\nu \simeq 11$ for positive $Cp_{mean}$ and $\nu \simeq 58$ for negative $Cp_{mean}$ when test building is placed in the city environment. It is implied by Figure 6.9 that this new technique for computing $\nu$ described herein is independent of the sampling rate. However, when applied to other pressure taps on the building, the technique did not yield reasonable results. The autocorrelation coefficient drops sharply even at the first lag number. This implies a high value of $\nu$ of order of magnitude 150 indep pk/sec. A possible explanation is that the new technique is sensitive to the degrees of pressure fluctuations. Tap No. 701 lies in the vortex formation region of the building where large fluctuation amplitudes occur, whereas other taps give relatively small fluctuations. It is thus recommended that

pressure fluctuation signals be amplified to within a reasonable range before further study. Nevertheless, for practical cladding design purpose, the vortex shedding phenomenon is the dominant factor that has to be taken into consideration. Information associated with this dominant phenomenon is significant enough to provide a general guideline in pursuing knowledge of local pressure fluctuations on buildings.

With the average effective fluctuation rate, $\nu$, available, the number of independent peaks, N, in time T is simply given by $N = \nu T$. And the distribution of the largest/smallest peak in time T is readily obtained by shifting by a factor of $\theta \ell n N$ the distribution of continuous maxima/minima.

The distribution for the largest/smallest peak in time T(= 5 sec in this thesis study) has been obtained for each tap location through wind-tunnel test. The long pressure fluctuation record (24 segments--each of size 16,384 samples at 250 Hz) provides 288 5-sec sampling intervals. Each sampling interval provides only one maximum/minimum. The extreme value distribution applies to a collection of maxima/minima derived from many such intervals. These distributions for the largest/smallest peak in time T(= 5 sec) are, traditionally, presented in histograms, as shown in Figures 6.10a-e. The peaks for the windward side of the building are fairly narrowly confined with very few extending above 4 to 5 standard deviations from the mean as can be seen in Figures 6.10a and b. The peak in the separated and vortex shedding regions of the building is observed to have higher values and the larger peaks tail off slowly to values of 9 standard deviations from the mean as illustrated in Figure 6.10c, d, and e. This result is not surprising in light of the probability distribution for the fluctuating

pressure presented earlier. The data presented by Peterka and Cermak (1974) for fluctuating pressures on a wind-tunnel test model are consistent with the present data. Dalgliesh et al. (1979) conducted measurements of peak pressures on a full-scale structure as well as wind tunnel model. The present results are also in good agreement with theirs.

The distributions of continuous peaks were shifted, according to the amount $\theta \ln N$, to best fit the histograms of peaks in order to obtain $\nu$. This method of "back-calculating" to determine $\nu$ gave reasonable agreement when compared with directly computed values of $\nu$ from the proposed autocorrelation technique. For example, the distribution of continuous peaks for Tap No. 116 would have to be shifted to the right an amount $\theta \ln N = 3.5$ to best fit its corresponding experimental extreme value distribution. Since $\theta = -0.861$ and $\theta \ln N = 3.5$, we have

$$(0.861) \ln(\nu T) = 3.5$$

$$\nu T \simeq 59$$

$$\nu \simeq 12.$$

This value is the same as that found by correlation analysis. Note that, from Eq. (3.21),

$$Q(x) = \exp\{-\exp[\frac{x + (\xi + \theta \ln N)}{\theta}]\} \tag{3.21}$$

a negative value of $\theta$ (as for positive $Cp_{mean}$ case) implies the translation of the curve to the right. Similarly, cases of negative $Cp_{mean}$ find $\theta$ to assume positive values, which means a translation of the curve to the left. The value of $\nu$ for Tap No. 417 was calculated to be 21, while $\nu = 55$ for Tap No. 419, $\nu = 20$ for Tap No. 613 and

$\nu = 60$ for Tap No. 701. Results are shown in Figure 6.10a-e. Distribution at $\hat{R} = 0.1$ and $\hat{R} = 0.3$ level (from Figure 6.9) were also shown for Tap No. 701 in Figure 6.10e. Note that the shifted amount $\theta\ \ell n(\nu T)$ is not sensitive to the estimated value of $\nu$ because of the nature of logarithmic function. Values of $\nu$ range from approximately 12 up to approximately 60, and are in reasonable agreement with estimates via autocorrelation technique as well as with other wind-tunnel test findings. Note that the test building is placed in the city environment as compared with previous wind-tunnel tests with only one or two block building(s). In summary, the theoretical extreme value distribution can be determined by shifting the distribution of continuous peaks if a knowledge of $\nu$ is obtained.

In fact, techniques have been developed to predict the peak wind loading values on a structure. Davenport (1961, 1964) provided a peak value theory for wind loads based in part on earlier statistical work of Cartwright and Longuet-Higgins (1956) and Rice (1944, 1945). The procedure involves the assumption of a Gaussian pressure distribution of local pressures acting on the structure in response to a Gaussian distribution of velocity in the turbulent flow about the structure. The peak probability density function is a function of sample time. The purpose of Davenport's statistical model is to relate the largest likely instantaneous value of the pressure force occuring during a period of time $T$ to the mean value, power spectrum, and probability distribution of the (continuous) peak fluctuations at the point of interest. The theory by Davenport is that given a stationary random function $x = f(t)$ having a normal probability distribution with mean $\bar{x}$, standard deviation $\sigma(x)$, and normalized variate $\eta$ defined as $(x-\bar{x})/\sigma(x)$, the assumed probability distribution of the function is

$$p(\eta) = \frac{1}{2\pi} \exp(-\frac{1}{2}\eta^2) \tag{6.4}$$

The probability distribution for the largest peak in time T is

$$P(\eta) = \eta\ \nu T \exp[-\frac{\eta^2}{2} - \nu T \exp(-\frac{\eta^2}{2})] \tag{6.5}$$

The quantity, $\nu$, is interpreted by Davenport to be the frequency at which most of the energy in the spectrum will generally be close to the natural frequency (for application to the building motion). In order to obtain this value (called average effective fluctuation rate) the power spectral density for the random function is required. And $\nu$ is given by

$$\nu = (m_2/m_0)^{1/2} \tag{6.6}$$

where

$$m_r = \int_0^\infty n^r\ S(n)\ dn \tag{6.7}$$

in which $S(n)$ is the power spectrum of the random function at the frequency $n$. It is attempted to apply Davenport's theory to Tap No. 116 (positive mean) and Tap No. 419 (negative mean). Spectra were formed for the positive and negative mean data (long time series sampled at 1,000 Hz) from the test building. Results are shown in Figures 6.11a and b. Appropriate moments of the spectrum were taken to form $\nu$ according to Equations (6.6) and (6.7). There is a drawback in the integration formula

$$m_2 = \int_0^\infty n^2\ S(n)\ dn.$$

It is well known that $S(n)$ is of order $n^{-5/3}$. The integrand $n^2\ S(n)$ is thus of order $n^{1/3}$. It is apparent that the indefinite integral

$$\lim_{n\to\infty} \int_0^n n^2\ S(n)\ dn \to \infty$$

The average effective fluctuation rate, $\nu$, thus assumes infinity. Actual integration upper limits used were frequencies intercepted with the extrapolated spectra curves shown in Figure 6.11a and b. The theoretical distributions based on Davenport's theory are shown in Figures 6.12a and b, together with those predicted by the present theory. Figure 6.12a shows that the data for the windward side of the building follows Davenport's distribution reasonably well, while the present theory doesn't quite match the data. However, the data in Figure 6.12b do not fit Davenport's theoretical curve at all well and yet the present theory works beautifully. This is significant because pressure coefficients in the flow separated and vortex formation regions are of primary concern in the practical design of claddings. Even for the positive mean case, it is argued that a slight increase of the value of $\eta = (Cp - Cp_{mean})/Cp_{rms}$ around the modes of two theoretical distributions, say at $\eta = 3.5$, would result in a cumulative probability of .846 predicted by Davenport's theory as compared with a value of .654 from the present theory. Design at this level based on the present theory is thus on the safe side.

The reason why Davenport's theory breaks down for the negative mean case is because of his assumption of a Gaussian parent distribution. It is discussed in Section 6.2 that parent distribution of pressure fluctuations on the windward side of the building can be approximated by a Gaussian distribution. It is thus not surprising that the data of positive pressures are predicted reasonably well by Davenport's theory. However, in strongly turbulent negative regions the tail of the parent distribution is distinctly non-Gaussian, and predictions based on Davenport's theory fall far short of observations. Measurements made

by Dalgliesh (1971) and Peterka and Cermak (1974) yield the same conclusions. It should be noted that the only assumptions made in the present theory are: 1) the pressure fluctuation process is stationary and 2) the tail of the parent distribution is of exponential type. These were actually verified in Section 6.1 and Figure 6.8. Dispute over whether the pressure fluctuations is Gaussian or not seems superfluous from the present point of view.

The average effective fluctuation rate formed by taking appropriate moments of power spectrum density are consistent with estimates from autocorrelation technique. As far as the available facilities and practical design purpose are concerned, the present theory provides an economic and convenient way to form $\nu$, which is just a by-product when constructing the distribution of continuous peaks. No extra work, like generating the power spectrum density and taking the appropriate moments, is necessary. Dalgliesh (1971) discussed the fluctuation rates at some length. He pointed out that for pressure fluctuations on cladding, $\nu$ is a random variable, i.e., the numerical value of $\nu$ differs somewhat from record to record in a random fashion. The information provided by fluctuation rate is useful for the checking and improvement of the theoretical methods for predicting peak pressures. Dalgliesh gave a theoretical interpretation of $\nu$. He argued that $\nu$ represents the average number of crossings of the zero (mean) value with positive slope (plus crossings) per second. For narrow-band random processes the plus crossing rate and the number of peaks per second are essentially the same; but for the wide-band process represented by local pressure fluctuations on cladding the actual number of peaks was found to be about twice or three times the

number of zero crossings. His viewpoint only leads to the conclusion that the peak rate is an upper bound for the effective fluctuation rate. Since we are mainly interested in the number of independent peaks in a period of time T, there is no way to tell, from Dalgliesh's argument, whether the peaks are correlated in some way. It is asserted in this thesis that the "continuous" peaks which passed the screening technique (see Figure 5.1) are dependent samples of a single random variable. There is a correlation within each sample of the random process, measured by the sample autocovariance function, $C_x(t, t+\tau)$, which is given by

$$C_x(t, t+\tau) = \frac{1}{n} \sum_{i=1}^{n} X_i(t)\, X_i(t+\tau) \qquad (6.8)$$

in which $\tau$ is referred to as time lag. If the process is stationary (at least in the weak sense) and the mean is removed from the process, Equation (6.8) is merely a re-statement of Equation (6.3), which is the formula used that ultimately yields an estimate of the effective fluctuation rate. This is so because once the autocovariance has reached zero (or some acceptable level) at certain lag time, the subsequent data essentially form an independent sample.

Noticing the difficulty of applying a Gaussian distribution to the negative fluctuating pressures, Dalgliesh et al. (1979) solved the problem by saying that intermittent "bursts" of turbulence are superimposed on a record which is otherwise Gaussian in nature. In other words, strong spikes of pressure occur at random intervals throughout the sample record and these spikes, because of their large values, end up in the tail of the parent probability distribution and usually this

is the only part of the distribution that is non-Gaussian. Instead of aiming at the entire population of points in the sampling interval, Dalgliesh et al. examined the spikes according to two rules:

"1) A spike value must be away from the mean by a threshold value at least twice the rms about the mean. Both mean and rmsm are measured over the entire sampling interval.

2) A spike must be separated from adjacent spikes by returns toward the mean that extend at least the threshold value from the spike value."

These two artificially imposed rules to the record enabled Dalgliesh et al. to deal with a new parent population of spike values whose distribution (CDF) is

$$F(g) = 1 - \exp[-(g-\theta)/(\bar{g}-\theta)] \tag{6.9}$$

in which $g$ is normalized spike value, $\theta$ is the threshold value (chosen to be 2), and $\bar{g}$ is the mean of the spike values in the interval. The extreme value distribution of peaks, $\hat{g}$, where each peak in the distribution is the maximum spike value from a sampling interval, is related to the above expression by only one parameter:

$$F_n(\hat{g}) = \{1 - \exp[-(\hat{g} - \theta)/(\bar{g} - \theta)]\}^n \tag{6.10}$$

The new parameter $n$ is the average number of spikes per interval. Histograms of peaks from many intervals can be matched rather well by their theory. Note that Equation (6.9) is simply a statement that the upper tail of the original parent distribution is of exponential type (refer to Equation (3.7)). The average number of spikes per interval, n, is converted, based on Equation (4.4), to be compatible with present wind-tunnel values of $V$. Dalgliesh et al. gave values of $V$ ranging

from approximately 10 up to approximately 55. Though Dalgliesh's spike-value theory bears a resemblance to the present theory, it differs from its counterpart mainly in the way of treating "peaks". The question arises, for example, what would be the effect on the spike value theory if a change of threshold value occurs? The present theory, however, is simple and mathematically complete.

## 6.4 Applications of Extreme Value Results

### i) Wind Tunnel Study

Ten thousand continuous peaks were used to construct each distribution shown in Figure 6.8. It was found that 16 seconds pressure fluctuation record at 250 samples per second provides approximately 1,120 continuous peaks. The fitted type I distribution of the first 1,400 continuous peaks, out of 10,000, for Tap No. 417 is given in Fig. 6.13. It is seen that this distribution does not differ significantly from that of 10,000 continuous peaks (the chi-square test result is $\hat{\chi}^2_{0.5,17} = 27.4$ as compared with the sum of normalized deviations 12.63). This finding enables us to recover the extreme value distribution from the regular wind-tunnel pressure study data. The very same data used to compute $Cp_{mean}$ and $Cp_{rms}$ also yield the distribution of continuous peaks. An estimate of the average effective fluctuation rate according to the nature of fluctuating pressures would then allow the establishment of the distribution of the largest/smallest peak in time T. The significance of the theory presented in this thesis roots right in this application.

### ii) Gust Factor Approach

A parameter which was suggested (Dalgliesh, 1971) to describe extreme design loading coefficient values in terms of the parent mean and rms values is the Gust Factor, defined by

$$g_d = (C_{\hat{p}} - Cp_{mean})/Cp_{rms} \tag{6.11}$$

where the symbol $\hat{}$ denotes the extreme value. This approach has been adopted by many other researchers (Akins, 1976; Mayne and Cook, 1979; Dalgliesh et al., 1979, ..., etc.). The assignment of a value for $g_d$ is not as straightforward as for $Cp_{mean}$ and $Cp_{rms}$ because the Gust Factor must account for the randomness inherent in pressure fluctuations. If a measurement of a mean or rms pressure coefficient for a given flow situation and building geometry is repeated, the values of each individual measurement fall within the repeatability of the measurement system. However, the peak pressure coefficient will vary in a random fashion. The definition of $g_d$ in Equation (6.11) is analagous to that for the standardized variate $\eta$ in Equation (5.3). Extreme "Gust Factor" type of approach is possible using $g_d$ in place of $\eta$. The extreme value distribution (of gust factors) expresses the risk of exceedance of the pressure coefficient in the observation period. A reasonable way of choosing a representative value for $g_d$ is then possible by picking one of the following:

a) the value that occurs most frequently (the mode),

b) the average value (the mean), or

c) the value with an acceptably small probability of being exceeded.

The advantage of extreme value analysis over the selection of a single extreme is that the probability of the extreme is correctly assessed and is described by the values of $\xi$ (the location factor) and $\theta$ (scaling factor).

iii) A First-order Method for Design

Extreme value analysis of fluctuating pressures yields information on the risk of exceedance of the pressure coefficient in the observation period. The risk of the design wind speed can also be known from a similar analysis of the wind data. Therefore, the actual risk of wind loads on a structure can be assessed from the joint risk of wind speed and pressure coefficient. A first-order method to this assessment has been proposed by Mayne and Cook (1978, 1979) and is briefly described in this thesis. The reader is referred to their work for a complete discussion.

Since climatological records commonly refer to hourly mean wind velocities, the sample duration of frequent interest is one hour. The first-order method assumes that the design load is formed by the combination of the extreme hourly-mean wind speed with the extreme pressure coefficient in that hour of wind through a simple convolution integral of the joint PDF of the annual extreme hourly-mean wind speed V and the extreme pressure coefficient Cp. If these two parameters are statistically independent*, then the joint PDF is simply the product of their individual PDFs. This is illustrated in Figure 6.14. The probability of a given load X is the integral of the joint PDF along the curved line

*This is so through a fundamental redefinition of dynamic pressure and pressure coefficient parameters. This redefinition makes use of the way that the Spectral Gap, shown in Figure 6.15, divides the frequency range into Macro- and Micrometeorological ranges. The dynamic pressure, being a function of Macro- range only, and the pressure coefficient, a function of Micro- range only, can be considered as being statistically independent since all cross-sepctral terms are identically zero. See Mayne and Cook (1979) for details.

$$X = \frac{1}{2} \cdot \rho \cdot V^2 \cdot Cp \qquad (6.12)$$

Note that the shape of the two individual PDFs is the type I form, the shape of the joint PDF is always known and geometric similarity reduces the four parameters $\xi_v$ and $\theta_v$, for the wind speed, and $\xi_c$ and $\theta_c$, for the pressure coefficient, to the two independent parameters $(\xi/\theta)_v$ and $(\xi/\theta)_c$, and the scaling function of Equation (6.12). The design load probability distribution functions can then be computed over some range of $\xi/\theta$ of both parameters. It is also possible to work backwards from the results of the first-order design method to determine, for a given return-period, the equivalent static pressure coefficient which gives the design result when applied in Equation (6.12) with the extreme mean-hourly wind speed of the same return-period. This actually calibrates the "Gust Factor Approach" resulting in the design value of $g_d$ for some specified return-periods.

Mayne and Cook (1979) reported that the first-order method underestimates by the order of a maximum 10%. More refined higher-order methods are possible but the extra complication associated is not necessary because of the other uncertainties concerning the behaviour and strength of structures.

The extreme value distribution in a period of time $T = 5$ sec is obtained in this thesis. What would be the distribution of extreme values over longer observation period, say, one hour? The distribution of extreme values over longer observation period can actually be related to the original extreme value distribution provided that there is no additional variability introduced into the parent data by extending the observation period and the original T time extremes (peak pressures)

are independent. The number of independent observations of the original extreme population in each of the new longer periods is the ratio of their lengths $r = T_r/T$. The probability that an extreme value is not exceeded in the new longer period $T_r$ is the probability that all of r original extreme values are not exceeded

$$Q_r(x) = [Q(x)]^r \tag{6.13}$$

Thus the CDF of the new extreme value distribution is merely the CDF of the original extreme value distribution raised to the power of the sample-size ratio.

# Chapter 7

# CONCLUSIONS AND RECOMMENDATIONS FOR FURTHER STUDY

## 7.1 Conclusions

The experimental findings of this thesis are limited to static structures where the dynamic response caused by wind loads is negligible and does not enter into the design considerations. With this in mind, several conclusions concerning the nature of local pressure fluctuations on buildings caused by turbulent boundary-layer winds are listed.

In this wind tunnel study, the pressure fluctuation process is assumed to be stationary if the approaching wind speed is stationary. Since there are no specific trends observed in the mean and rms from the experimental data, the assumption was regarded as confirmed at least in the weak sense.

i) The distribution of fluctuating pressures for positive $Cp_{mean}$ is skewed to the right, while for the negative $Cp_{mean}$, the distribution is skewed to the left. Two parameters, namely, the mean pressure coefficient ($Cp_{mean}$) and the coefficient of skewness of fluctuating pressures (S{P}) summarily describe the nature of local pressure fluctuations. For a positive mean pressure distribution, the deviation from a normal distribution is not pronounced, therefore, a Gaussian approximation for pressures on windward face of a building is valid.

ii) The distributions of the positive-going and negative-going continuous peaks are of type I form. This fact tends to justify the assumption that the tails of the parent distribution are of the exponential type.

iii) The average effective fluctuation rate, $\nu$, can be obtained through the use of autocorrelation coefficients between continuous peaks of parent population for various time lags. Once the autocorrelation has reached zero (or close to zero) at some lag time, the subsequent peaks essentially form an independent sample. Note that $\nu$ is defined as number of independent peaks per unit time. This technique is independent of the sampling rate. Results from this technique are consistent with other reported values of $\nu$. It is observed that $\nu$ assumes values typically in the range of 10-60 peaks per second in wind-tunnel models.

iv) The distribution of the largest (positive or negative) peak in time $T$ can be obtained by shifting an amount $\theta \ell n(\nu T)$ the distribution of continuous peaks. The shifted result agrees well with the experimental extreme value distribution. Note that the prime advantage of the present theory, in addition to its convenience, is that it avoids detailed knowledge of the spectral content of the parent distribution.

v) Recovery of the extreme value distribution from regular wind-tunnel test data, e.g., 16 seconds record at 250 samples per second, is possible.

## 7.2 Recommendations for Further Study

Numerous extensions to the work discussed in this study is evident.

i) Study of the effect of fluctuating pressure amplitude on the proposed autocorrelation scheme for establishing the average effective fluctuation rate, $\nu$.

ii) Study of the slope and shapes of extreme pressure peaks. Also the acquiring of more information on the response of cladding as well as the characteristics of the loading.

iii) Investigation of the effect of the approach turbulence level on the local pressure fluctuations, especially on the largest peak negative values.

iv) Further research on the space correlations of the large negative peak fluctuations.

v) Any upper and lower bounds for the average effective fluctuation rate?

# REFERENCES

American National Standards Institute, 1972, Building Code Requirements for Minimum Design Loads in Buildings and Other Structures, ANSI A58.1-1972.

Akins, R. E. and Peterka, J. A., 1975, "Computation of Power Spectral Densities and Correlations Using Digital FFT Techniques," Technical Report CER75-76REA-JAP13, Fluid Dynamics and Diffusion Laboratory, Colorado State University, Fort Collins, Colorado.

Akins, R. E. and Cermak, J. E., 1976, "Wind Pressures on Buildings," Technical Report CER76-77REA-JEC15, Fluid Dynamics and Diffusion Laboratory, Colorado State University, Fort Collins, Colorado.

Bendat, J. S. and Piersol, A. G., 1971, Random Data: Analysis and Measurement Procedures, Wiley Interscience.

Benjamin, J. R. and Cornell, C. A., 1970, Probability, Statistics, and Decision for Civil Engineers, McGraw-Hill Book Company.

Bury, K. V., 1975, Statistical Models in Applied Science, John Wily & Sons, New York.

Cermak, J. E., 1958, "Wind Tunnel for the Study of Turbulence in the Atmospheric Surface Layer," Technical Report CER56-JEC42, Fluid Dynamics and Diffusion Laboratory, Colorado State University, Fort Collins, Colorado.

Cermak, J. E. and Sadeh, W. Z., 1971, "Pressure Fluctuations on Buildings," Proceedings of the Third International Conference on Wind Effects on Buildings and Structures, Tokyo, Japan.

Cermak, J. E., 1971, "Laboratory Simulation of the Atmospheric Boundary Layer," AIAA Journal, Vol. 9, No. 9, pp. 1746-1754.

Cermak, J. E., 1975, "Applications of Fluid Mechanics to Wind Engineering--A Freeman Scholar Lecture," ASME Journal of Fluids Engineering, Vol. 97, Ser. 1, No. 1, March, pp. 9-38.

Cermak, J. E., 1976, "Aerodynamics of Buildings," Annual Review of Fluid Mechanics, Vol. 8, pp. 75-106.

Dalgliesh, W. A., 1971, "Statistical Treatment of Peak Gusts on Cladding," Journal of the Structural Division, ASCE, Vol. 97, ST3, pp. 2173-2187.

Dalgliesh, W. A., 1975, "Comparison of Model/Full Scale Wind Pressures on a High-Rise Building," Journal of Industrial Aerodynamics, Vol. 1, No. 1, pp. 55-66.

Dalgliesh, W. A., Templin, J. T. and Cooper, K. R., 1979, "Comparisons of Wind Tunnel and Full-Scale Building Surface Pressues with Emphasis on Peaks," Proceedings Fifth International Conference on Wind Engineering, Cermak, J. E. (ed.) Fort Collins, Colorado, U.S.A., 9-14 July 1979, Pergamon Press, Vol. 1, Sessions I-V.

Davenport, A. G., 1961, "The Application of Statistical Concepts to the Wind Loading of Structures," Proceedings of the Institution of Civil Engineers, Vol. 19, pp. 449-471.

Davenport, A. G., 1964, "Note on the Distribution of the Largest Value of a Random Function with Application to Gust Loading," Proceedings of the Institution of Civil Engineers, Vol. 28, pp. 187-196.

Davenport, A. G., 1967, "Gust Loading Factors," Journal of the Structural Division, ASCE, Vol. 93, ST3, pp. 11-34.

Davenport, A. G., 1976, Discussion on "Wind Pressures on Buildings--Probability Densities by Peterka and Cermak (1975)," Journal of the Structural Division, ASCE, Vol. 102, ST11, pp. 2235-2237.

Epstein, B., 1960, "Elements of the Theory of Extreme Values," Technometric, Vol. 3, No. 1.

Gumbel, E. J., 1958, Statistics of Extremes, Columbia University Press.

Mayne, J. R. and Cook, N. J., 1979, "Acquisition, Analysis and Application of Wind Loading Data," Proceedings Fifth International Conference on Wind Engineering, Cermak, J. E. (ed.), Fort Collins, Colorado, U.S.A., 9-14 July 1979, Pergamon Press, Vol. 2, Sessions VI-X.

Ostrowski, J. S., Marshall, R. D., Cermak, J. E., 1967, "Vortex Formation on Pressure Fluctuations on Buildings," Proceedings of the International Seminar on Wind Effects on Buildings and Structures, Ottawa, Canada, pp. 459-484.

Peterka, J. A. and Cermak, J. E., 1974, "Simulation of Atmospheric Flows in Short Wind Tunnel Test Sections," Technical Report CER73-74JAP-JEC32, Fluid Dynamics and Diffusion Laboratory, Colorado State University, Fort Collins, Colorado.

Peterka, J. A. and Cermak, J. E., 1975, "Wind Pressures on Buildings-Probability Densities," Journal of the Structural Division, ASCE, Vol. 101, ST6, June, pp. 1255-1267.

Peterka, J. A. and Cermak, J. E., 1979, "Wind-Tunnel Study of Mountain Bell Utah State Headquarters Building, Salt Lake City," Technical Report CER79-80JAP-JEC14, Fluid Dyanmics and Diffusion Laboratory, Colorado State University, Fort Collins, Colorado.

Peterka, J. A., 1979, Personal communication.

Rice, S. O., 1944, 1945, "Mathematical Analysis of Random Noise," Bell System Technical Journal, Vol. 23, pp. 282-332, and Vol. 24, pp. 46-157.

Sockel, H., "Local Pressure Fluctuations," 1979, Proceedings Fifth International Conference on Wind Engineering, Cermak, J. E. (ed.), Fort Collins, Colorado, U.S.A., 9-14 July 1979, Pergamon Press, Vol. 1, Sessions I-V.

Templin, J. T. and Cermak, J. E., 1976, "Wind Pressures on Buildings: Effect on Mullions," Technical Report CER76-77JTT-JEC24, Fluid Dynamics and Diffusion Laboratory, Colorado State University, Fort Collins, Colorado.

University Computer Center, 1976, Computer User's Manual, Colorado State University, Fort Collins, Colorado.

Van der Hoven, I., 1957, "Power Spectrum of Horizontal Wind Speed in the Frequency Range from 0.0007 to 900 Cycles per Hour," Journal of Meteorology, 14, pp. 160-164.

Velozzi, J. and Cohen, E., 1968, "Gust Response Factors," Journal of the Structural Division, ASCE, Vol. 94, No. ST6, pp. 1295-1313.

Vickery, B. J., 1966, "Fluctuating Lift and Drag on a Long Cylinder of Square Cross-Section in a Smooth and Turbulent Stream," Journal of Fluid Mechanics, Vol. 25, Pt. 3, pp. 481-494.

Vickery, B. J., 1970, "On the Reliability of Gust Loading Factors," Wind Loads on Buildings and Structures, National Bureau of Standards, Building Science Series No. 30, pp. 93-106.

Zambrano, T. G. and Peterka, J. A., 1978, "Wind Load Interaction on an Adjacent Building," Technical Report CER77-78TGZ-JAP26, Fluid Dynamics and Diffusion Laboratory, Colorado State University, Fort Collins, Colorado.

# TABLES

Table 6.1. Test for Stationarity of Pressure Fluctuation Data Obtained at Tap No. 116, WD = 000°.

Tap No. 116
WD = 000°

| Interval No. | $C_{pmean}$ | $C_{prms}$ |
|---|---|---|
| 1 | 0.416 | 0.133 |
| 2 | 0.426 | 0.127 |
| 3 | 0.425 | 0.143 |
| 4 | 0.431 | 0.131 |
| 5 | 0.470 | 0.126 |
| 6 | 0.427 | 0.135 |
| 7 | 0.447 | 0.112 |
| 8 | 0.423 | 0.138 |
| 9 | 0.476 | 0.133 |
| 10 | 0.435 | 0.123 |
| 11 | 0.469 | 0.127 |
| 12 | 0.443 | 0.134 |
| 13 | 0.452 | 0.143 |
| 14 | 0.449 | 0.145 |
| 15 | 0.434 | 0.128 |
| 16 | 0.448 | 0.135 |

Table 6.2. Chi-square Test Result for the Distribution of Continuous Peaks of Tap No. 701.

| | | Type I Model: $\xi$=.033, $\theta$=.874 | |
|---|---|---|---|
| Class Intervals | Observed No. of Occurrences | Expected No. of Occurrences | Normalized Squared Deviation (see Equation 5.7) |
| 1(from $\lambda$ = -8.625) | 0 | 0.25 | 0.25 |
| 2 | 0 | 0.25 | 0.25 |
| 3 | 0 | 0.25 | 0.25 |
| 4 | 0 | 0.25 | 0.25 |
| 5 | 0 | 0.5 | 0.5 |
| 6 | 0 | 0.75 | 0.75 |
| 7 | 0 | 0.75 | 0.75 |
| 8 | 2 | 1.25 | 0.45 |
| 9 | 2 | 1.5 | 0.17 |
| 10 | 0 | 2 | 2 |
| 11 | 1 | 2.75 | 1.11 |
| 12 | 3 | 3.5 | 0.07 |
| 13 | 2 | 4.75 | 1.59 |
| 14 | 5 | 6.25 | 0.25 |
| 15 | 4 | 8.5 | 2.38 |
| 16 | 11 | 11.25 | 0.006 |
| 17 | 18 | 14.75 | 0.95 |
| 18 | 20 | 19.75 | 0.003 |
| 19 | 28 | 26.25 | 0.117 |
| 20 | 27 | 34.75 | 1.728 |
| 21 | 45 | 46.25 | 0.034 |
| 22 | 60 | 61.25 | 0.026 |
| 23 | 94 | 80.75 | 2.174 |
| 24 | 111 | 106.5 | 0.19 |
| 25 | 149 | 140 | 0.579 |
| 26 | 182 | 183.25 | 0.008 |
| 27 | 236 | 238.25 | 0.02 |
| 28 | 318 | 307.75 | 0.34 |
| 29 | 387 | 393.5 | 0.107 |
| 30 | 529 | 496.5 | 2.127 |
| 31 | 579 | 615.5 | 2.165 |
| 32 | 778 | 745 | 1.46 |
| 33 | 861 | 874 | 0.19 |
| 34 | 954 | 983.25 | 0.87 |
| 35 | 1034 | 1046.5 | 0.149 |
| 36 | 1073 | 1034 | 1.47 |
| 37 | 898 | 926 | 0.847 |
| 38 | 710 | 727 | 0.4 |
| 39 | 475 | 479.25 | 0.038 |
| 40 | 264 | 250.5 | 0.728 |
| 41 | 109 | 96 | 1.76 |
| 42 | 23 | 24.5 | 0.092 |
| 43 | 7 | 3.5 | 3.5 |
| 44(to $\eta$ = 2.125) | 1 | 0 | 1 |
| | 10,000 | 10,000 | 34.1 |
| | | | $\chi^2_{0.05,41}$=42.7 |

Table 6.3. Average Time Interval between Continuous Peaks for Tap No. 701

Tap No. 701
1 tape-record = 4096 data points

| Tape-record Number | Number of Continuous Peaks | | | |
|---|---|---|---|---|
| | Sample Rate=250 HZ | Average Time Interval between Peaks (sec) | Sample Rate=1,000 HZ | Average Time Interval between Peaks (sec) |
| 1 | 1145 | .0143 | 1368 | .0030 |
| 2 | 1153 | .0142 | 1372 | .0030 |
| 3 | 1132 | .0145 | 1363 | .0030 |
| 4 | 1136 | .0144 | 1370 | .0030 |
| 5 | 1143 | .0143 | 1343 | .0031 |
| 6 | 1163 | .0141 | 1318 | .0031 |
| 7 | 1156 | .0142 | 1334 | .0031 |
| 8 | 1153 | .0142 | (532) | -- |
| 9 | (819) | -- | -- | -- |
| Σ | 10,000 | | 10,000 | |
| Average No. of Peaks per Tape-record | 1148 | | 1353 | |
| Average Time Interval between Peaks for Overall Series (sec) | .0143 | | .0030 | |

Table 6.4. Autocorrelation Coefficients between Continuous Peaks at Various Lag Times for Tap No. 701.

| Lag No. | Sample Rate=250 HZ | | Sample Rate=1,000 HZ | |
|---|---|---|---|---|
| | Lag Time (sec) | $\hat{R}$ | Lag Time (sec) | $\hat{R}$ |
| 0 | 0. | 1.000 | 0. | 1.000 |
| 1 | .0143 | .256 | .003 | .356 |
| 2 | .0286 | .196 | .006 | .336 |
| 5 | .0715 | .094 | .015 | .281 |
| 10 | .143 | .033 | .030 | .220 |
| 15 | .215 | .004 | .045 | .178 |

# FIGURES

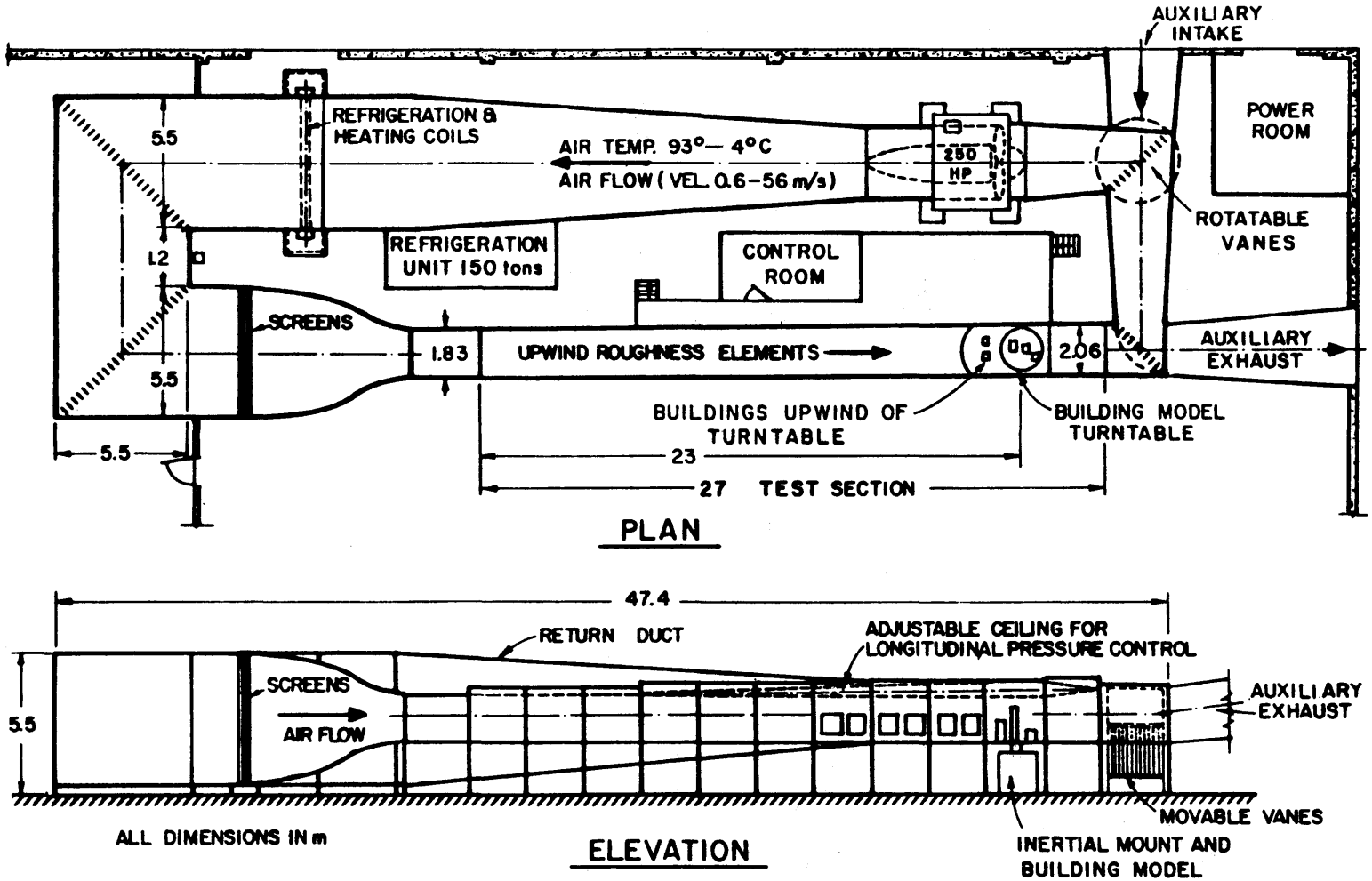


Figure 4.1. Meteorological Wind Tunnel, Fluid Dynamics and Diffusion Laboratory, Colorado State University.

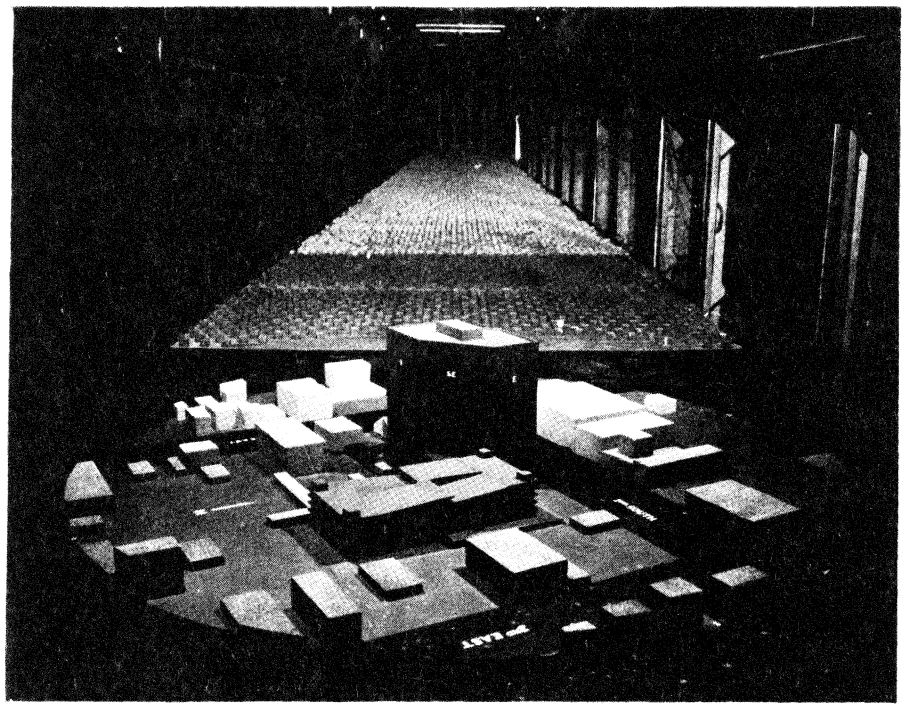

Figure 4.2. Completed Model in Wind Tunnel--Mountain Bell Utah State Headquarter Building.

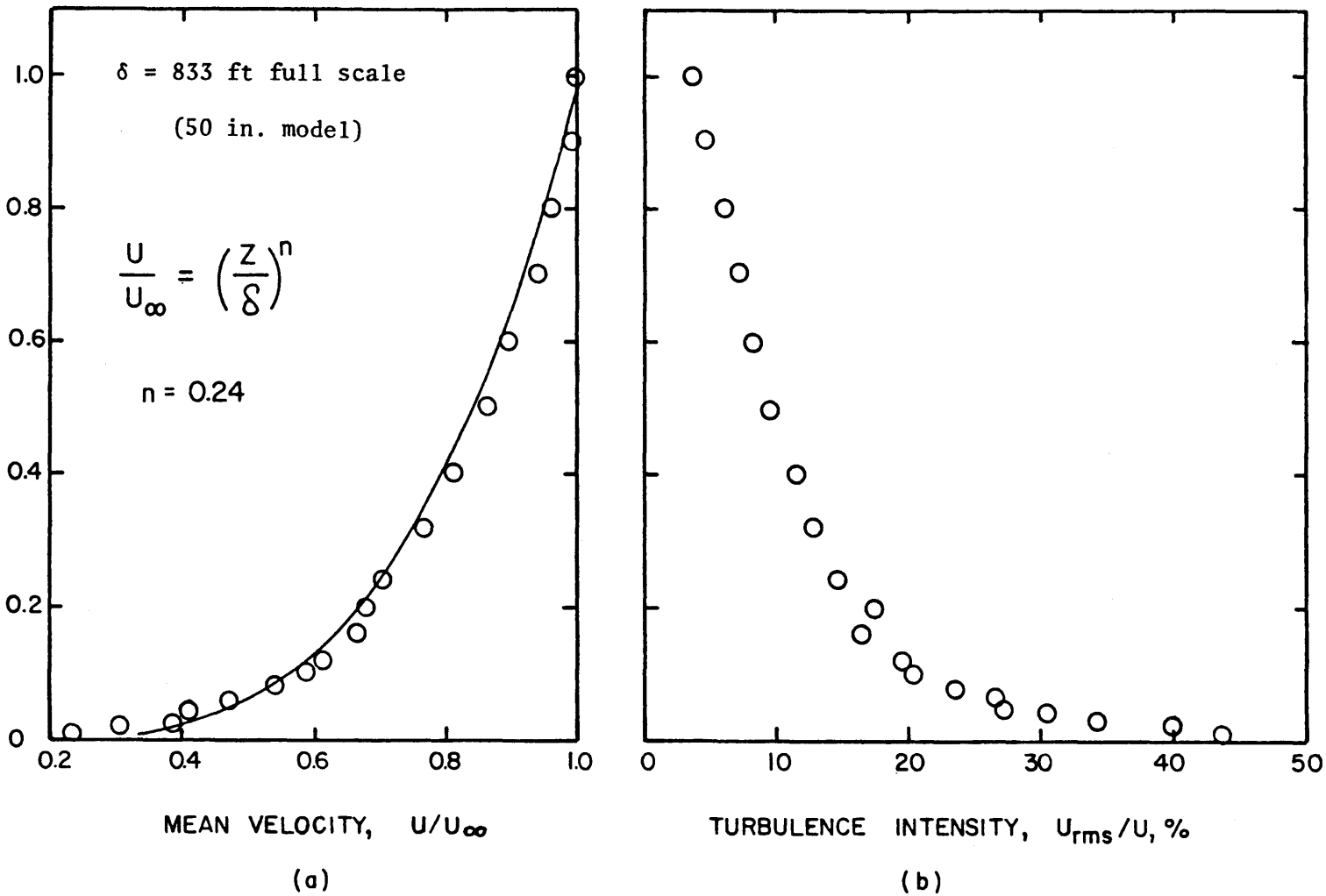


Figure 4.3. Mean Velocity and Turbulence Profiles Approaching the Model.

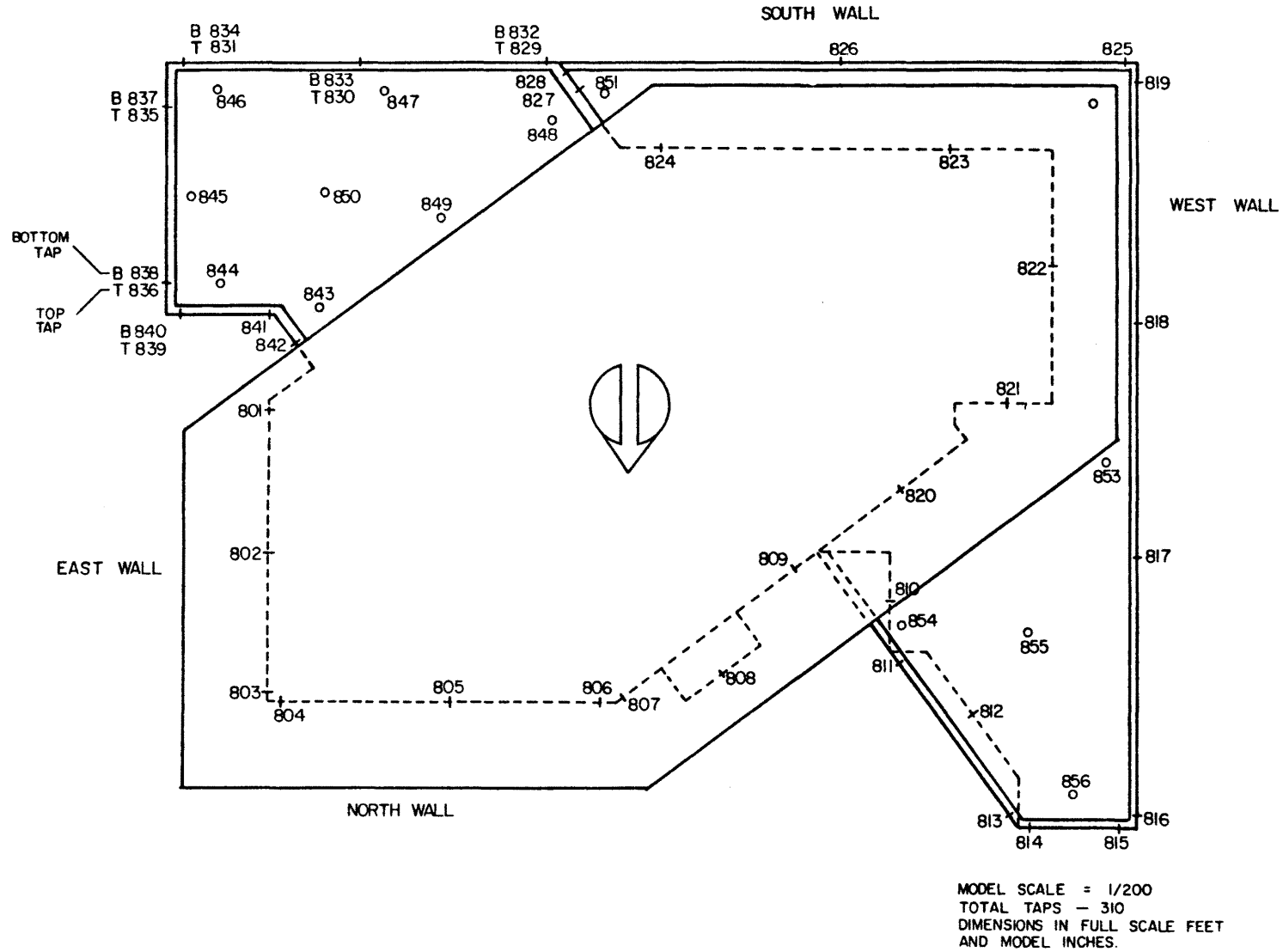


Figure 4.4a. Dimensions of the Model and Pressur Tap Locations.

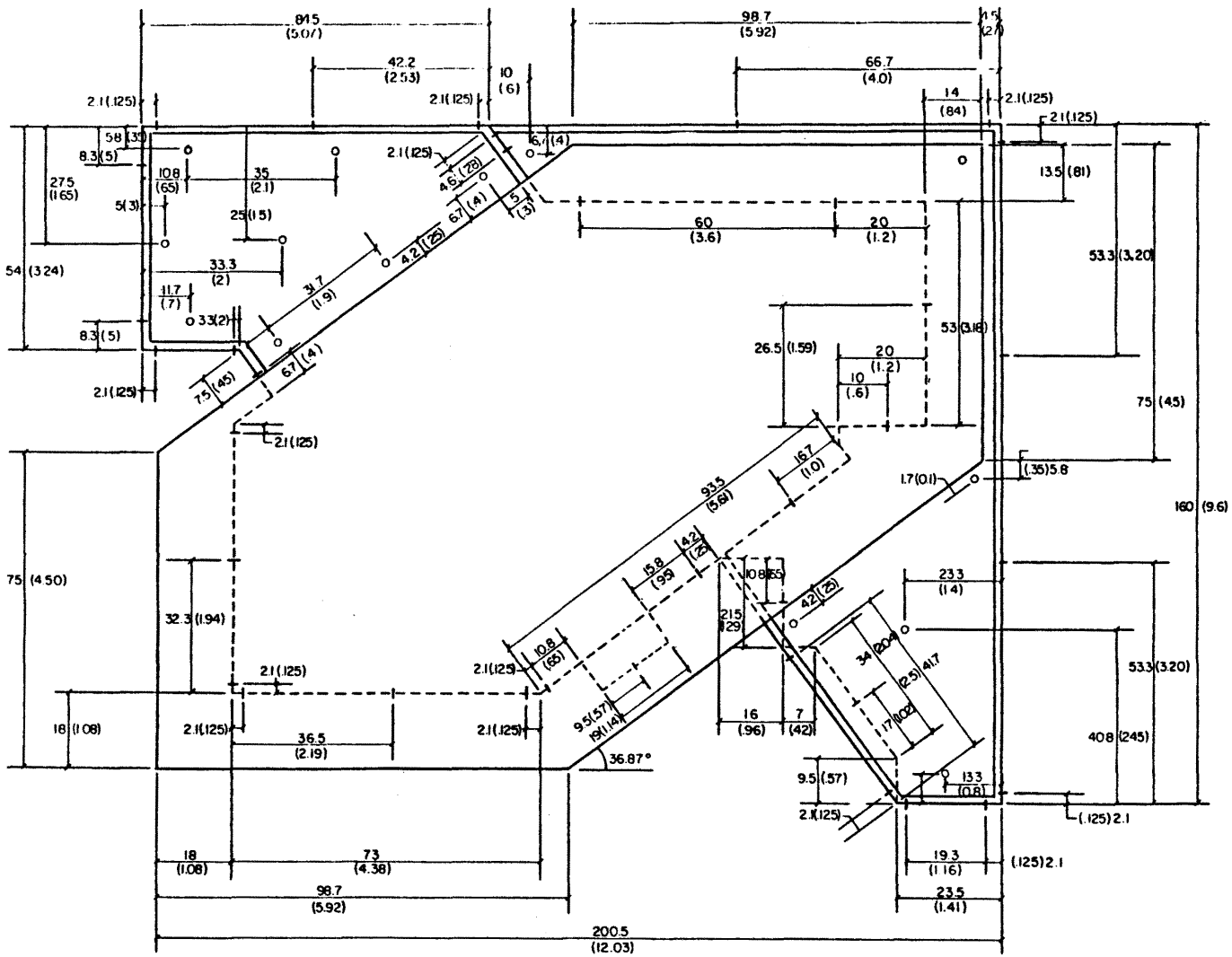


Figure 4.4b. Dimensions of the Model and Pressur Tap Locations.

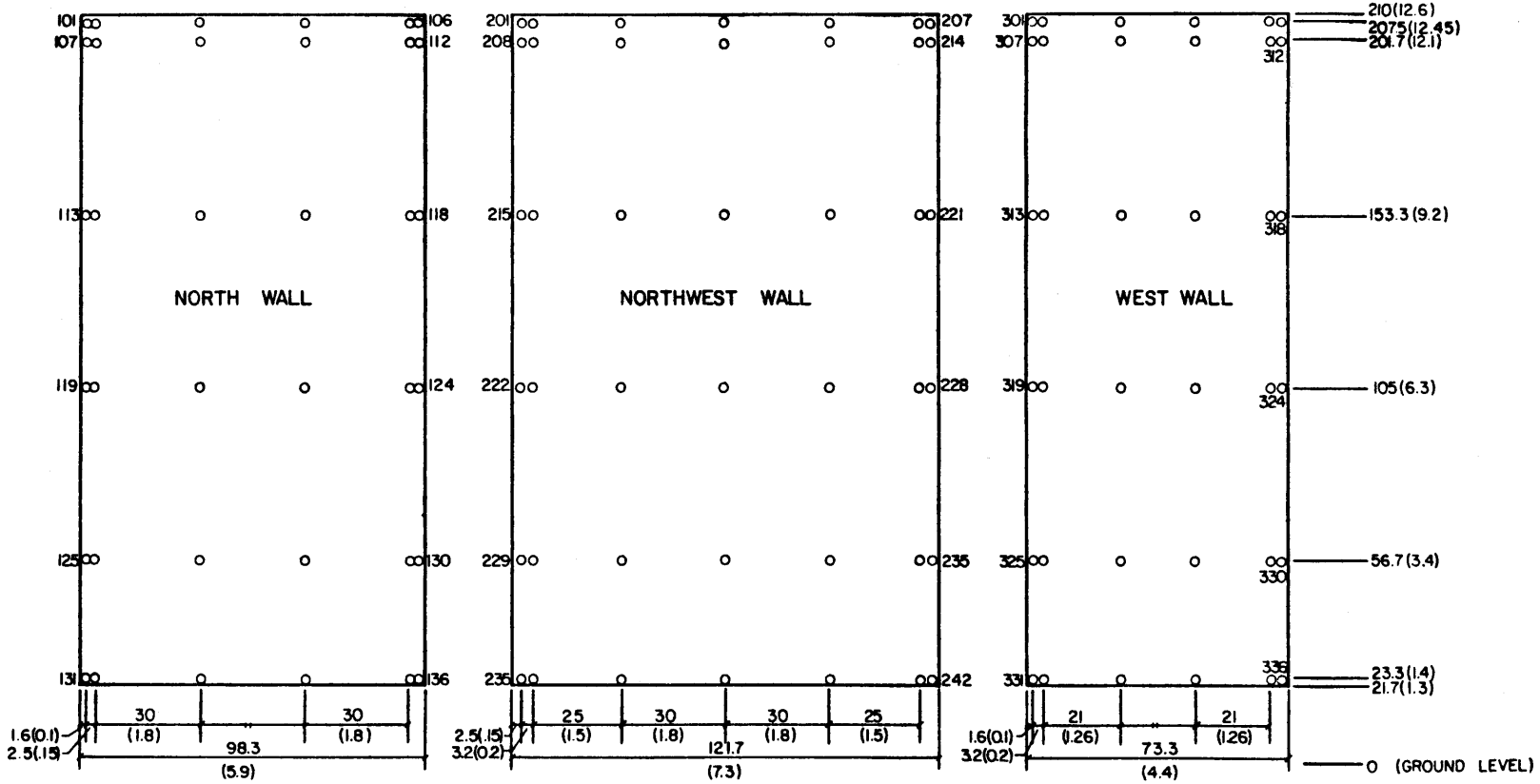


Figure 4.4c. Dimensions of the Model and Pressur Tap Locations.

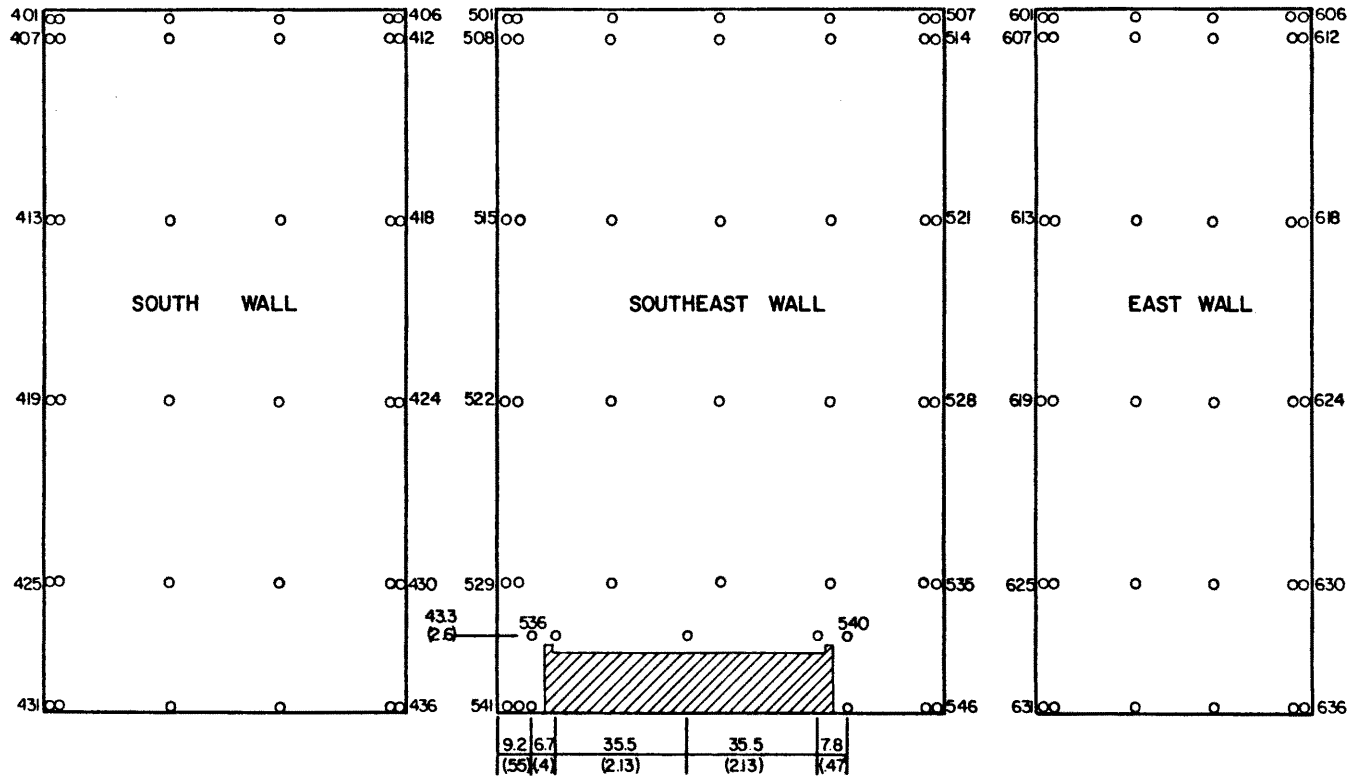


Figure 4.4d. Dimensions of the Model and Pressur Tap Locations.

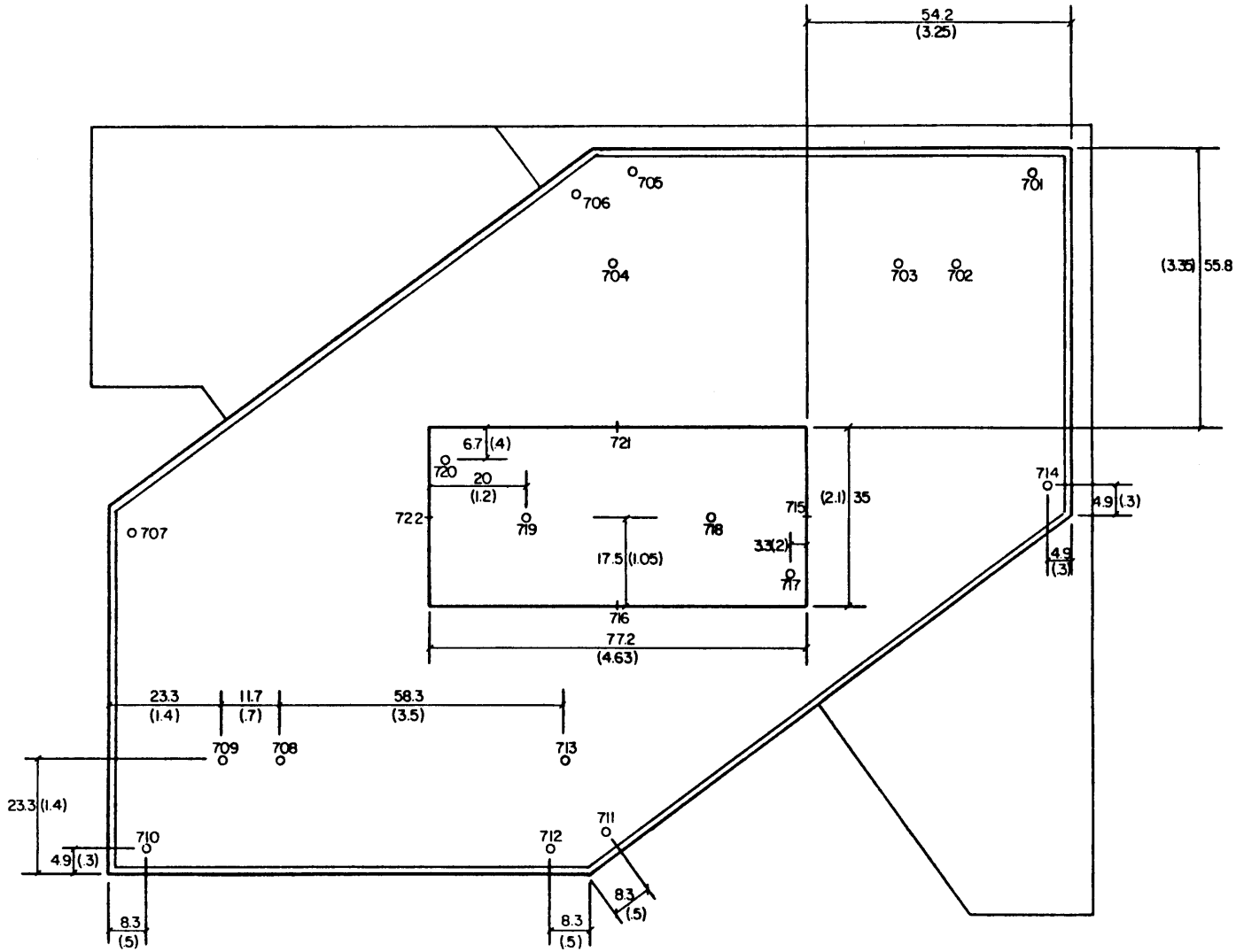


Figure 4.4e. Dimensions of the Model and Pressur Tap Locations.

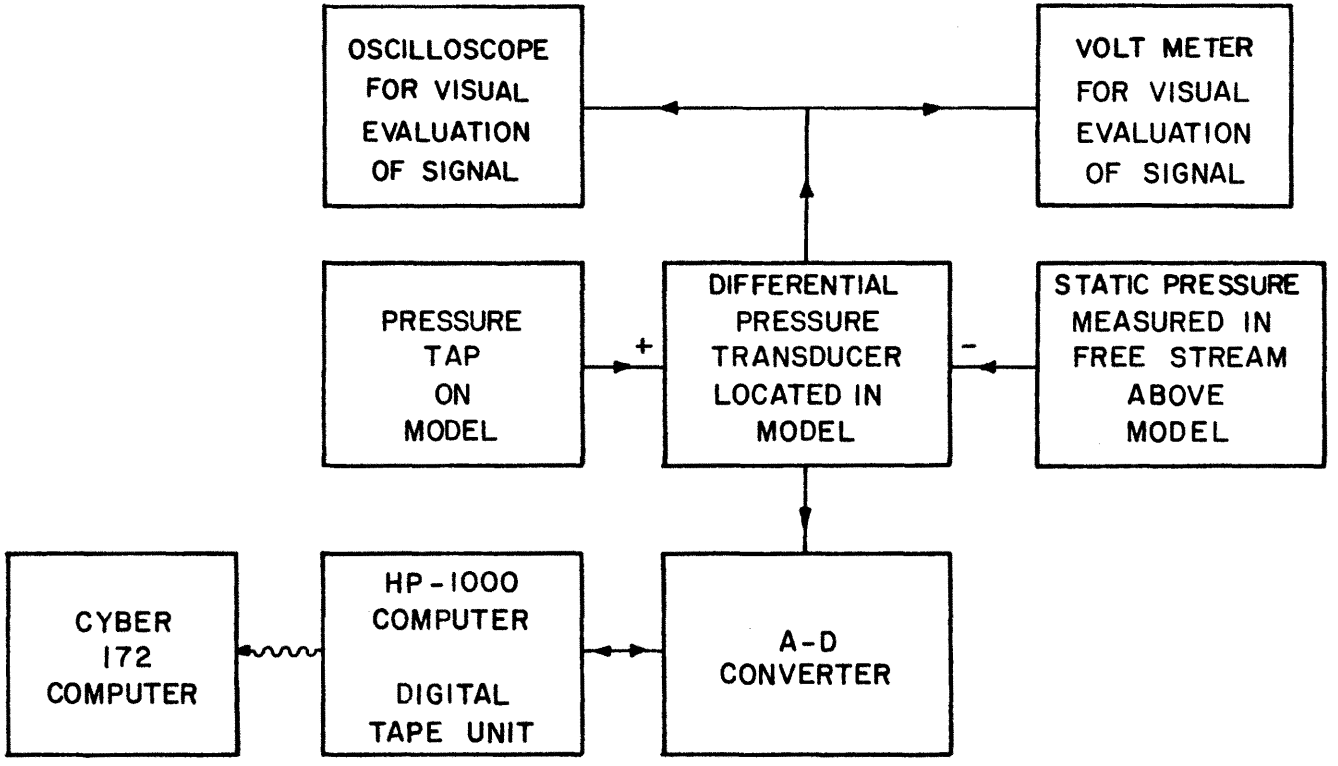


Figure 4.5. Schematic of Data-Acquisition System.

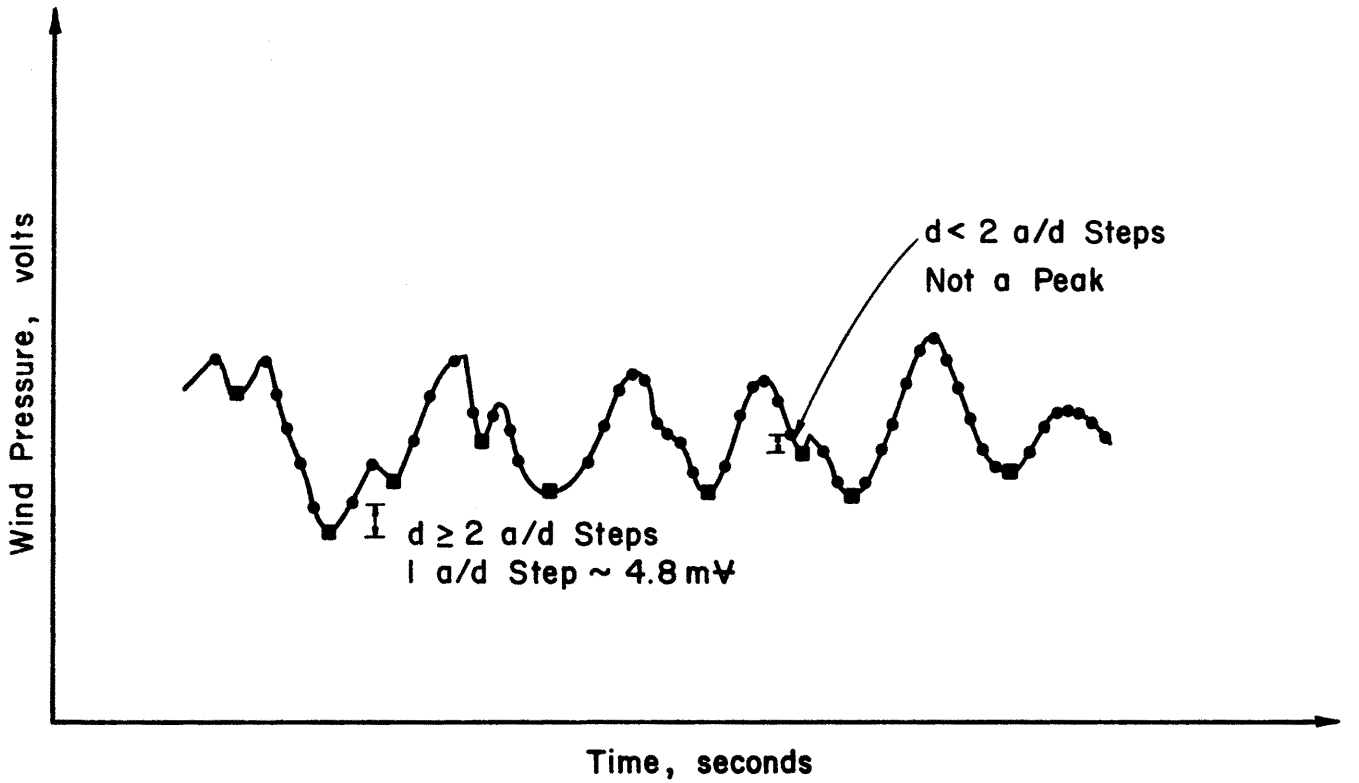


Figure 5.1. Definition of Peaks in Sequence.

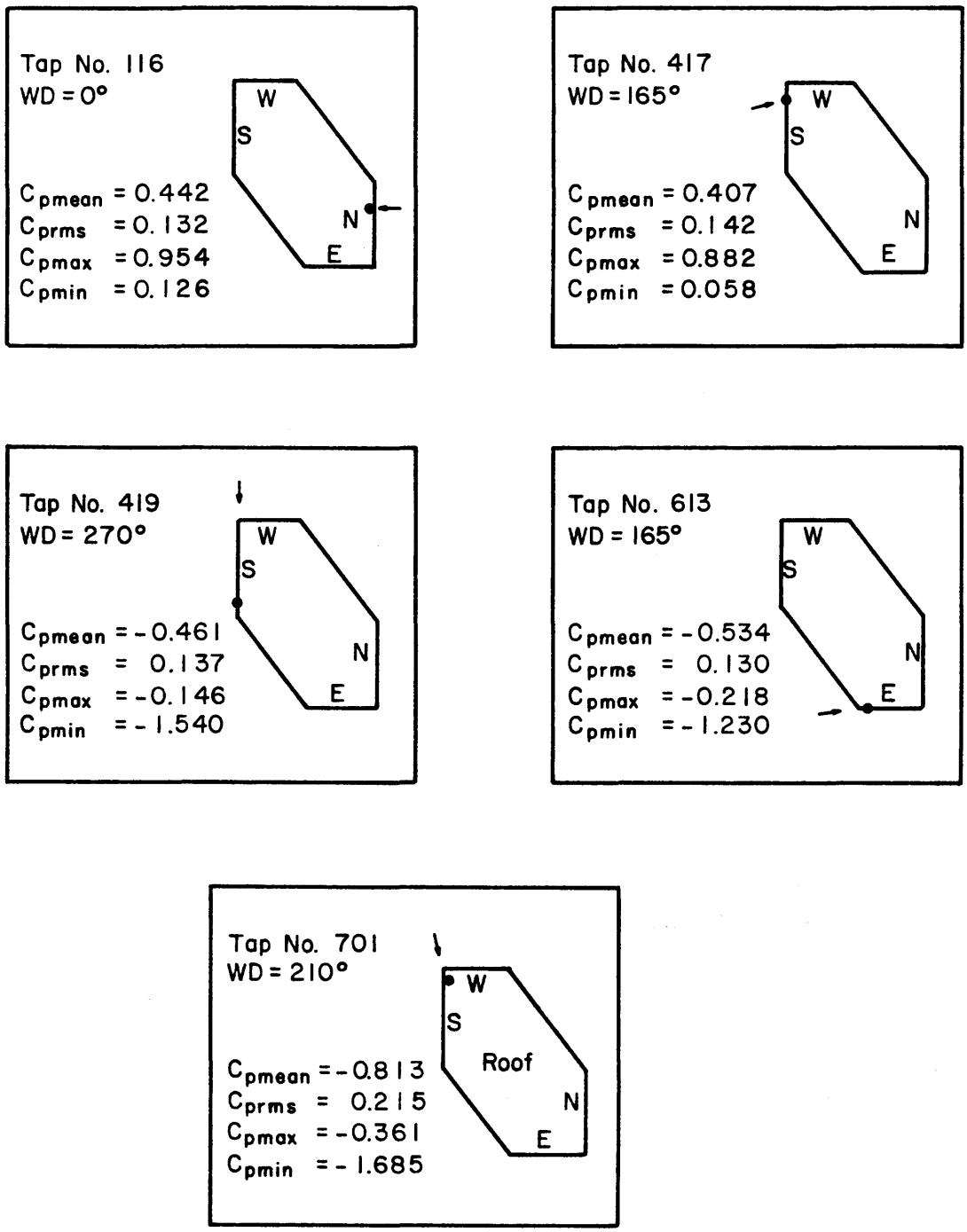


Figure 6.1. General Characteristics of Taps Selected--Mountain Bell Utah State Headquarters Building.

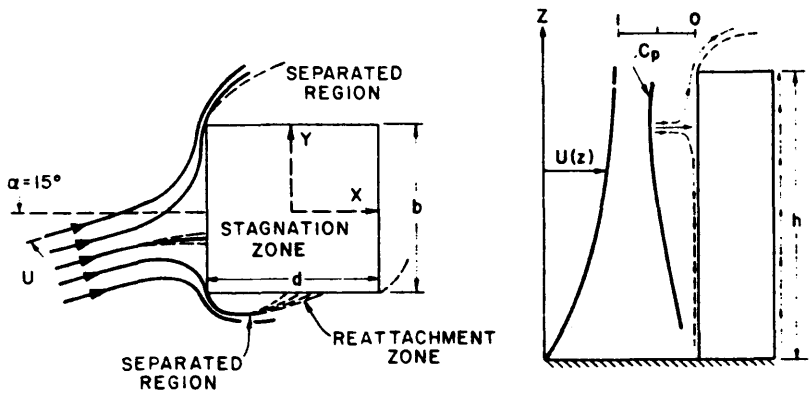


Figure 6.2a. Typical Flow Pattern Around a Tall Block Building in a Boundary-Layer Flow (Cermak, 1976).

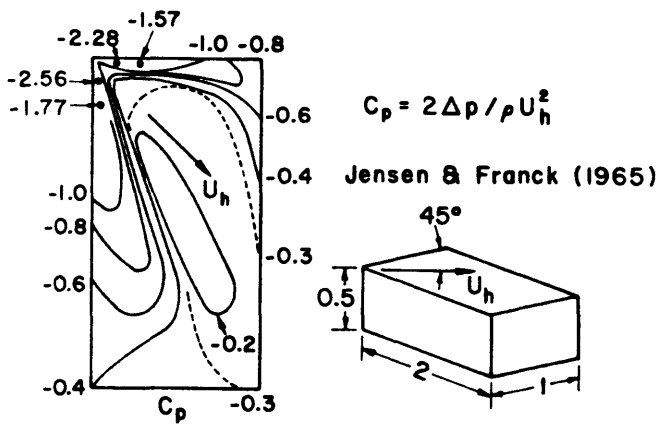


Figure 6.2b. Effect of Vortex Formation on the Mean Pressure Distribution over a Flat-roof Building (Cermak, 1976).

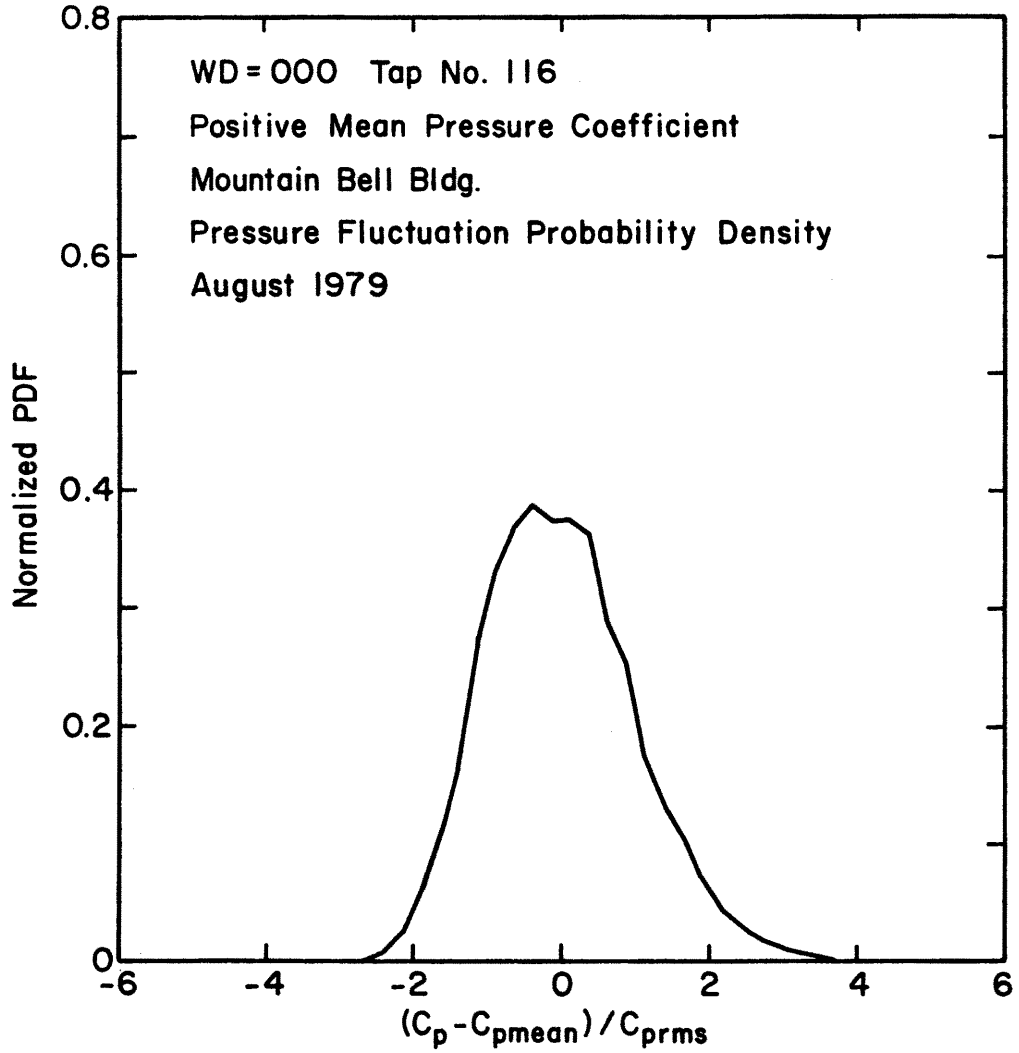


Figure 6.3a. Probability Density for Pressure Fluctuations in Direct Impingement Regions.

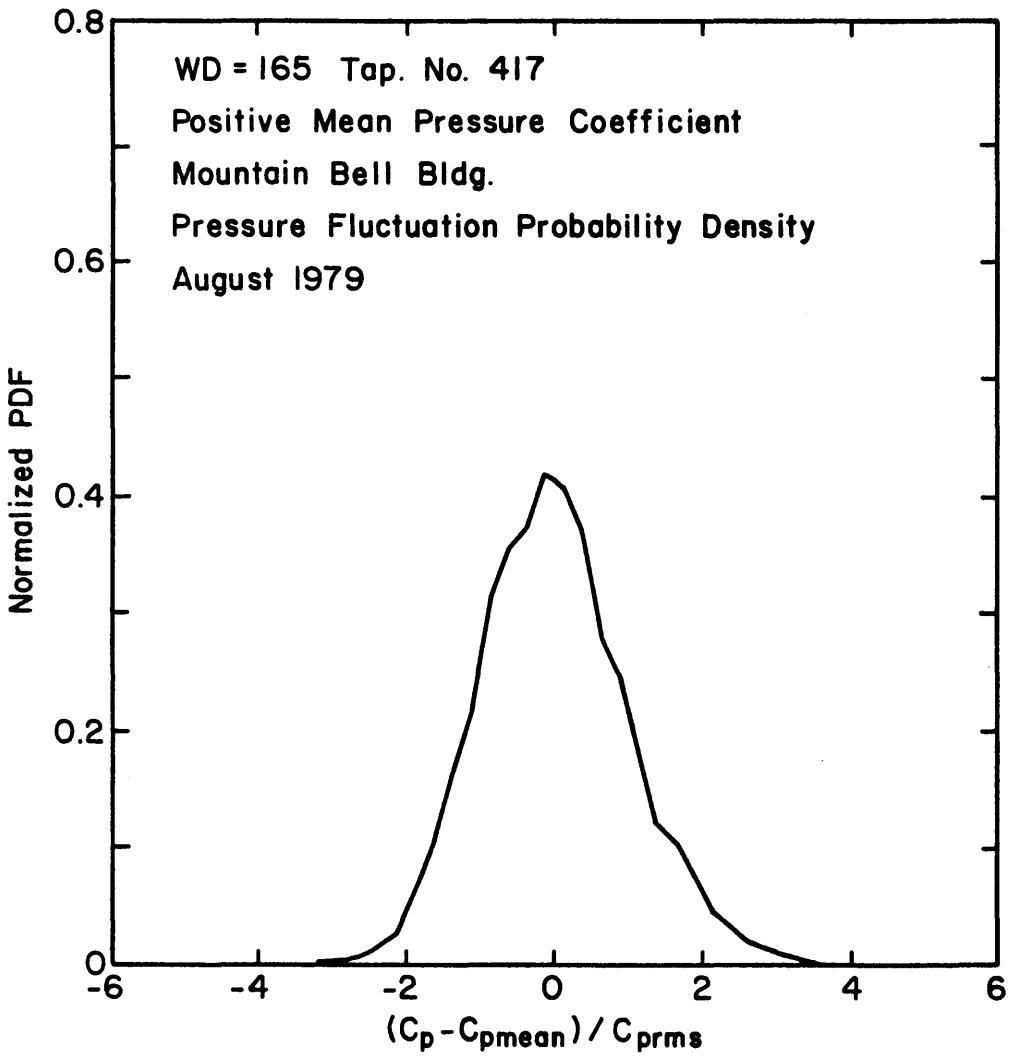


Figure 6.3b. Probability Density for Pressure Fluctuations in Direct Impingement Regions.

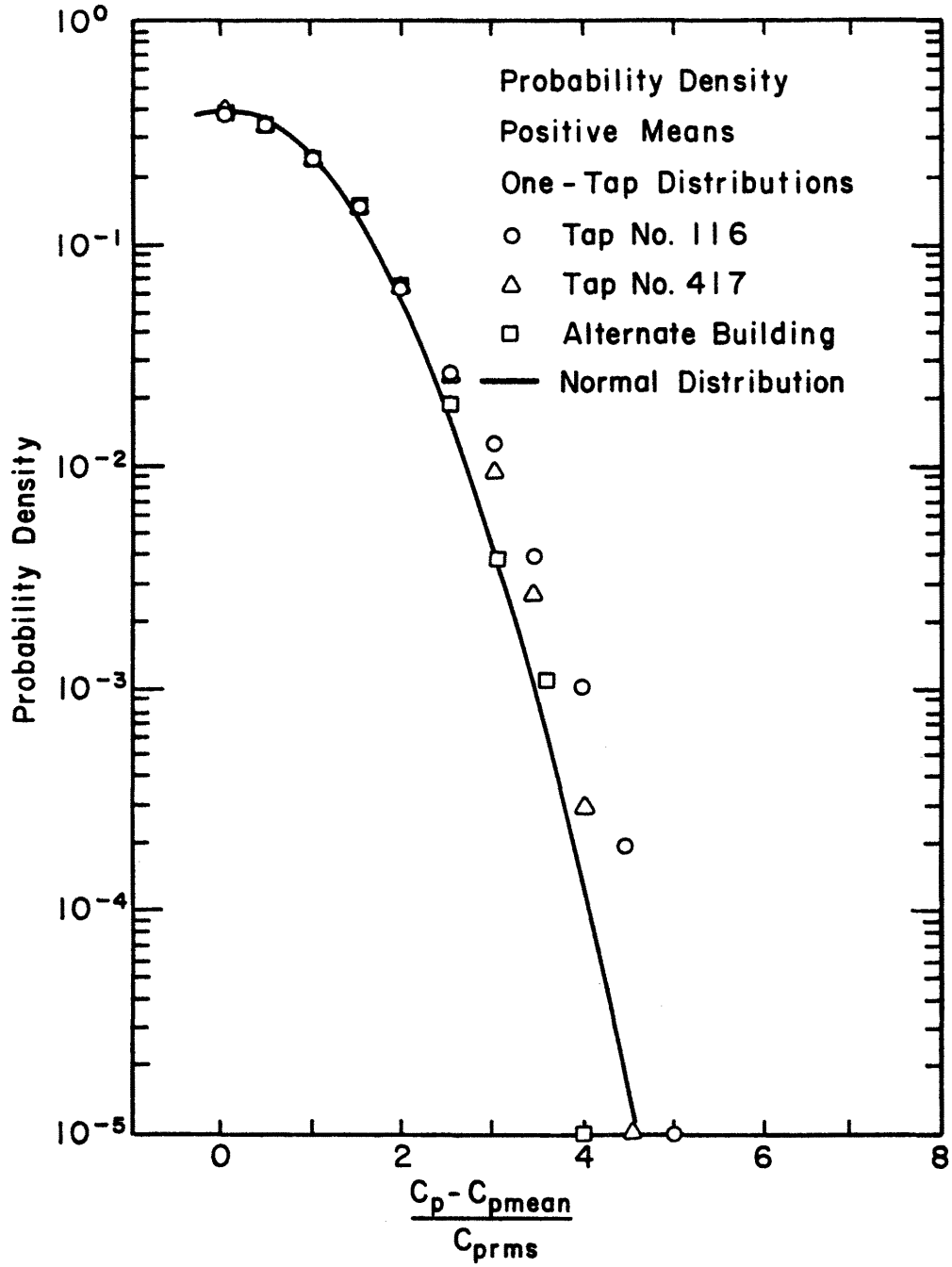


Figure 6.4. Positive Tails of the Probability Densities for Pressure Fluctuations in Direct Impingement Regions.

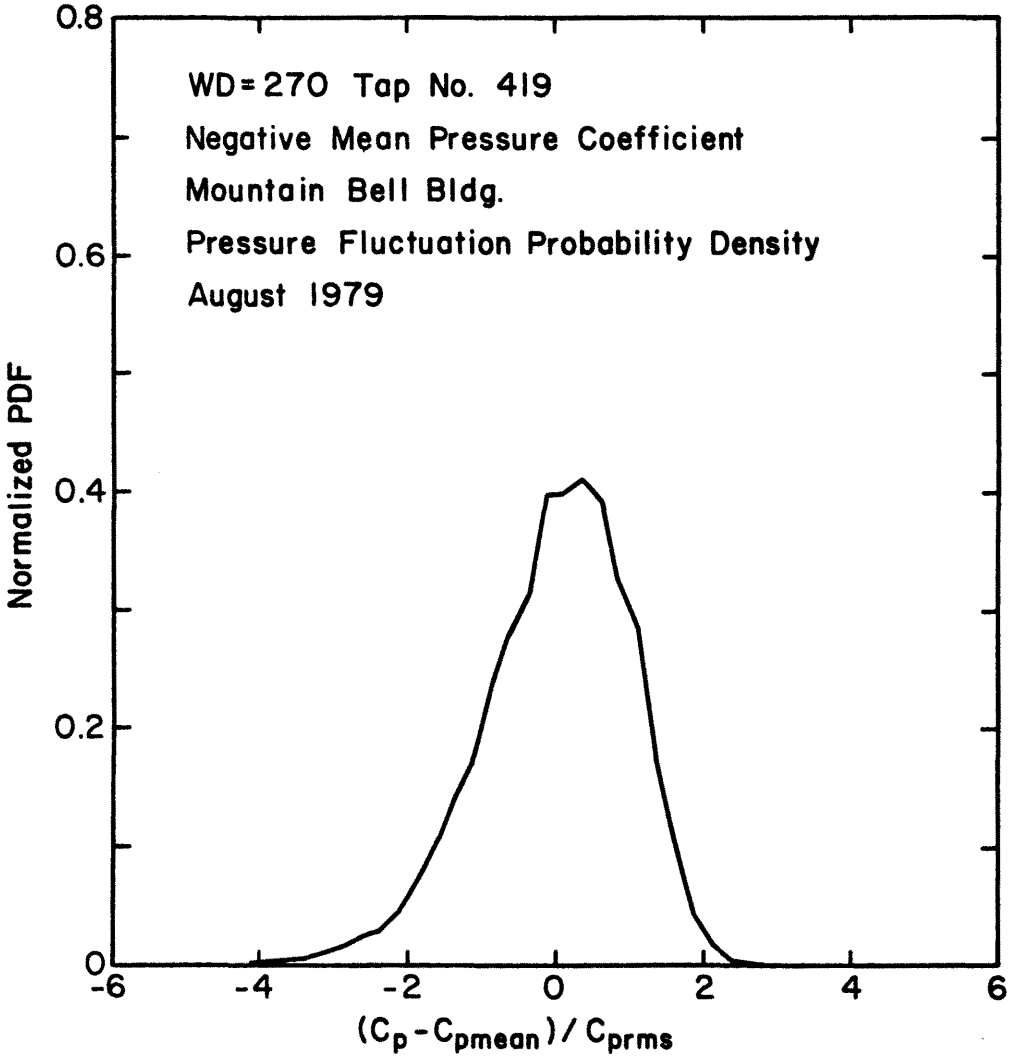


Figure 6.5a. Probability Density for Pressure Fluctuations in Separated Regions.

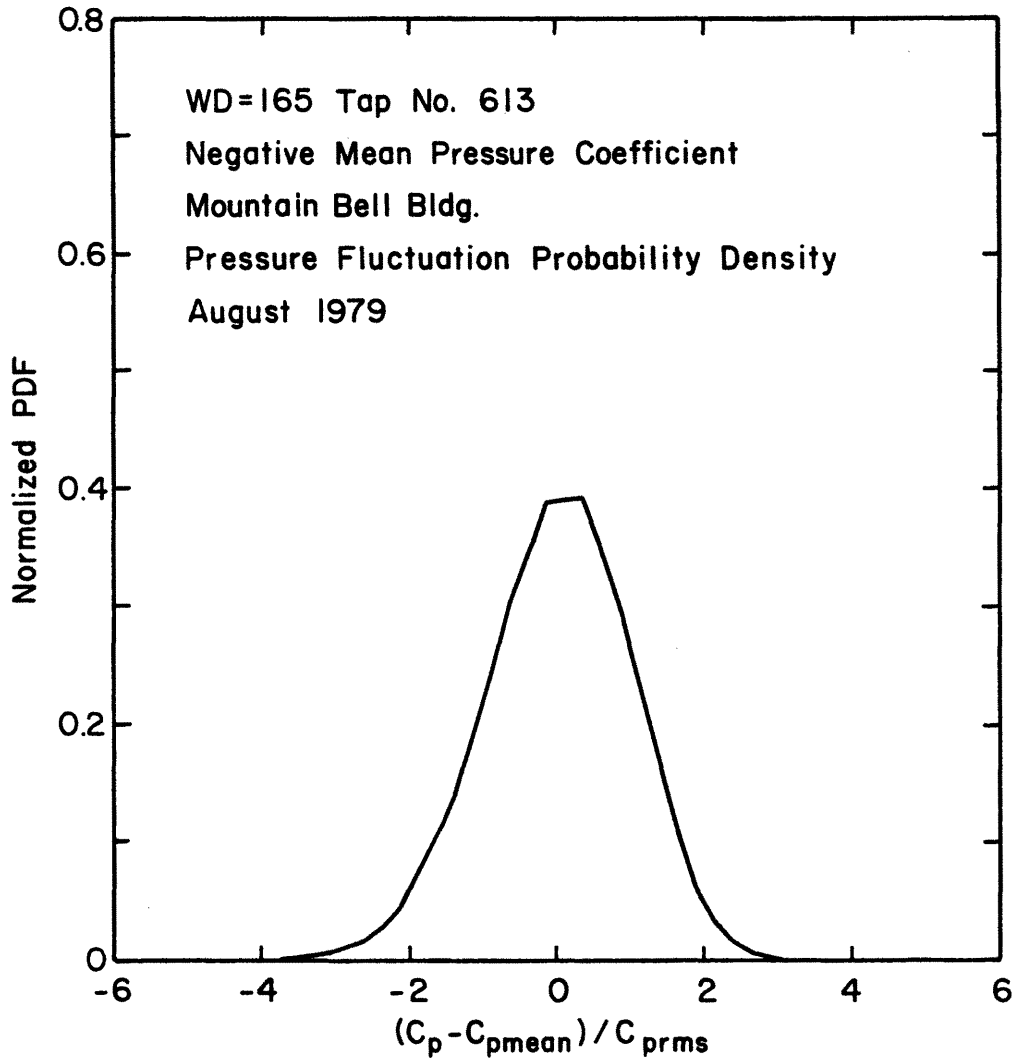


Figure 6.5b. Probability Density for Pressure Fluctuations in Separated Regions.

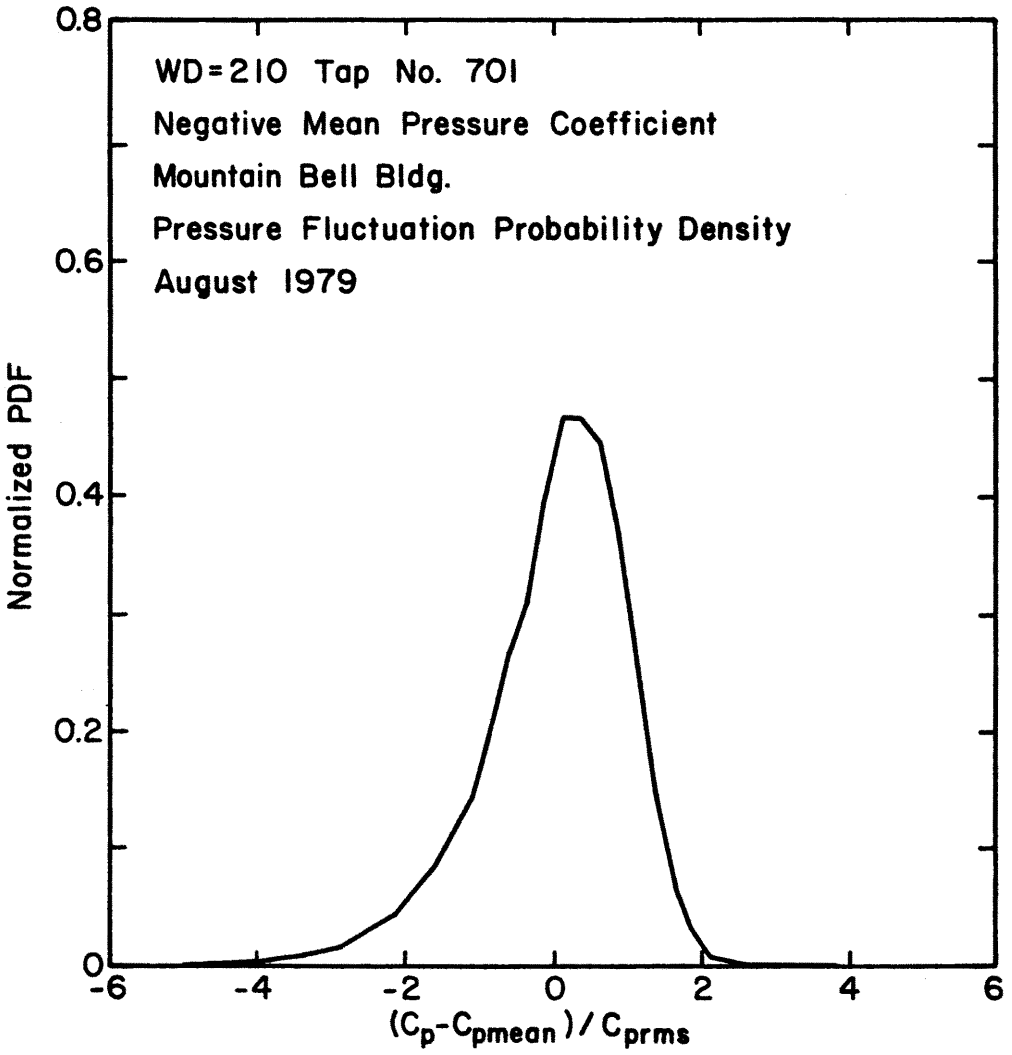


Figure 6.5c. Probability Density for Pressure Fluctuations in Vortex Formation Regions.

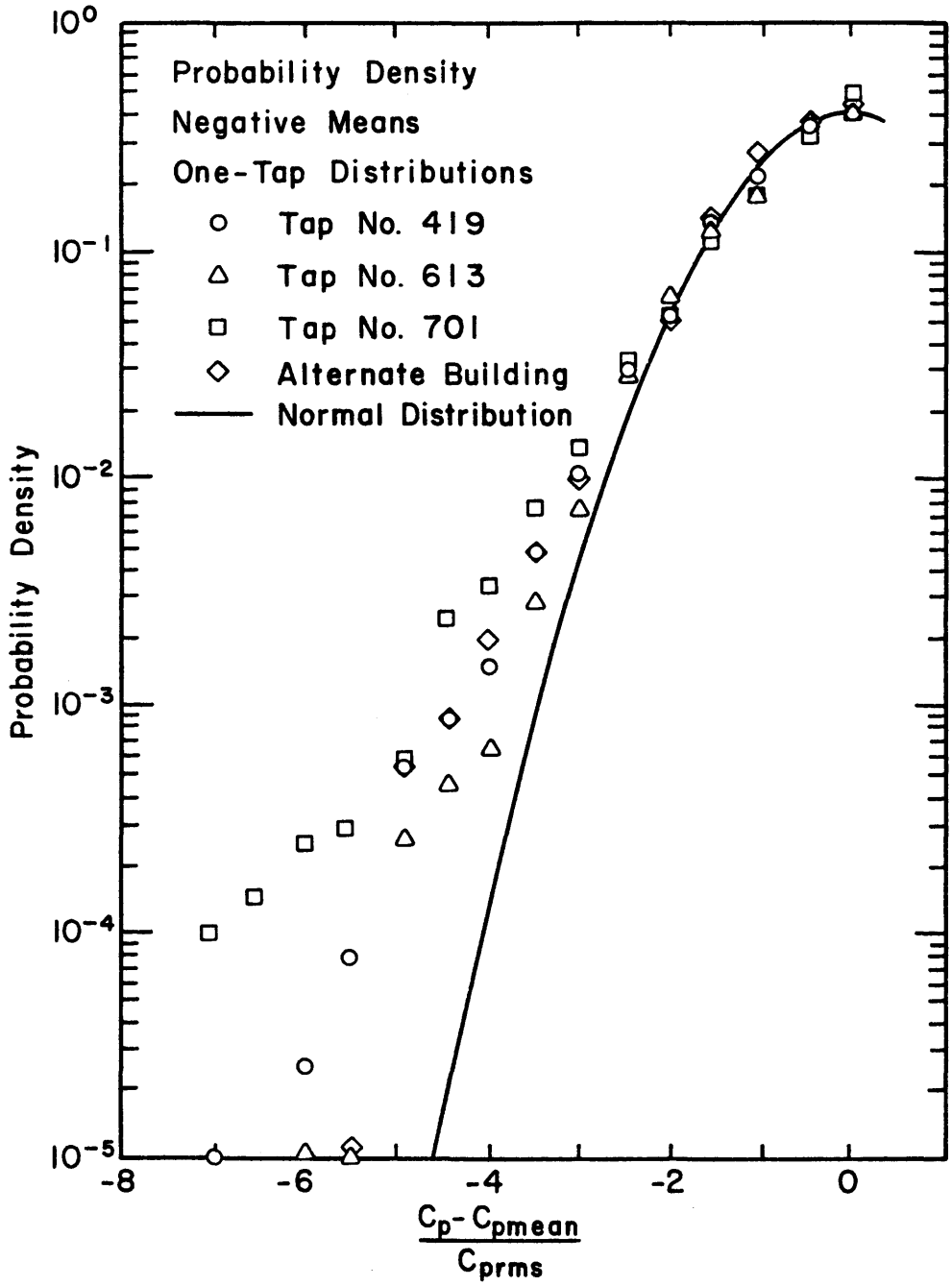


Figure 6.6. Negative Tails of the Probability Densities for Pressure Fluctuations in Separated Regions.

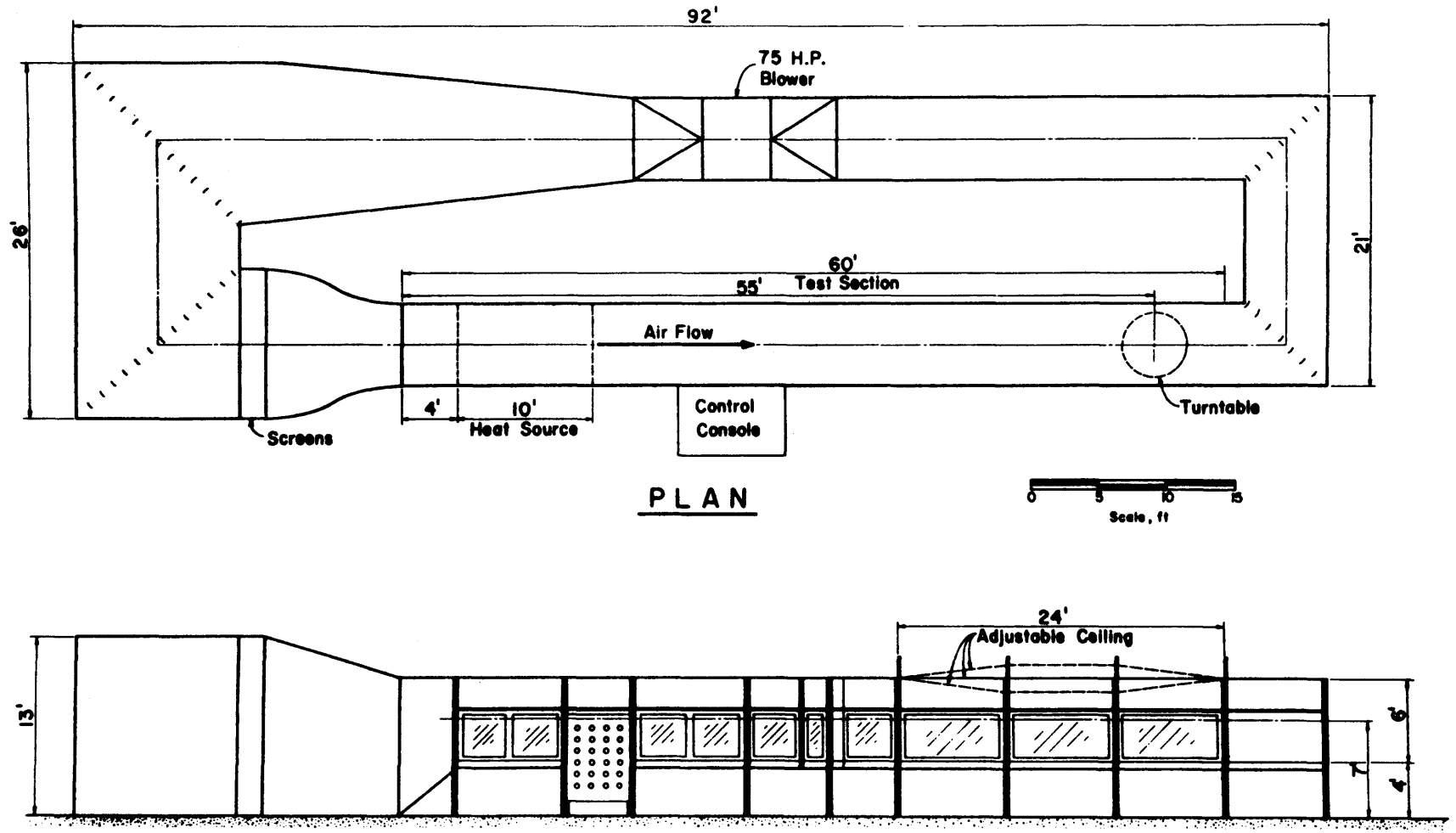


Figure 6.7. Industrial Aerodynamics Wind Tunnel, Fluid Dynamics and Diffusion Laboratory, Colorado State University.

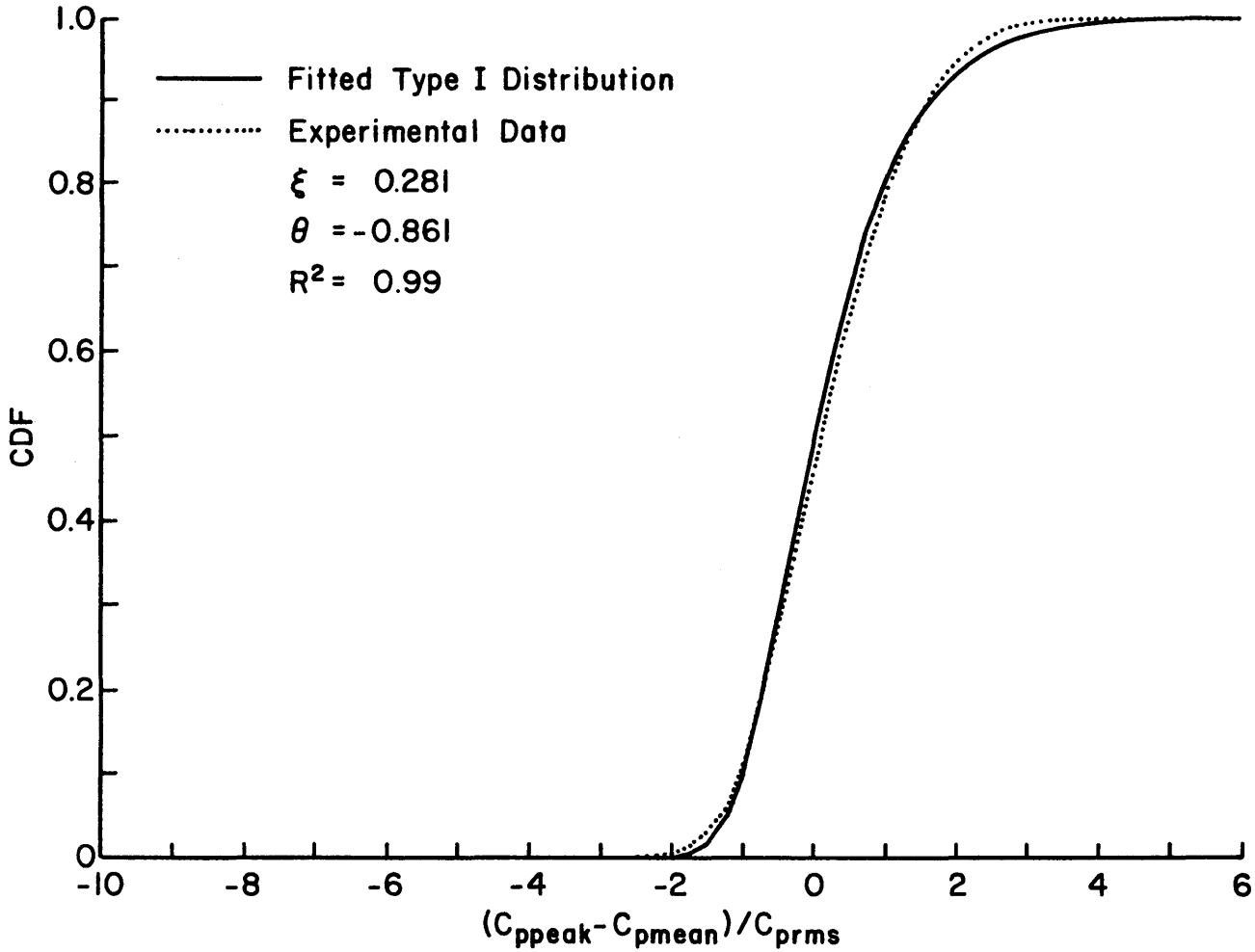


Figure 6.8a. Distribution of Continuous Peaks for WD=000, Tap No. 116.

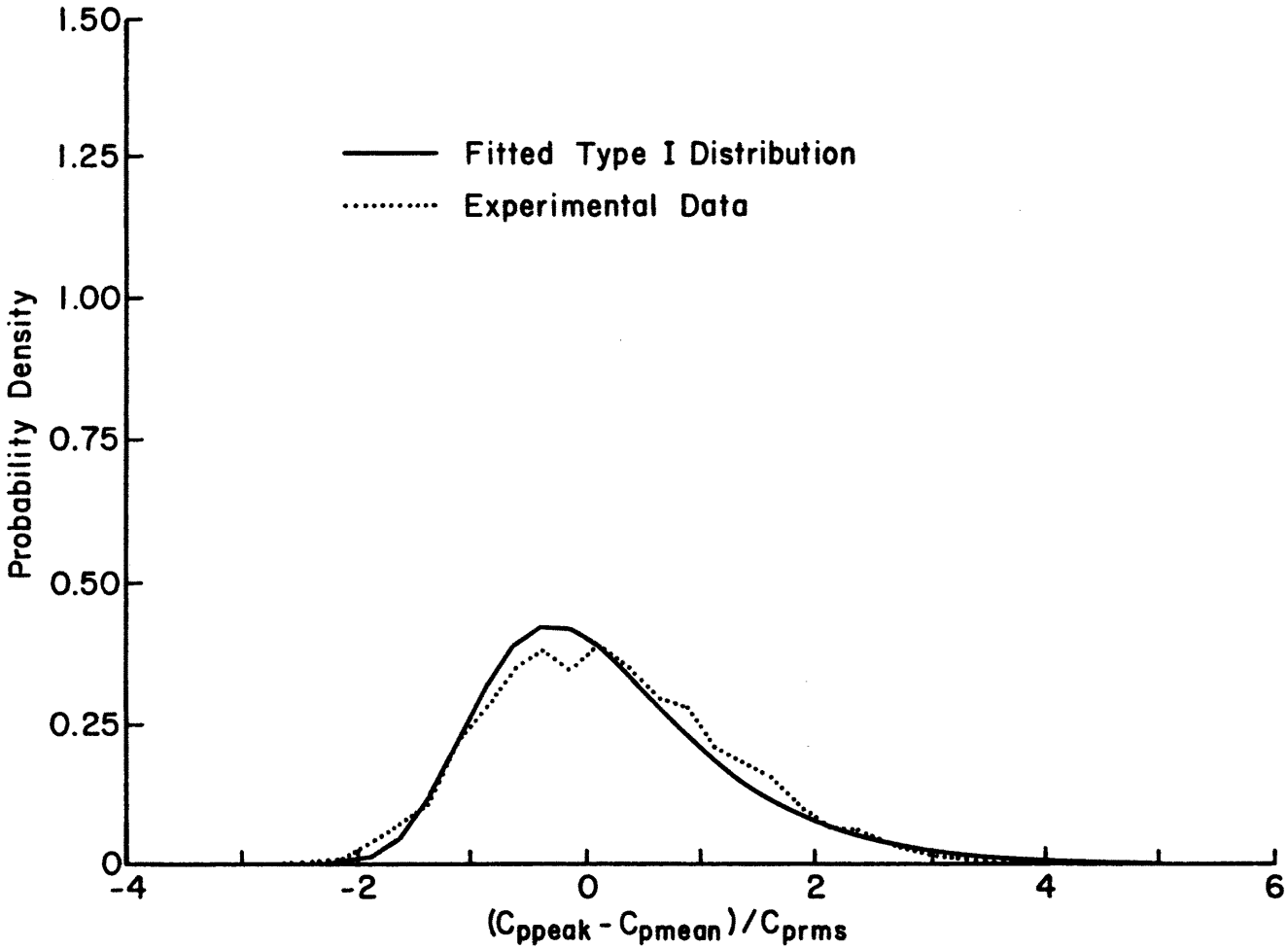


Figure 6.8b. Distribution of Continuous Peaks for WD=000, Tap No. 116.

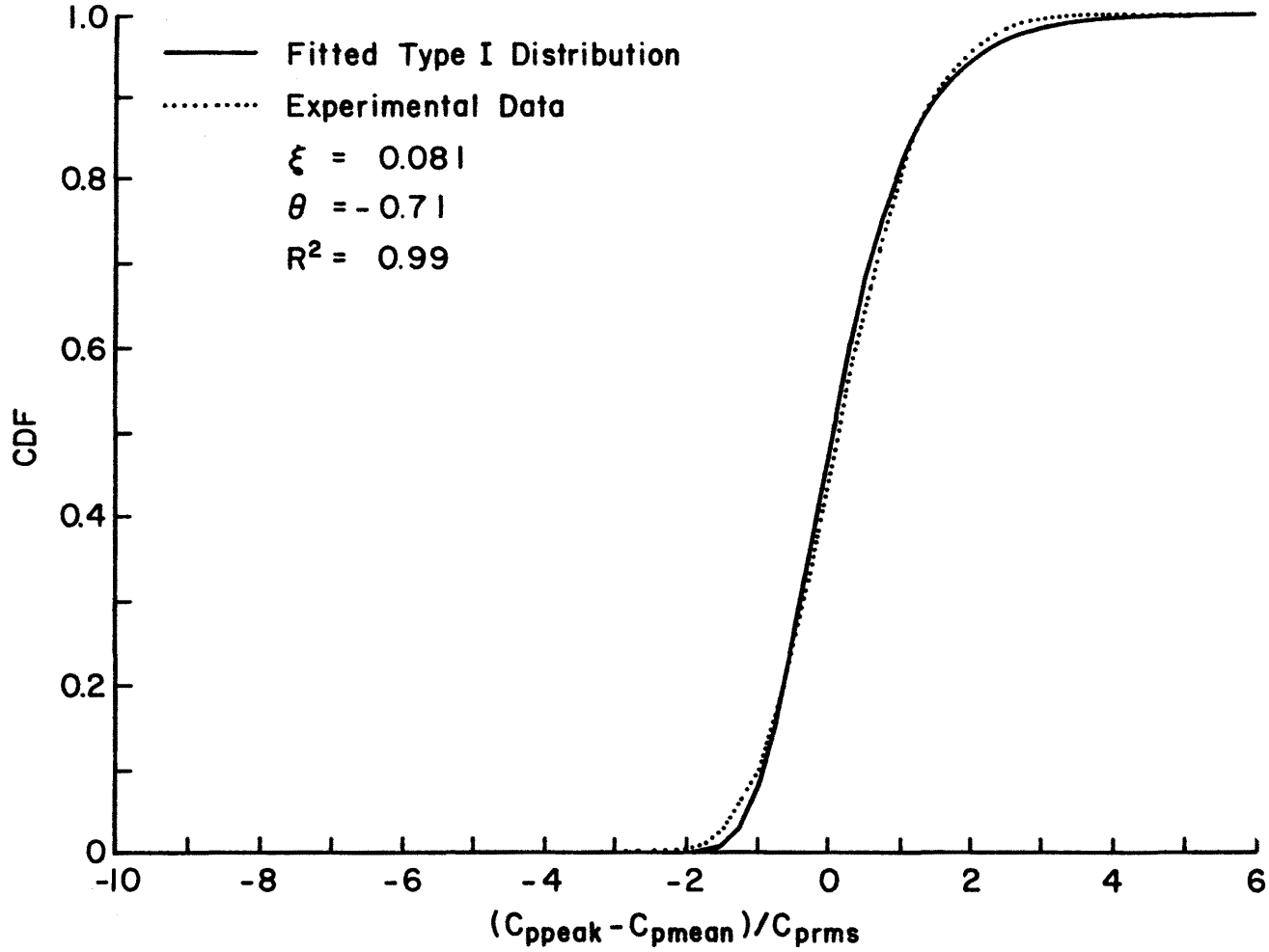


Figure 6.8c. Distribution of Continuous Peaks for WD=165, Tap No. 417.

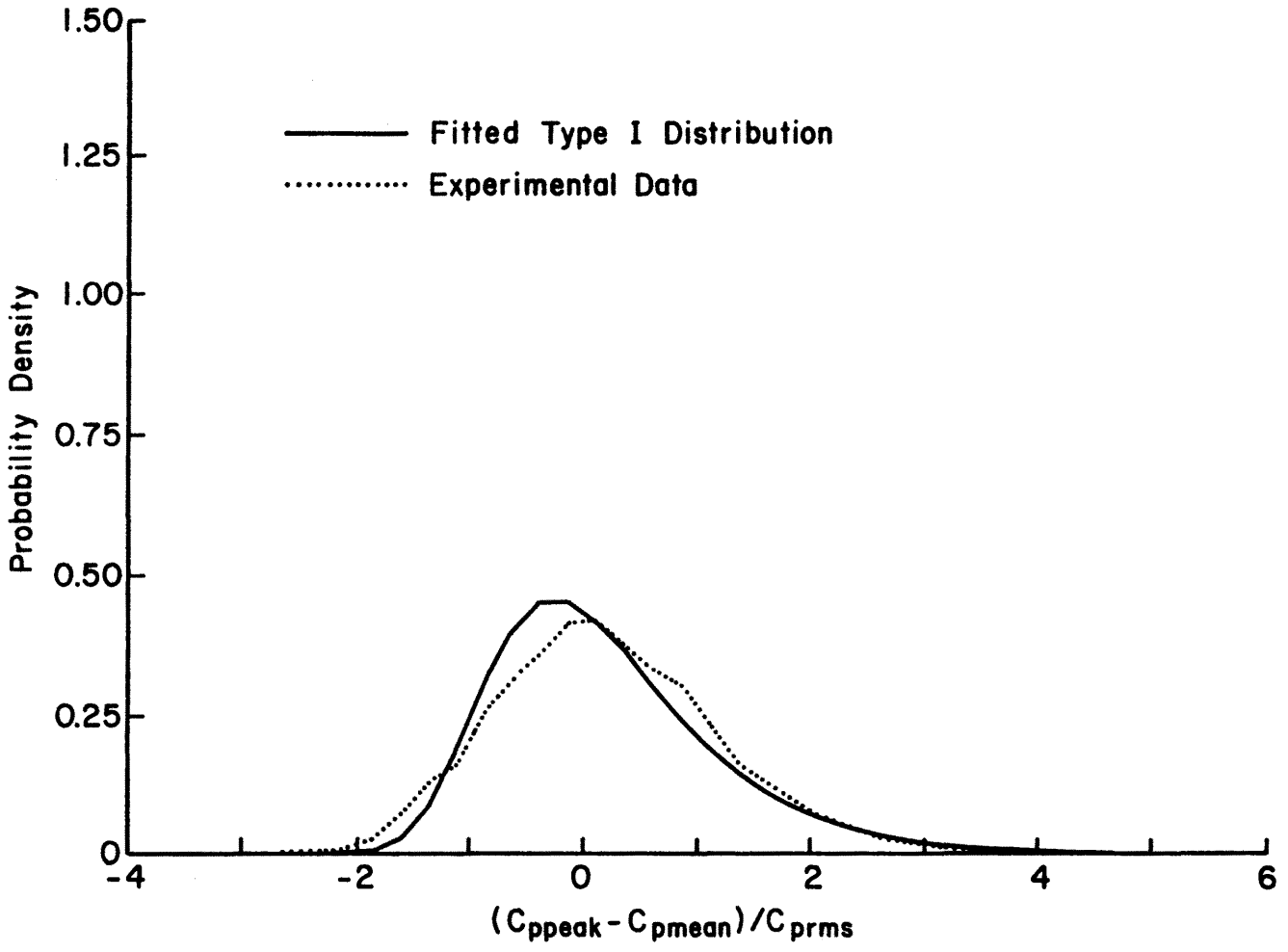


Figure 6.8d. Distribution of Continuous Peaks for WD=165, Tap No. 417.

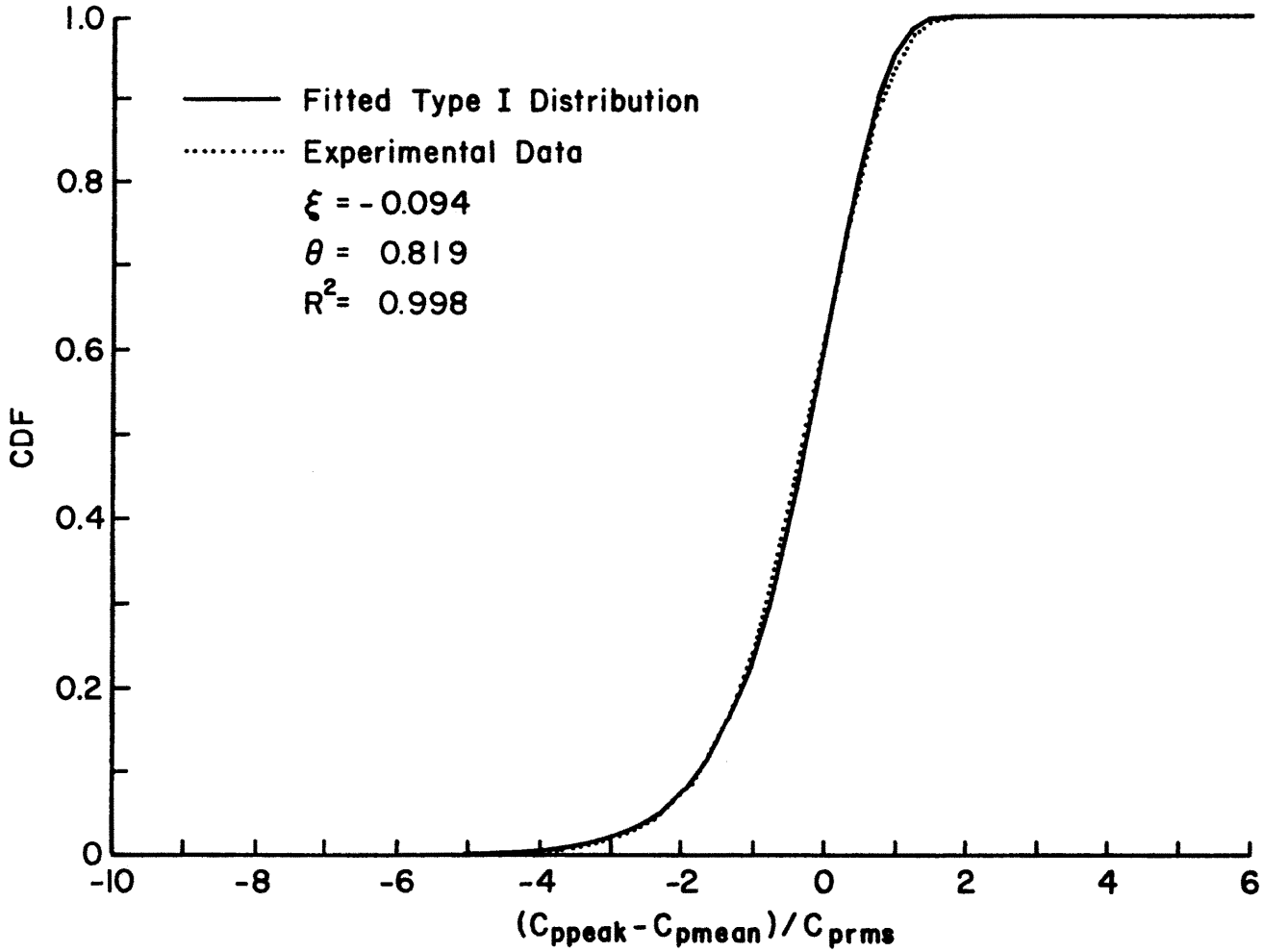


Figure 6.8e. Distribution of Continuous Peaks for WD=270, Tap No. 419.

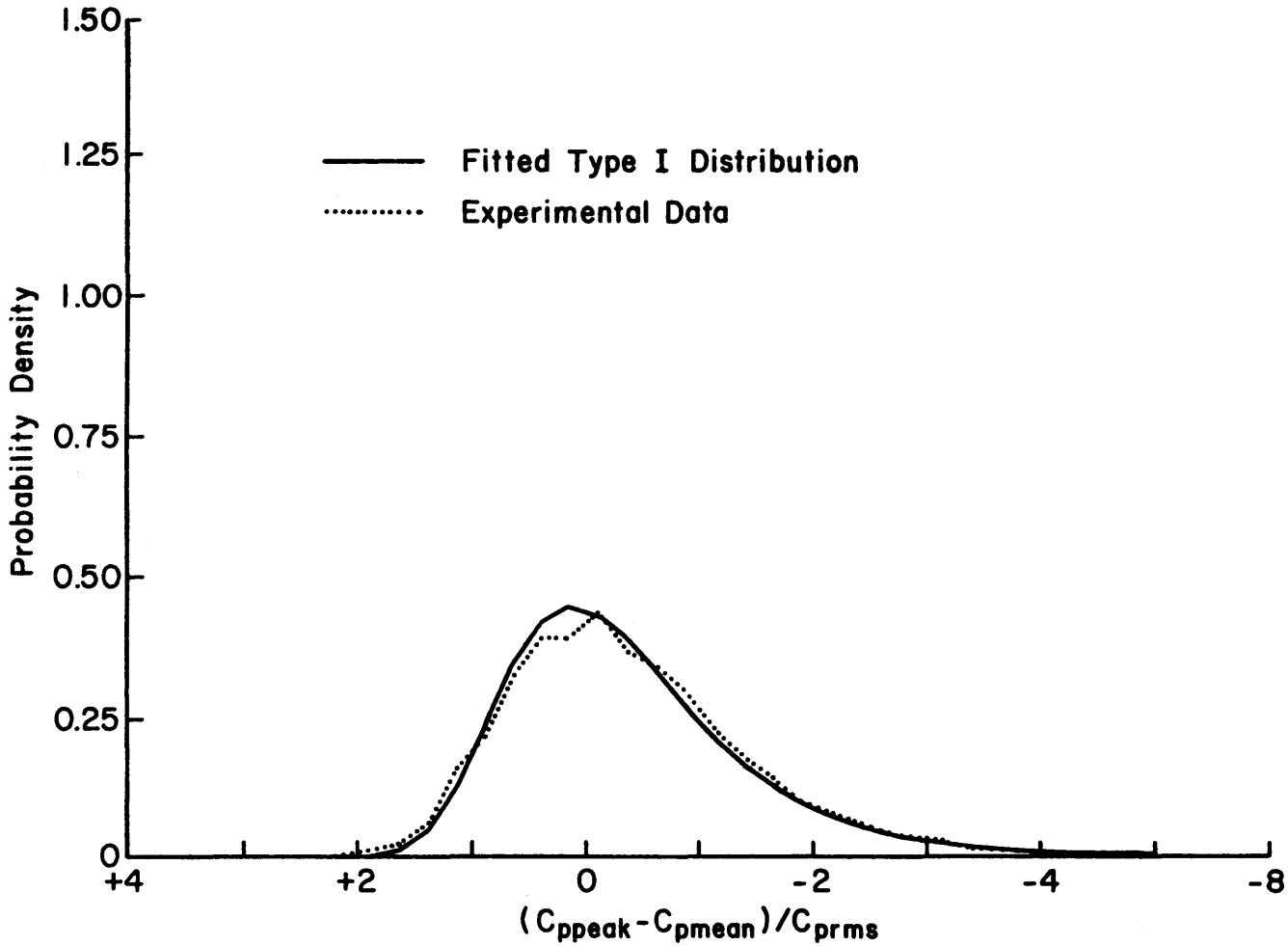


Figure 6.8f. Distribution of Continuous Peaks for WD=270, Tap No. 419.

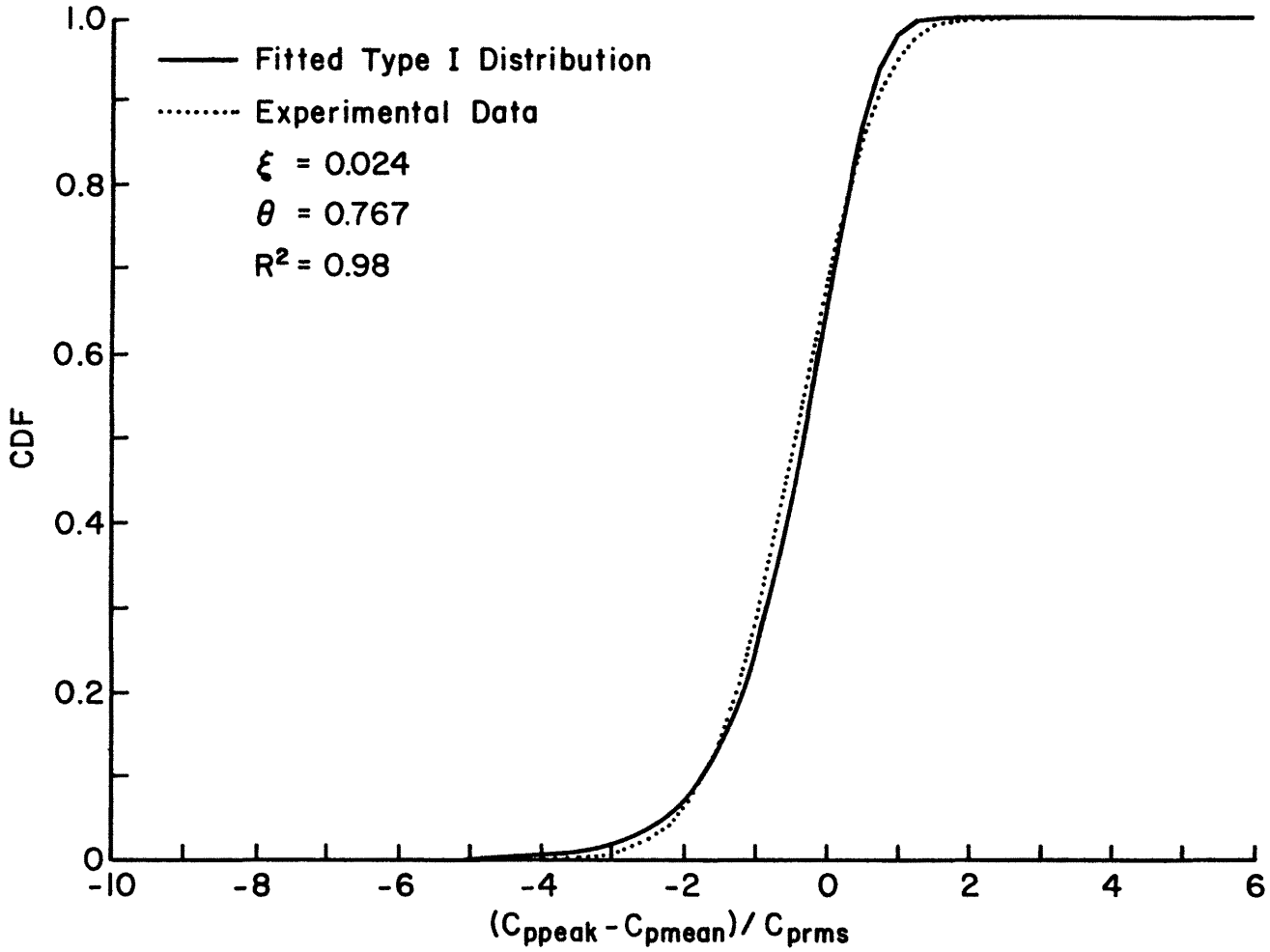


Figure 6.8g. Distribution of Continuous Peaks for WD=165, Tap No. 613.

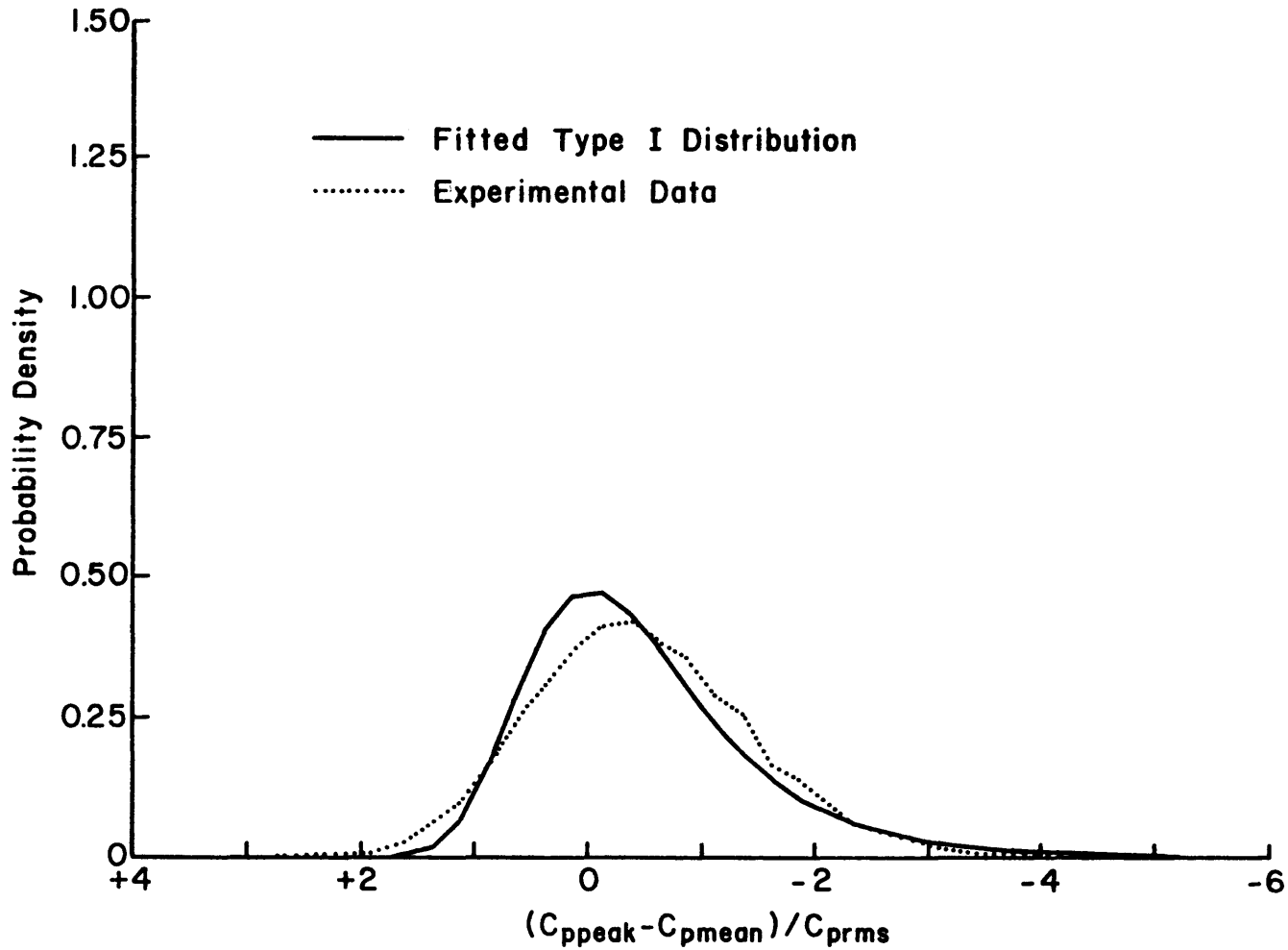


Figure 6.8h. Distribution of Continuous Peaks for WD=165, Tap No. 613.

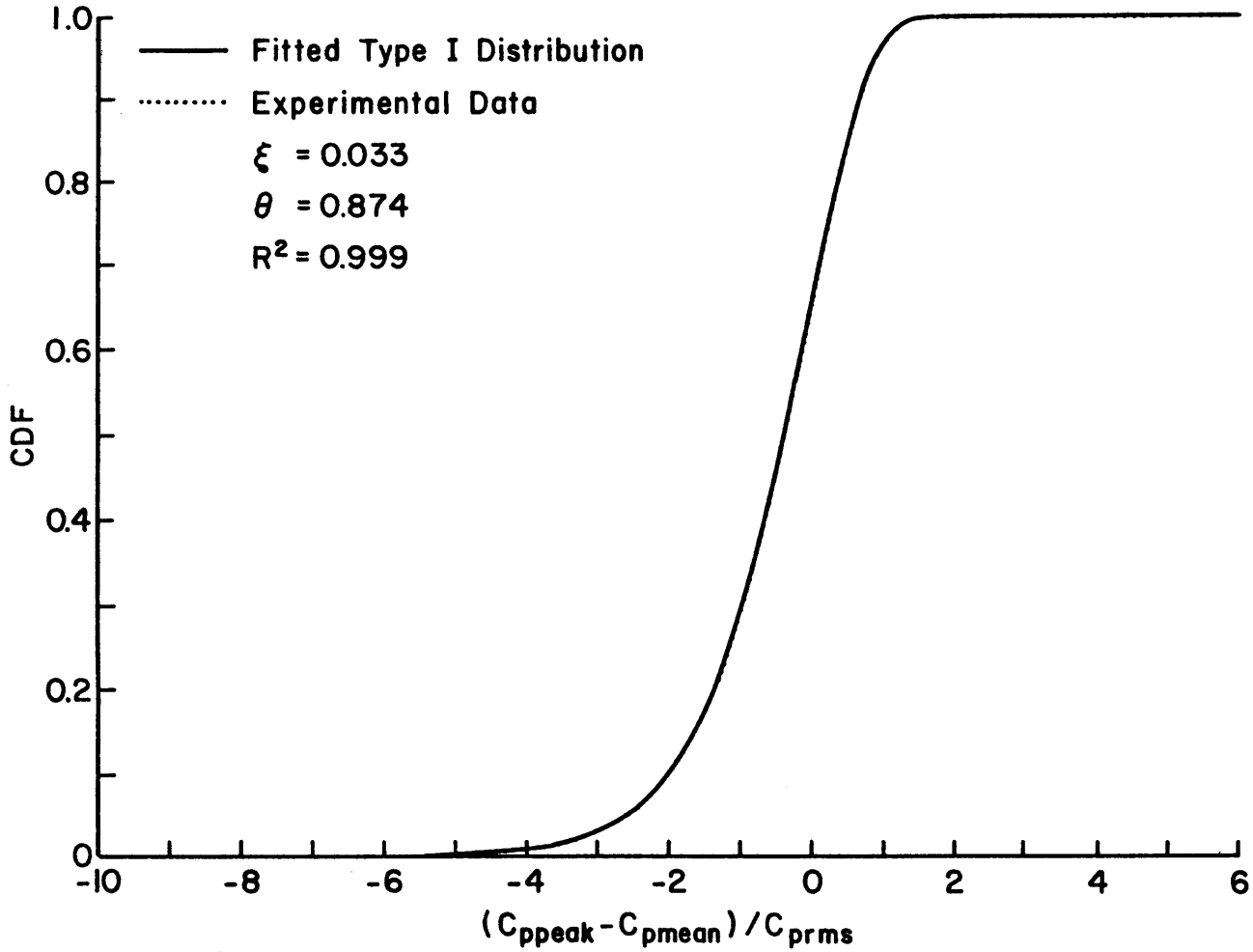


Figure 6.8i. Distribution of Continuous Peaks for WD=210, Tap No. 701.

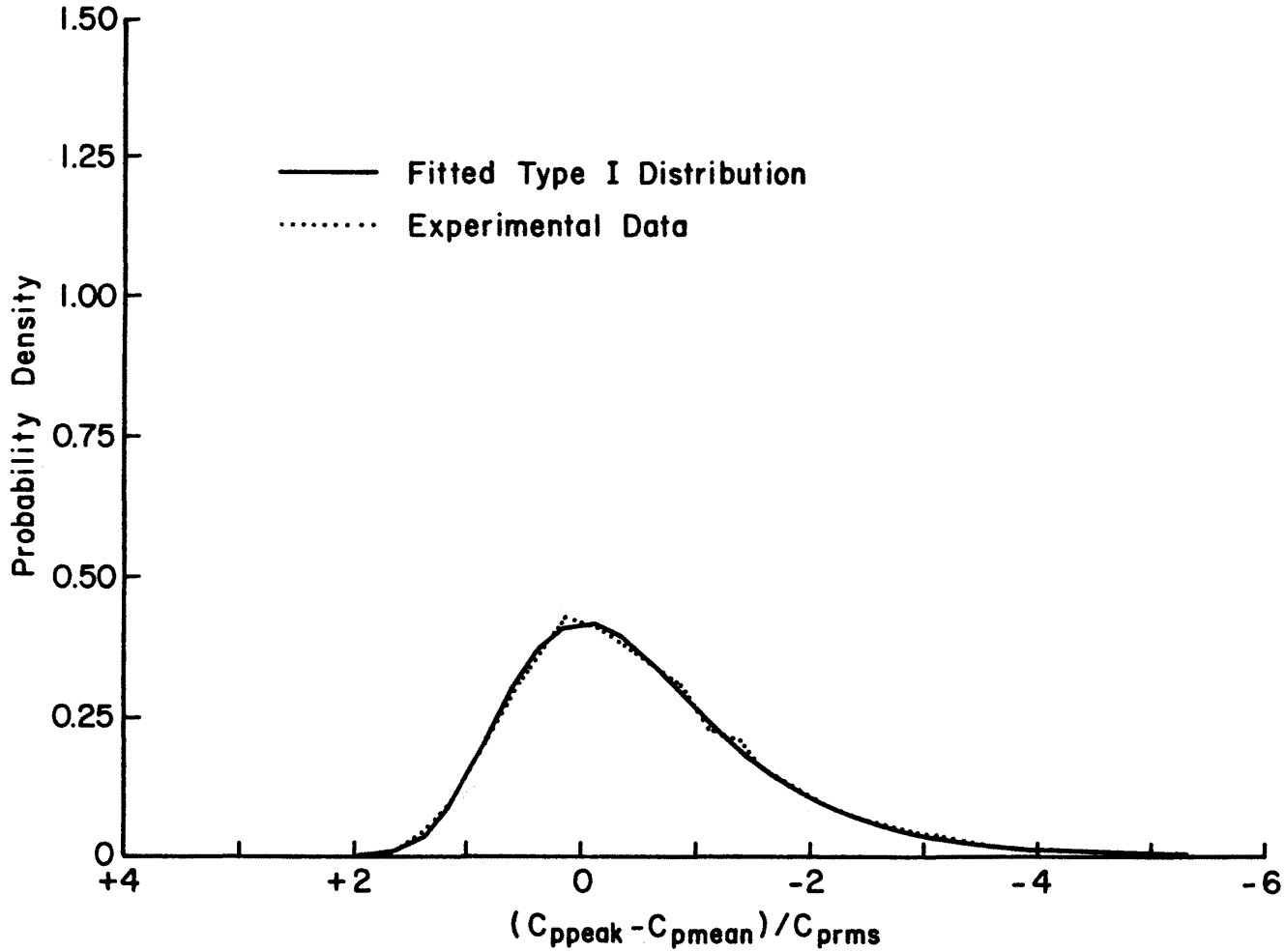


Figure 6.8j. Distribution of Continuous Peaks for WD=210, Tap No. 701.

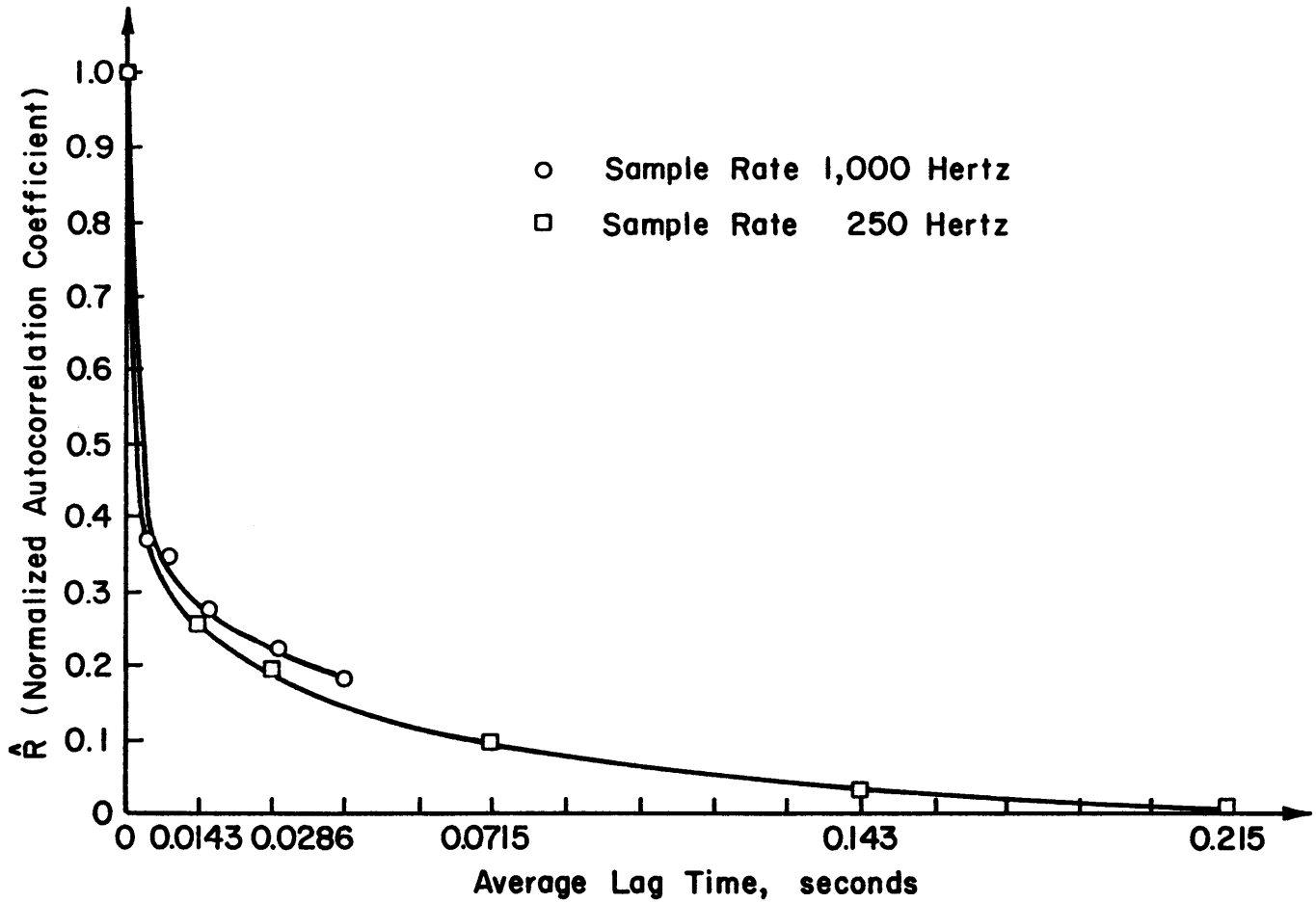


Figure 6.9 Normalized Autocorrelation Coefficients between Continuous Peaks at Various Lag Times, shown for Tap 701.

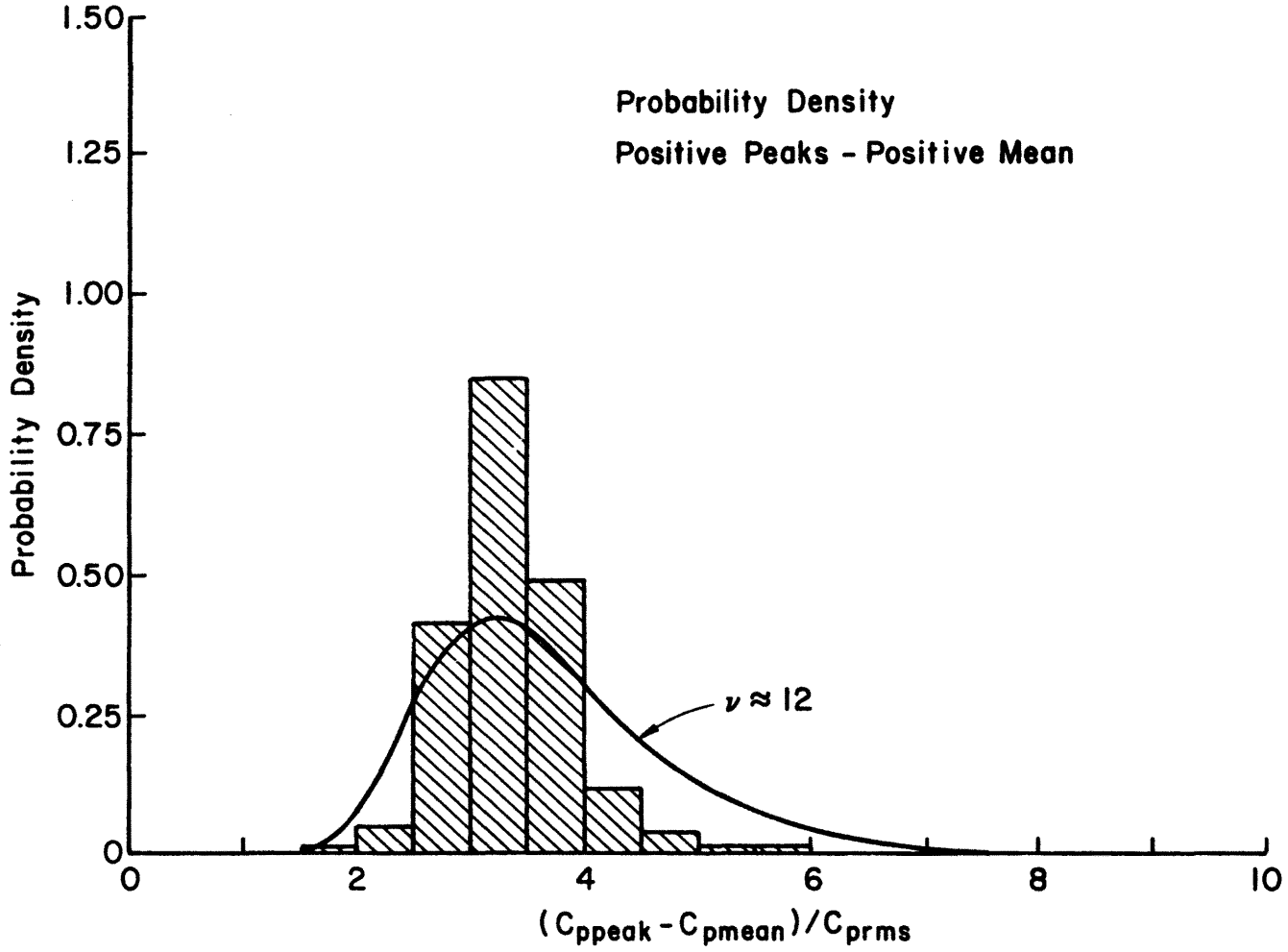


Figure 6.10a. Experimental Extreme Value Distribution for WD=000, Tap No. 116 (in histogram) and the Shifted Distribution of Continuous Peaks.

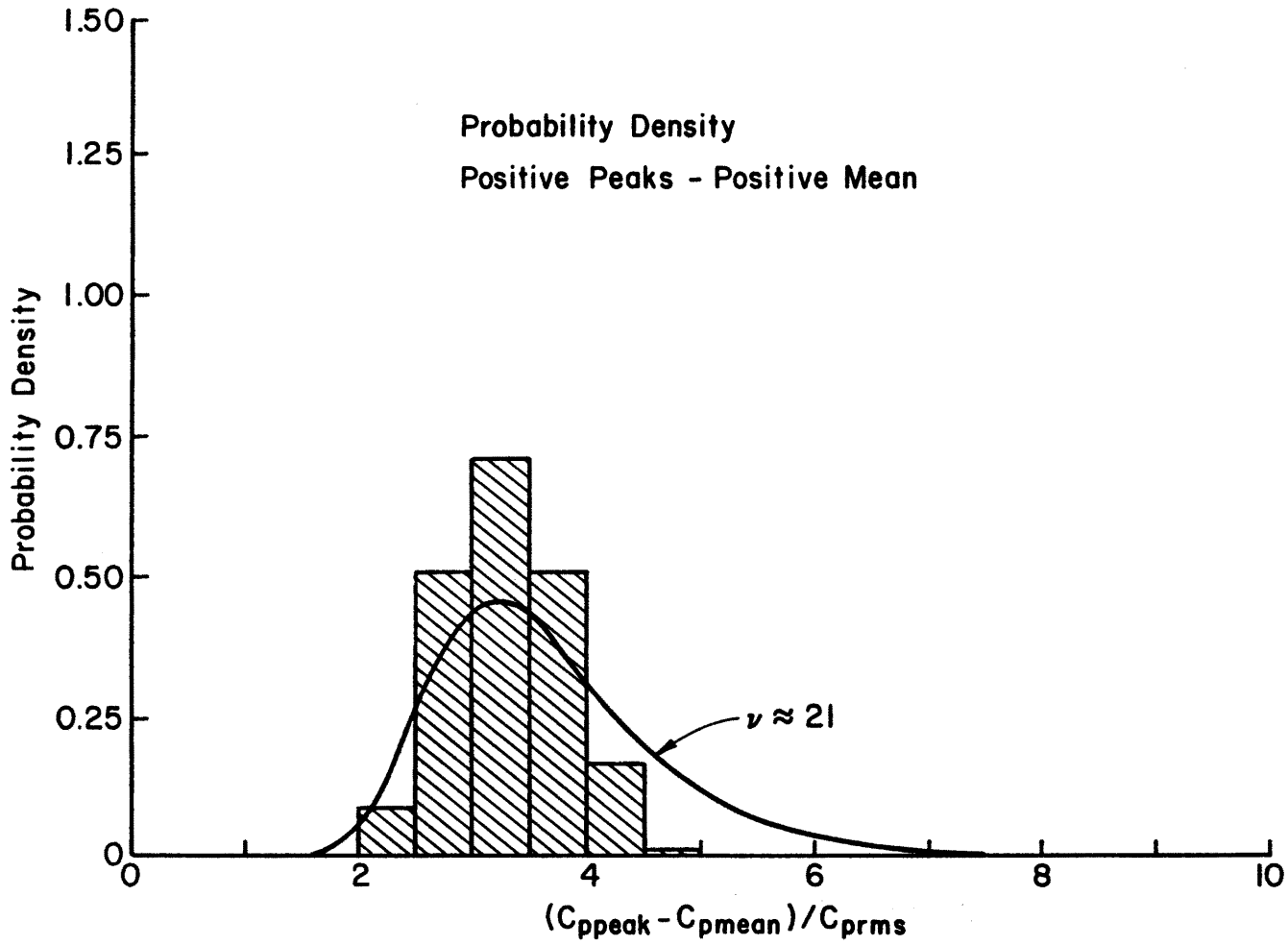


Figure 6.10b. Experimental Extreme Value Distribution for WD=165, Tap No. 417 (in histogram) and the Shifted Distribution of Continuous Peaks.

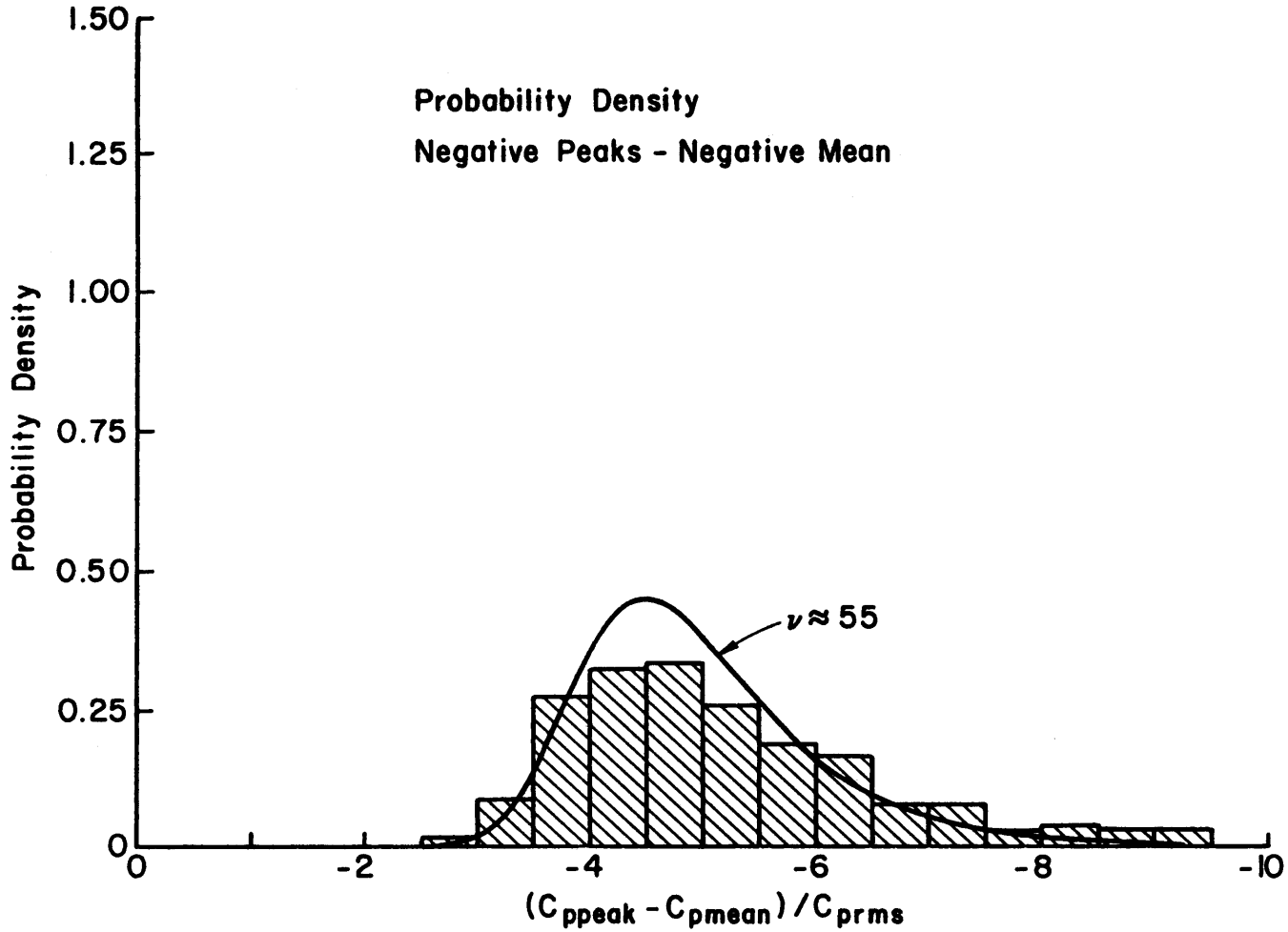


Figure 6.10c. Experimental Extreme Value Distribution for WD=270, Tap No. 419 (in histogram) and the Shifted Distribution of Continuous Peaks.

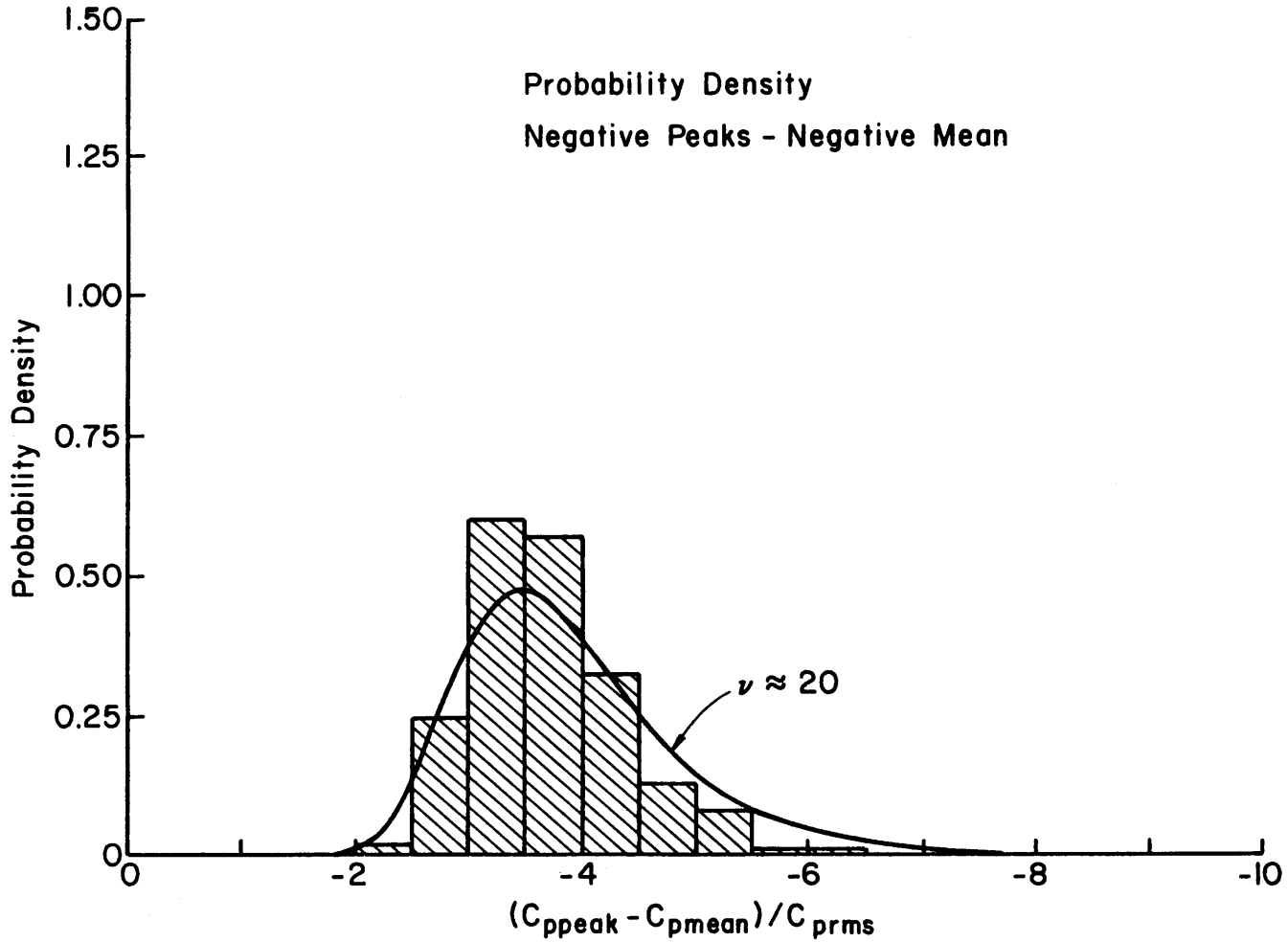


Figure 6.10d. Experimental Extreme Value Distribution for WD=165, Tap No. 613 (in historgram) and the Shifted Distribution of Continuous Peaks.

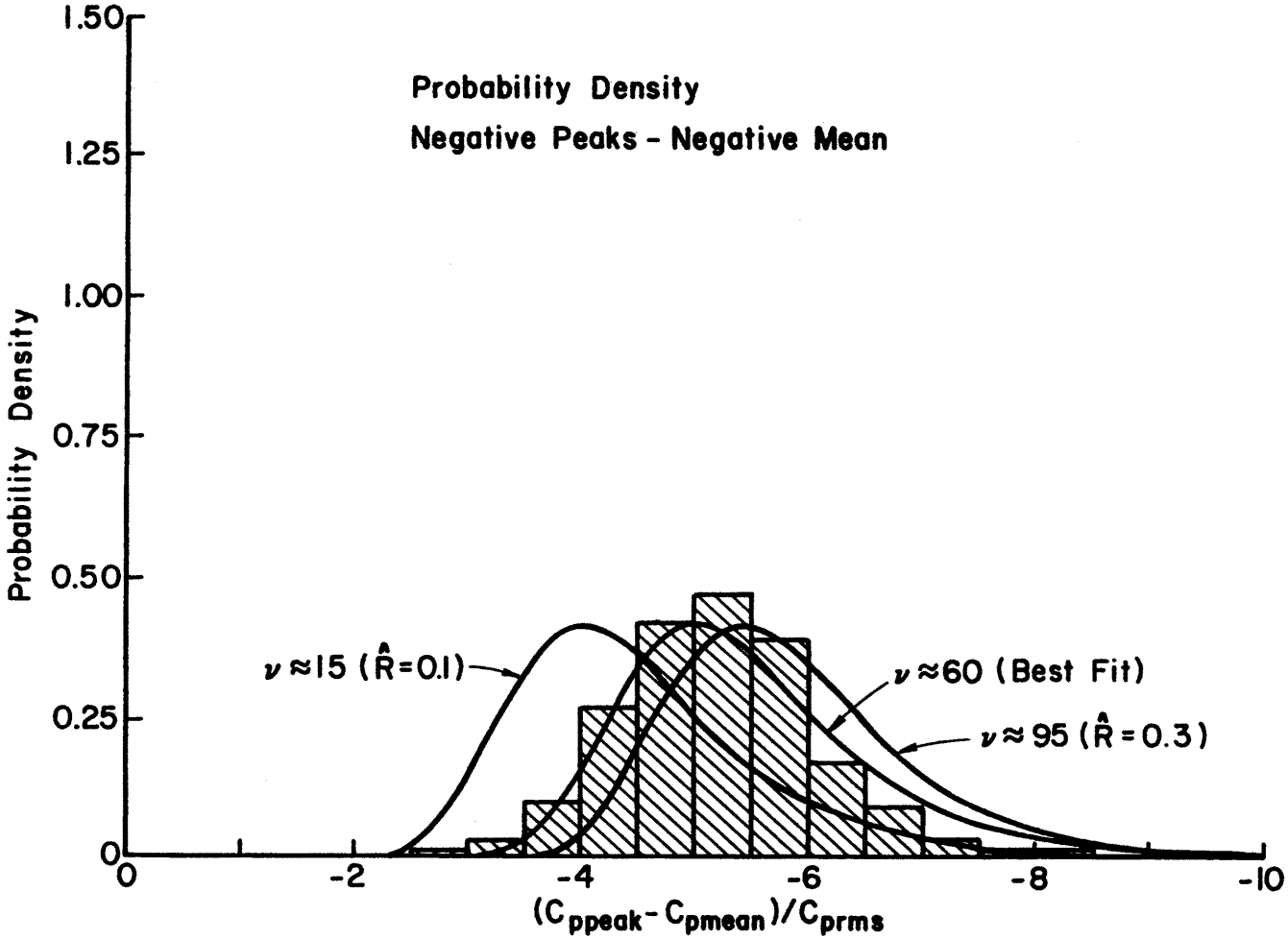


Figure 6.10e. Experimental Extreme Value Distribution for WD=210, Tap No. 701 (in histogram) and the Shifted Distribution of Continuous Peaks.

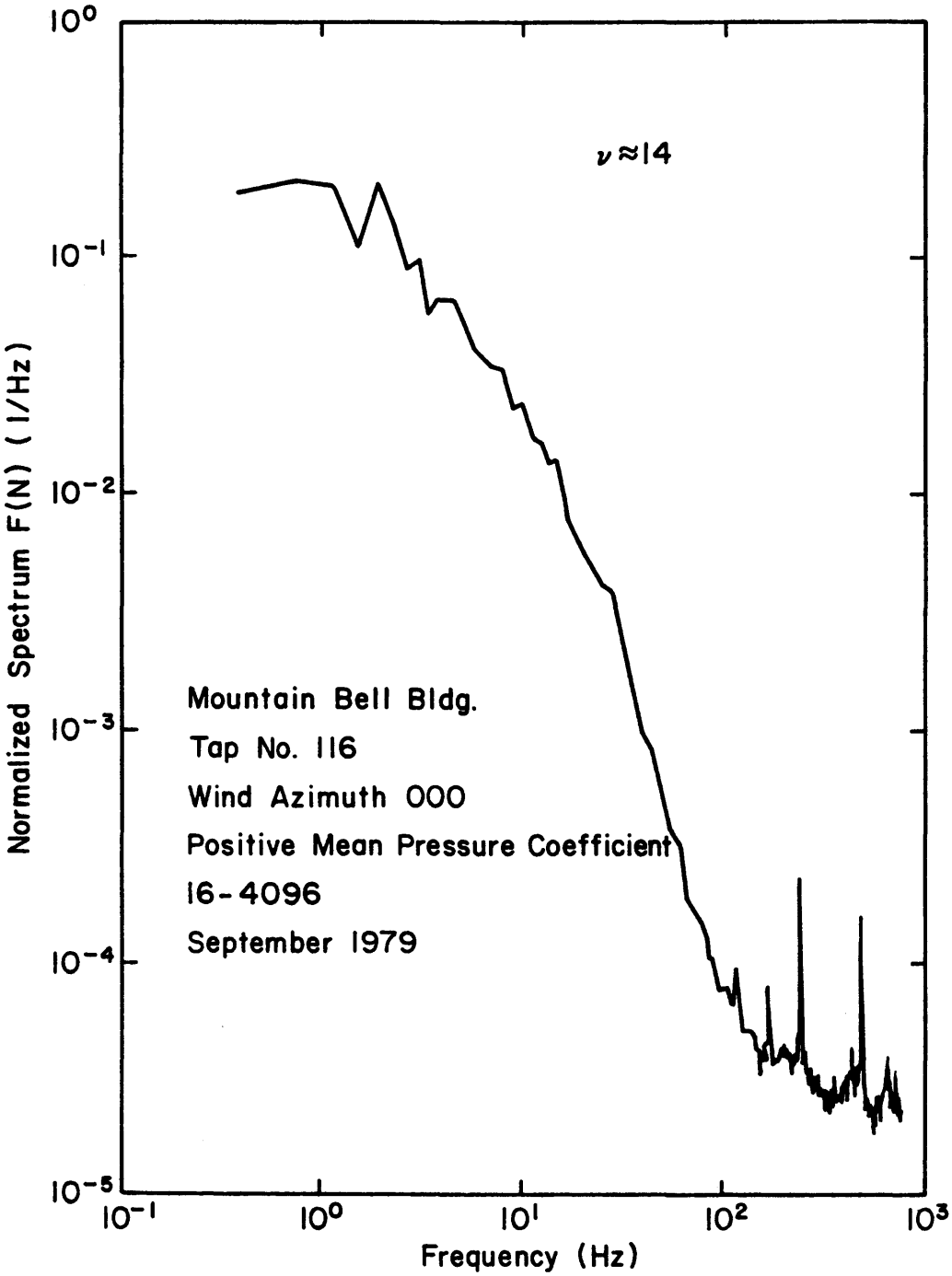


Figure 6.11a. Power Spectral Density Function of Pressure Fluctuations (Positive $Cp_{mean}$).

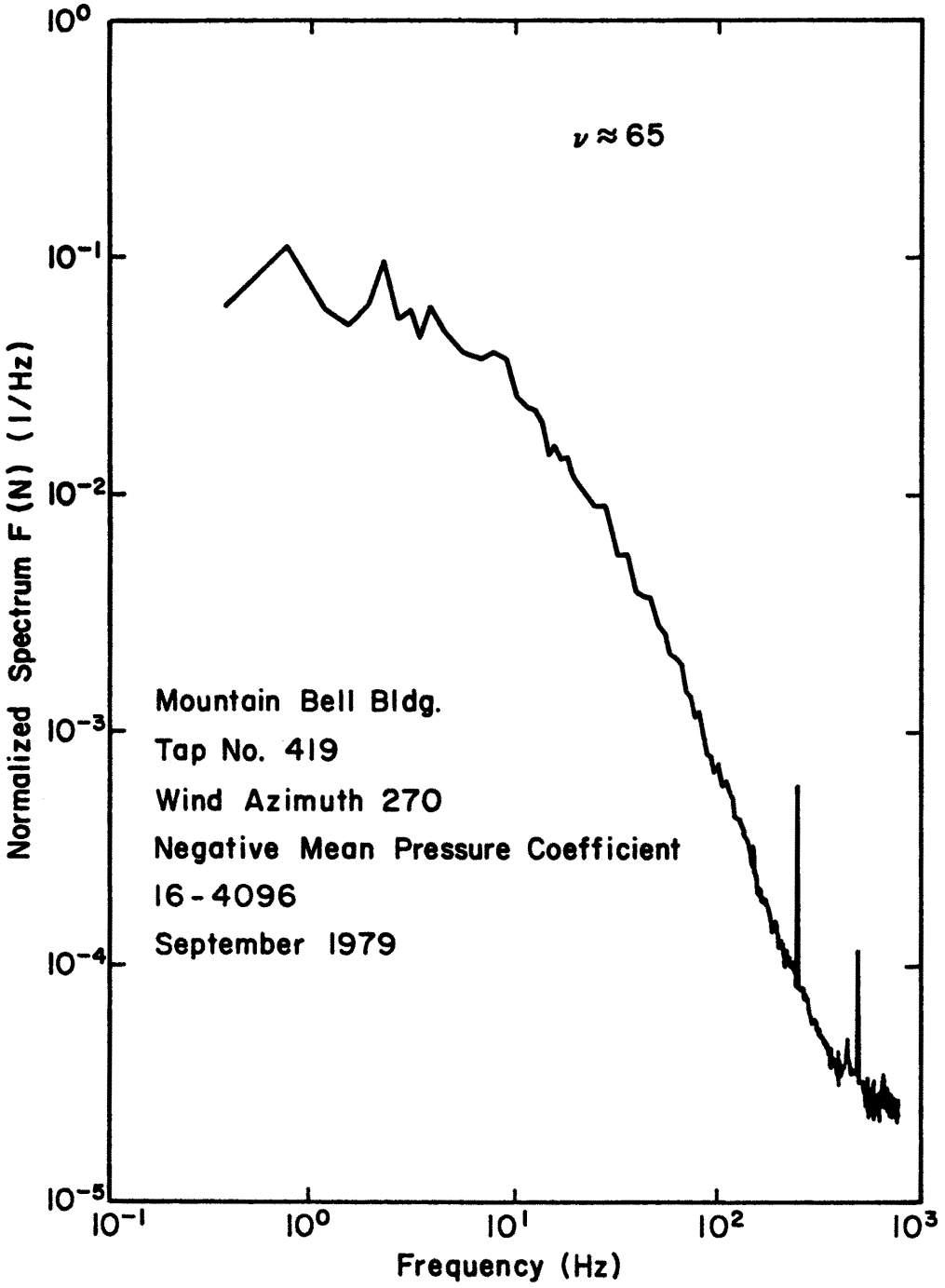


Figure 6.11b. Power Spectral Density Function of Pressure Fluctuations (Negative $Cp_{mean}$).

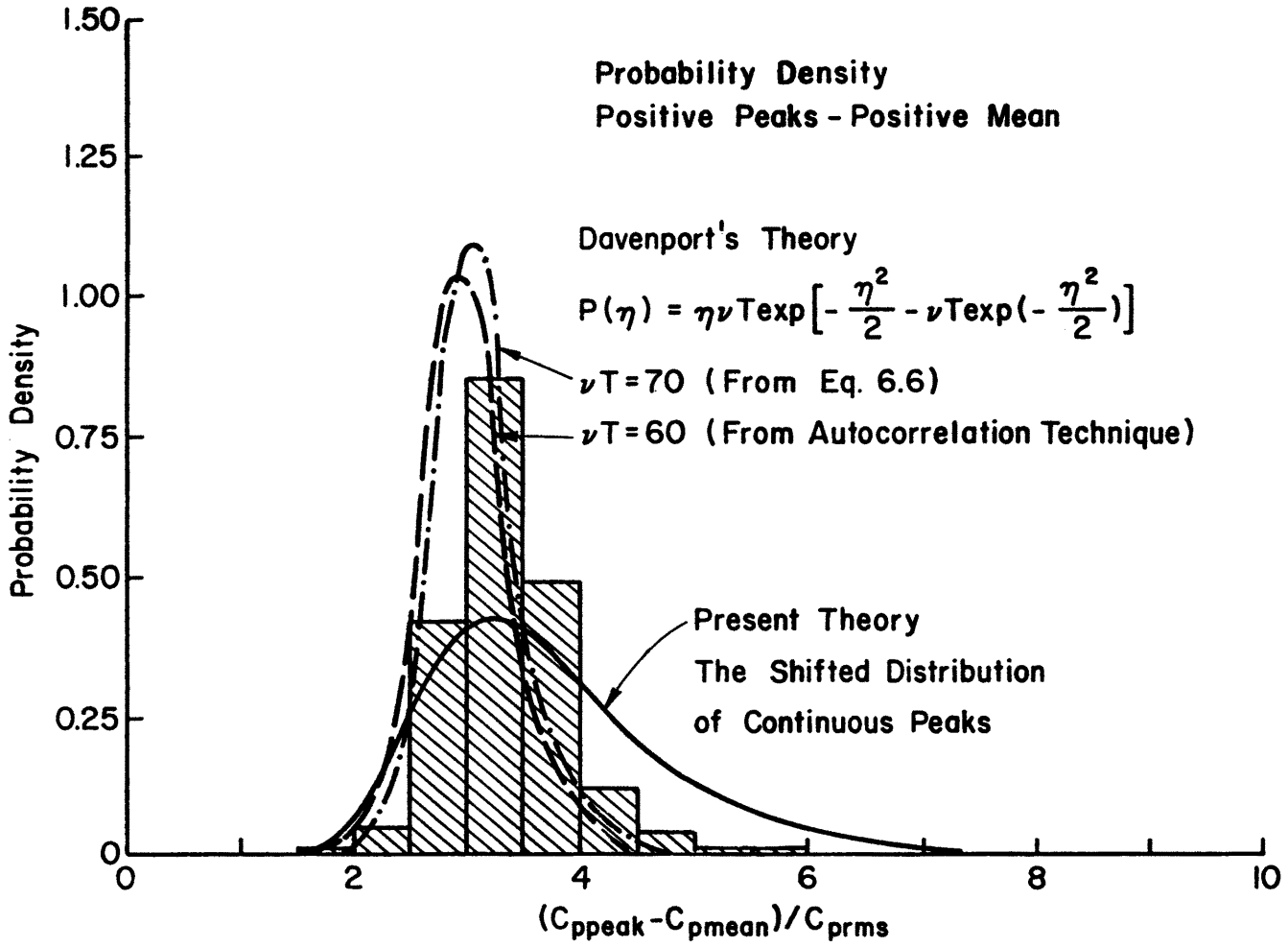


Figure 6.12a. Extreme Value Distribution for WD=000, Tap No.116, A Comparison between Present and Davenport's Theory (Positive Peaks).

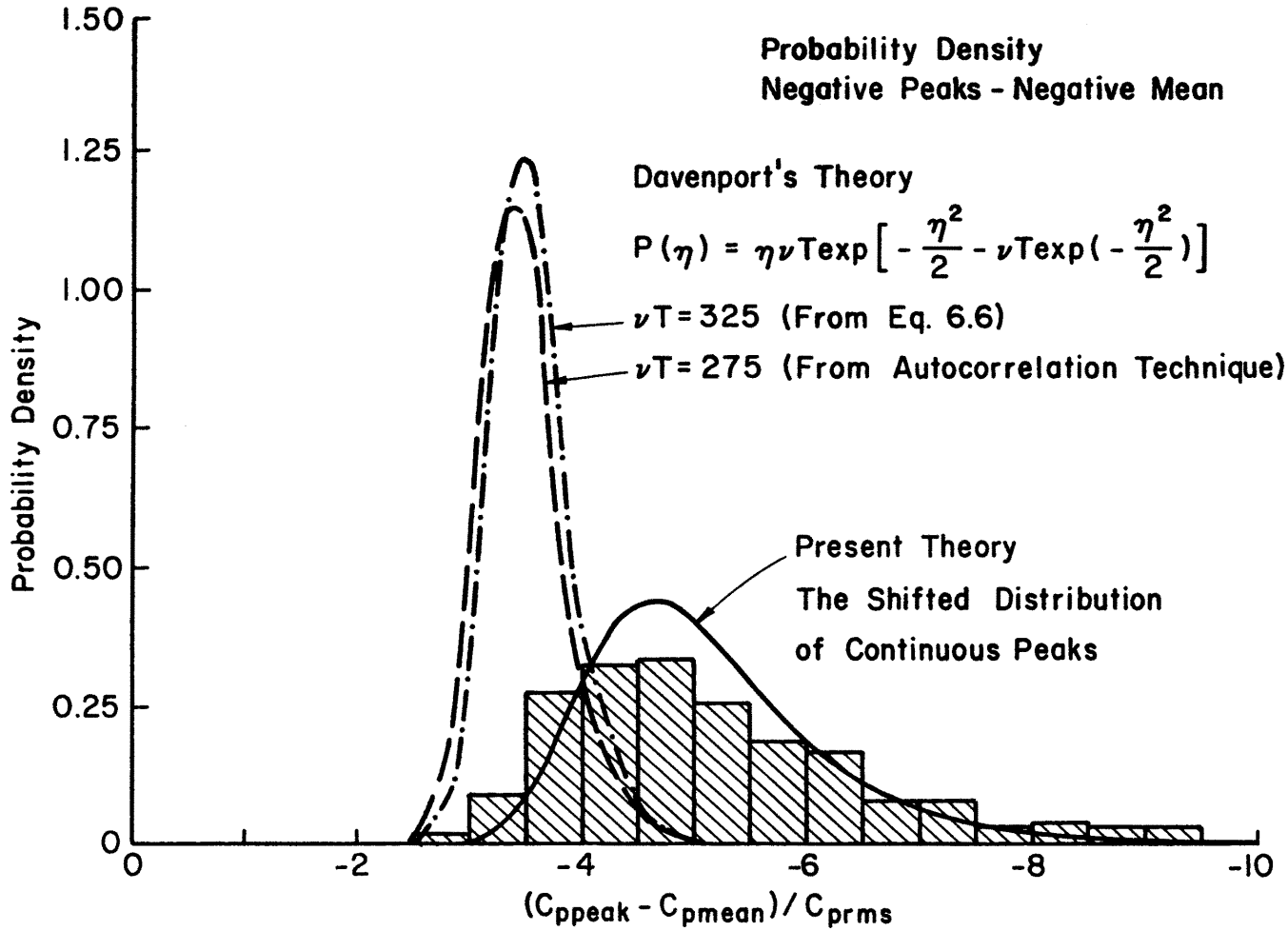


Figure 6.12b. Extreme Value Distribution for WD=270, Tap No. 419, A Comparison between Present and Davenport's Theory (Negative Peaks).

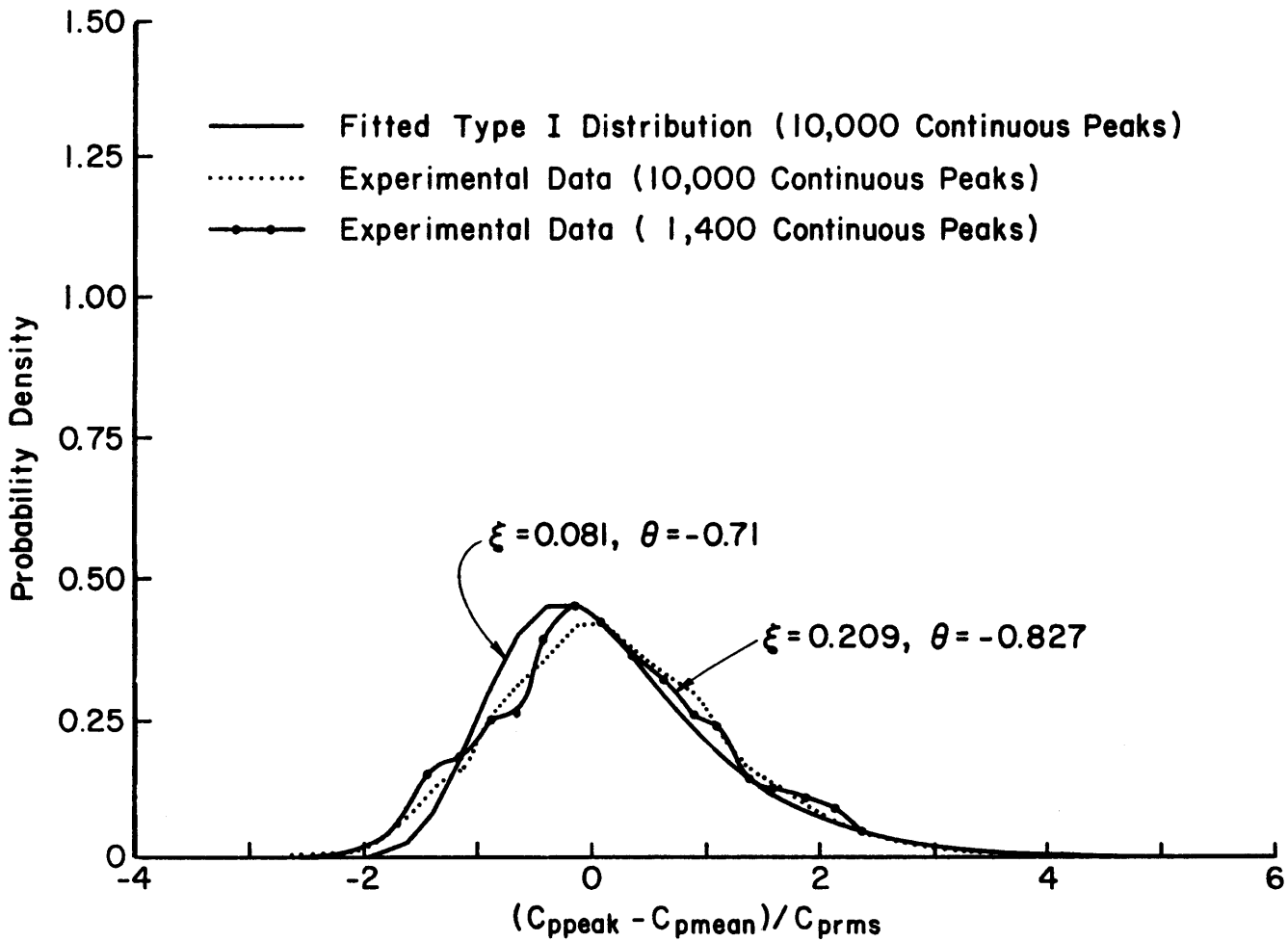


Figure 6.13. Comparison between Distributions of Continuous Peaks for WD=165, Tap No. 417 with 10,000 and 1,400 Peaks.

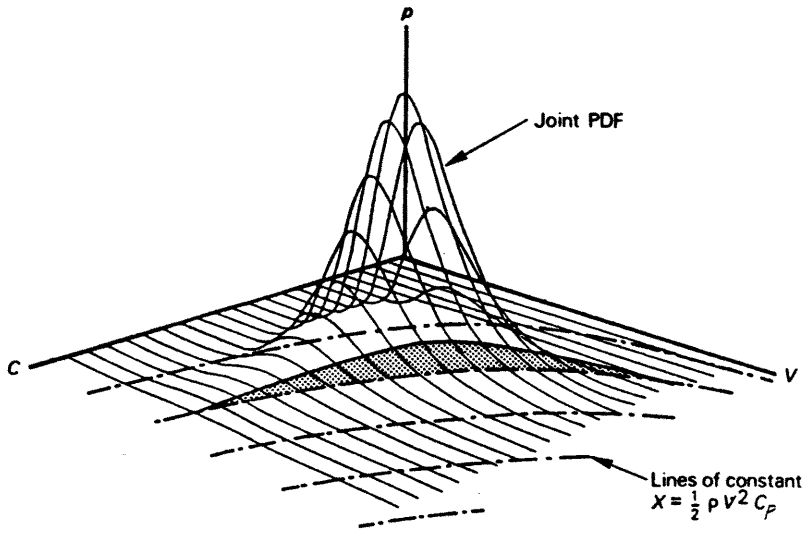


Figure 6.14. Joint PDF of Cp and V after Mayne and Cook (1979).

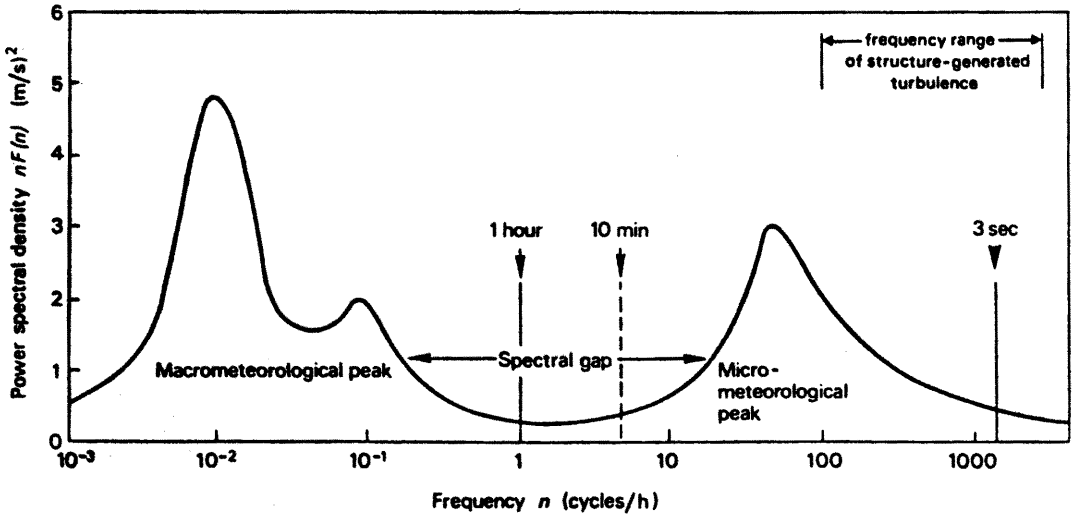


Figure 6.15. Spectrum of Horizontal Wind Speed after Van der Hoven (1957).